Thesis for a Ph.D. Degree

Long-term Changes in Tropical Cyclone Intensity and its Impacts on Coastal Countries of East Asia

열대저기압 강도의 장기변화와 동아시아 국가에서의 그 영향에 관한 연구

Doo-Sun Park

August 2013

School of Earth and Environmental Sciences

The Graduate School

Seoul National University

열대저기압 강도의 장기변화와 동아시아 국가에서의 그 영향에 관한 연구

Long-term Changes in Tropical Cyclone Intensity and its Impacts on Coastal Countries of East Asia

지도교수 허 창 회

이 논문을 이학박사 학위논문으로 제출함
2013년 4월

서울대학교 대학원
지구환경과학부
박 두 선

박 두 선 의 이학박사 학위논문을 인준함
2013년 6월

위 원 장 임 규 호 (인)
부위원장 허 창 회 (인)
위 원 김 광 열 (인)
위 원 이 혜 상 (인)
위 원 박 신 기 (인)

Long-term Changes in Tropical Cyclone Intensity and its Impacts on Coastal Countries of East Asia

By

Doo-Sun Park

Dissertation Submitted to the Faculty of the Graduate School of Seoul National University in Partial Fulfillment of the Requirement for the Degree of Doctor of Philosophy

Degree Awarded

August 2013

Advisory committee:

Professor	Gyu-Ho Lim, Chair
Professor	Chang-Hoi Ho, Advisor
Professor	Kwang-Yul Kim
Doctor	Hee-Sang Lee
Professor	Seon Ki Park

이학박사학위논문

열대저기압 강도의 장기변화와 동아시아 국가에서의 그 영향에 관한 연구

Long-term Changes in Tropical Cyclone Intensity and its Impacts on Coastal Countries of East Asia

2013년 8월

서울대학교 대학원

지구환경과학부

박 두 선

ABSTRACT

Long-term Changes in Tropical Cyclone Intensity and its Impacts on Coastal Countries of East Asia

Doo-Sun Park
School of Earth and Environmental Sciences
The Graduate School
Seoul National University

Tropical cyclones (TCs), accompanied with strong wind and heavy rainfall, always cause immeasurable loss of life and property after their landfalls on the coastal countries. Despite of their destructiveness, it is still unclear whether or not TC intensity became stronger in the western North Pacific (WNP) under the notable warming of sea surface temperature (SST) there. This study examined the long-term trends in TC intensity over the WNP during the period 1977−2010 by using five TC datasets. In addition, changes in landfall strength of TCs over East Asia with their potential and socioeconomic impacts on South Korea were also investigated.

It was found that there is a consistent spatial inhomogeneity of the trends in TC intensity, with a weakening in the tropical Philippine Sea (TP) and a strengthening in southern Japan and its southeastern ocean (SJ). This spatial distribution can be described by TC intensification rate and genesis frequency, with the aid of the climatological direction of TC movement. The increasing intensification rate around the center of the WNP can mostly account for the increasing intensity over the SJ region owing to the less genesis effect there,

whereas the influence of both intensification rate and local genesis frequency matters, due to the effect of the newly generated and less developed weak TCs on the TC intensity, in the TP region.

Thermodynamic variables (e.g., sea surface temperature, potential intensity, and 26℃ isotherm depth) show almost homogeneous changes in space, possibly favoring intensification rate and genesis frequency over the entire WNP. However, the decreasing intensification rate and genesis frequency in some tropical regions conflict with the impact of thermodynamic variables, but rather accord with the impact of dynamic variables (i.e., vorticity and wind shear). Thus, the spatially inhomogeneous trends in TC intensity can be explained by considering the thermodynamic and dynamic aspects in combination through intensification rate and genesis frequency.

These changes in thermodynamic and dynamic environments also could shift spatial positions of the maximum intensity of TCs to near coastal seas. This results in the robust increase in landfall intensity over East Asia (e.g., east China, Korea, and Japan). In contrast, an increase of TC genesis frequency over the northern part of the South China Sea leads to a reduction in the maximum TC intensity before landfall, because of their short lifetime; thus, there are no clear tendencies in the landfall intensity across Vietnam, south China, and Taiwan. In the midlatitudes countries, Korea and Japan, the stronger landfall TCs made their own duration longer after their landfalls. Hence, the potential impacts (e.g., power dissipation index and TC-induced rainfall) could have remarkably increased there.

The other factors (e.g., tracks, translational speeds, mean drift lengths and weakening rates of TCs) could also affect the TC duration, but they are found to be not significant.

Finally, changed relationships between potential damage parameters, defined by wind and rainfall, and real socioeconomic damages were analyzed by using 51 TCs that stroke South Korea during the period 1979–2010. The results displayed that TCs have caused less damages at the same intensity over the country. This reduced vulnerability could be explained by the improved national infrastructures of disaster prevention.

Keywords: Tropical Cyclones, Climate Variability, Trends, Damage Assessment
Student number: 2009-30862

PREFACE

The thesis includes the following papers:

I. **Park, D.-S. R.**, C.-H. Ho, J.-H. Kim, and H.-S. Kim, 2011: Strong landfall typhoons in Korea and Japan in a recent decade, *Journal of Geophysical Research*, **116**, D07105, doi:10.1029/2010JD014801.

II. **Park, D.-S. R.**, C.-H. Ho, J.-H. Kim, and H.-S. Kim, 2013: Spatially inhomogeneous trends of tropical cyclone intensity over the western North Pacific for 1977–2010, *Journal of Climate*, **26**, 5088–5101, doi:http://dx.doi.org./10.1175/JCLI-D-12-00386.1.

III. **Park, D.-S. R.**, C.-H. Ho, and J.-H. Kim, 2013: Growing threat of intense tropical cyclones to East Asia, *Climatic Change*, (to be submitted).

IV. **Park, D.-S. R.**, C.-H. Ho, C.-H. Nam, K.-H. Chang, and S. Park, 2013: Reduced typhoon vulnerability in South Korea possibly due to improved national infrastructures of disaster prevention, *WIREs Climate Change*, (in preparation).

Table of Contents

List of Tables

List of Figures

1. Introduction

Tropical cyclones (TCs), accompanied by strong wind and torrential rainfall, always give rise to numerous casualties and severe property losses after their landfalls on the countries bordering the warm ocean basins. Figure 1 shows each ratio of global economic losses by extreme weather that includes TCs, local/undefined storms, extratropical cyclones, drought, and extreme temperature over the past 30 years. As shown in Figure 1, TCs caused the largest economic losses accounting for about 59% of the total damages by severe weather phenomena over the globe. It is no wonder that TC activity is an old interest of not only policy makers and scientists but also the public in coastal countries.

For the western North Pacific (WNP), recent notable increase in sea surface temperature (SST) [*Cane et al*., 1997; *Rayner et al*., 2003; *An et al*., 2011; *Zhang et al*., 2011], a key factor for TC intensification [*Emanuel*, 1986; *Merrill*, 1988; *Holland*, 1997], aroused curiosity about whether TC activities to increase under this changing climate. Many researchers have investigated long-term changes in TC activities (i.e., genesis frequency, track density, and intensity) linked with the SST warming in the WNP. These scientific efforts made general agreement about changes in genesis frequency and track density, but not intensity.

In both cases of genesis frequency and track density, their own decadal

variations are more dominant regardless of the monotonically rising SST. TC genesis frequency continues to fluctuate with a virtually decadal cycle during the last years in which TC best-track data are available [*Chan and Shi*, 1996; *Yumoto and Matsuura*, 2001; *Yumoto et al*., 2003; *Liu and Chan*, 2012]. This decadal variability of genesis frequency is highly associated with warm and cold phases of SST in the central Pacific [*Matsuura et al*., 2003], whereas SST in the WNP is not a focal factor [*Chan*, 2005]. Meanwhile, most studies on track density consistently showed that major tracks of TCs over the WNP tend to move toward Taiwan and Japan for recent three decades and that the shifted track density is attributable to eastward retreat of the subtropical high and northeastward tropospheric mean flow in the subtropics [*Wu et al*., 2005; *Tu et al*., 2009]. However, there are no scientific evidences that these changed large-scale environments results from the increasing SST in the WNP; the changes in main tracks highly depend on the analysis period. *Ho et al*. [2004] argued that more number of TCs head to the South China Sea and eastern coast of Japan during the last five decades.

In contrast, intensity change is a still controversial topic in the WNP. Analysis of observational records produced conflicting interpretations of historical trends of TC intensity for the WNP basin [*Grossmann and Morgan*, 2011]. Some studies insisted that the overall TC intensity and the number of

intense TCs show significant increasing trends with tropical ocean warming [*Emanuel*, 2005; *Webster et al*., 2005], whereas others raised a counterargument that decadal variations are more dominant than specific trends [*Chan and Liu*, 2004; *Chan*, 2006, 2008]. These incompatible results mainly arose from uncertainty in the available TC intensity records. There is an obvious inconsistency in terms of wind speed among various TC best track datasets over the WNP [*Wu et al*., 2006; *Kamahori et al*., 2006; *Song et al*., 2010; *Ren et al*., 2011] because different modifications have been made to the Dvorak technique used for evaluating TC intensity in each agency that issuing TC best-track data [e.g., *Dvorak*, 1975; *Velden et al*., 1998; *Velden et al*., 2006]. Some studies also asserted that an uncertainty remains due to changed observing technologies: new satellites and cessation of aircraft reconnaissance, so that it is hard to find a reliable trend in TC intensity [*Landsea et al*., 2006, 2010; *Knutson et al*., 2010]. To enhance the reliability of trends in the TC intensity, efforts have been made to reanalyze or reproduce the TC intensity records in a homogeneous way [*Knapp and Kossin*, 2007; *Kossin et al*., 2007; *Wu and Zhao*, 2012]. However, it is still uncertain which data is definitely dependable. Thus, to find consistent trend in TC intensity is an important and challeging research topic.

In this study, an alternative approach to assessing changes in TC intensity were adopted; that is horizontal distribution, thereby illuminating sub-regions

where the intensity changes were statistically significant and consistent in recent decades. This idea is based on the assumption that there would be regional distinction in trend of TC intensity because changes in thermodynamic and dynamic environments vary in different localities in the WNP. For example, in the low latitudes, the recently enhanced Hadley and Walker circulations induce drier conditions in the subtropics [*Sohn and Park*, 2010]. Otherwise, more notable SST rising and remarkable vertical wind shear weakening in the midlatitudes were observed [*Ho et al.*, 2004; *Kwon et al.*, 2007; *Archer and Caldeira*, 2008; *Zhu et al.*, 2011]. These lead to infer the existence of consistent strengthening and weakening of TCs somewhere in the WNP.

Consistent with our inference, *Wu and Zhao* [2012] recently demonstrated a spatially inhomogeneous distribution of TC intensity change (see their Figure 6). However, they did not conduct an in-depth analysis of the horizontal distribution, but related it to the basin-wide change of TC intensity. Thus, it is worth further concentrating attention on the spatial pattern of the intensity changes.

In addition to long-term changes in TC intensity, landfall intensity and its socioeconomic damages are also a matter of concern for the present study. Although some researchers have examined the strength of TCs at landfall from a global perspective [*Weinkle et al*. 2012], the increasing intensity of TCs striking the extensive East Asian area in recent decades has yet to be investigated.

Meanwhile, it was revealed that socioeconomic damages over the globe notably increase under global warming possibly due to economic growth and more frequent emergence of extreme TCs [*Pielke and Landsea*, 1998; *Pielke et al.*, 2003; *Pielke et al*., 2008; *Zhang et al*., 2009; *Fengjin and Ziniu*, 2010; *Crompton et al*., 2011; *Emanuel*, 2011; *Mendelsohn et al*., 2012]. However, no one considered the improved national infrastructures of disaster prevention, which could successfully reduce TC-induced damages.

Thus, the objective of this study is (1) to finding consistent trends of TC intensity in sub-regions of the WNP, (2) to examining landfall strength of TCs striking East Asia, and (3) to confirm changed statistical relationships between potential damage parameters and real socioeconomic damages as focusing on TCs to make a landfall on South Korea. The remaining sections are organized as follows. Section 2 illustrates the data and analysis methods used. Section 3 shows spatial distributions of changes in TC intensity and other TC activity parameters (e.g., intensification rate, genesis, and passage). Section 4 illustrates increase in landfall intensity of TCs over East Asia. Section 5 represents reduction of TC damages in South Korea. Finally, concluding remarks are given in Section 6.

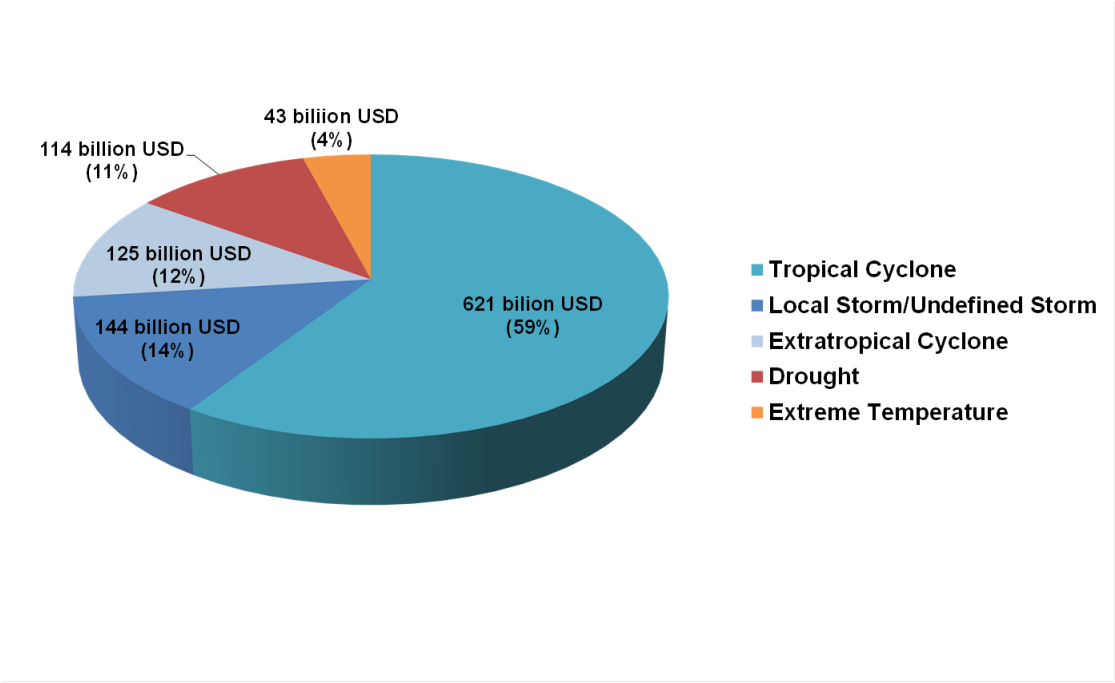

Figure 1. Ratios of economic losses by severe weather phenomena, such as tropical cyclones, local/undefined storms, extratropical cyclones, drought, and extreme temperature, over the globe during the period 1984–2012. Loss data from EM-DAT: The OFDA/CRED International Disaster Database - www.emdat.be, Universite Catholique de Louvain, Brussels (Belgium).

2. Data and Method

a. Best-track Data

Four TC best-track datasets were used to examine the consistency of changes in TC intensity over the WNP. The best track datasets include the Regional Specialized Meteorological Center - Tokyo (RSMC), Joint Typhoon Warning Center (JTWC), Hong Kong Observatory (HKO), and Shanghai Typhoon Institute (STI). Notable distinctions in TC intensities were reported among the four datasets [*Knapp and Kruk*, 2010]. The datasets commonly include the locations of TC centers and maximum sustained wind speeds at six-hour intervals. Details of the all datasets are summarized in Table 1.

The datasets have some non-trivial inconsistencies; especially for the definition of maximum sustained wind. The consistency of the definition of maximum sustained wind is essential in order to compare intensity records of the four best-track data on approximately equal terms. In this study, 10-min averaged maximum sustained wind speed was adopted as a reference; the correction factors for the JTWC and STI datasets are 0.88 and 0.871, respectively [*Knapp and Kruck*, 2010]. In addition, the unit is expressed in the International System of Units (m s^{-1}) using the multiplicative factor, 0.514 for the RSMC, JTWC, and HKO datasets. These methods do not change the original properties of individual best track data.

The TC records with maximum sustained wind speeds in excess of 17 m s^{-1} were used in the analysis. TCs are categorized into four types on the basis of the 10-min averaged maximum sustained wind speeds (v_{max}): tropical depressions (TDs, $v_{max} < 17$ m s^{-1}), tropical storms (TSs, 17 m $s^{-1} \leq v_{max} < 25$ m s^{-1}), severe tropical storms (STSs, 25 m $s^{-1} \leq v_{max} < 33$ m s^{-1}), and typhoons (TYs, $v_{max} \geq 33$ m s^{-1}). This categorization is based on the definitions provided by the World Meteorological Organization. In other words, tropical storms, severe tropical storms, and typhoons were only considered in this study.

The analyses were limited to the period 1977–2010; this is because of the following reasons: (1) operation of the Geostationary Meteorological Satellite launched by Japan Meteorological Agency commenced in 1977 and (2) the RSMC data for the maximum sustained wind speed are available for the period after 1977 [*Kamahori et al*., 2006; *Wu and Zhao*, 2012]. The TC season was defined as 5 months, from July to November, when the formation of intense TCs (i.e., Saffir–Simpson categories 4 and 5) is more frequent in the WNP [*Tu et al*., 2011].

To evaluate the trends found in the best-track data, the TC dataset of University of Wisconsin/National Climatic Data Center (UW/NCDC), introduced by *Kossin et al*. [2007], was also utilized. The data is reproduced by a simple multivariate log-linear regression model based on the new globally consistent satellite data [*Knapp and Kossin*, 2007]. This reanalyzed data covers only the period 1982–2006, so that the linear trends were calculated for the best-track datasets during the period 1977–2010 and for the UW/NCDC data during the

period 1982–2006. Because the UW/NCDC data were trained for the North Atlantic, it may contain a substantial bias when the data are applied in intensity analyses for other basins. For instance, in Figure 4a, absolute values of the UW/NCDC data are considerably lower than those of the best track data. Thus, the UW/NCDC data was excluded when calculating spatial distributions and averages of datasets. Nevertheless, the UW/NCDC data is a good estimator for evaluating whether the trends based on the best track data are reliable, because it is regarded as the most homogeneous data at present [*Kossin et al*., 2007]. Although the intensity estimates of the UW/NCDC data for the WNP TCs are not complete, the consistent trends between the best track and UW/NCDC data indicate that the trends are less likely to be artificial due to the heterogeneity of the best track records (J. P. Kossin 2012, Personal communication).

To examine the horizontal distribution of changes in TC activity parameters (e.g., intensity, intensification rate, genesis frequency, track density, translation speed, and location of maximum intensity), an overlapping latitude–longitude gridding method [*Kim et al*., 2010] was adopted. Based on the center of any grid point, a 5° × 5° square window was set up, in which annual TC activity parameters were calculated by averaging all six-hourly records observed during the TC season for the year. By shifting the window at a 1° interval in latitude and longitude (far less than the size of the window), gridded data with a 1° × 1° horizontal resolution were constructed, by which the distribution of annual TC activity parameters was spatially smoothed without modifying the original data

properties. As no averaged records were obtained in grid points where no TCs passed during a year, these grid points were given a missing value and were not used for the calculation of trends in TC intensity, intensification rate, and translational speed. However, as the non-recorded points are meaningful for frequency-related parameters (e.g., genesis frequency, track density, and location of maximum intensity), the zero values were included in the calculation of trends for these parameters. The linear trends in TC intensity, intensification rate, and translational speed (genesis frequency, track density, and location of maximum intensity) were not calculated for the grid points where missing (zero-valued) years were detected for more than 14 (25) years. The selected threshold years are sufficient to show the major regions with significant trends. It is noted that replacements in the threshold years just alter the extension of the area without changing the calculated trends.

To estimate the time of TC landfall with greater accuracy, the TC data, generally recorded at six-hour intervals, were linearly interpolated with one-hour intervals. Figure 2 displays the target landfall regions (i.e., gray shaded area), which include Indochina, Hainan Island, Taiwan, mainland China, the Korean Peninsula, and the Japanese archipelago. The intensity at landfall is defined as the wind speed of the TC when its interpolated center enters the landfall region for the first time.

Table 1. Characteristics of four best-track datasets over the WNP.

	RSMC	JTWC	HKO	STI
Record period	1951–present	1945–present	1961–present	1949–present
Time for maximum sustained wind	10 minutes	1 minute	10 minutes	2 minutes
Unit for maximum sustained wind	Knot	Knot	Knot	$m\ s^{-1}$
Time interval of record	6 hours (3 hours near Japan)	6 hours	6 hours	6 hours
Multiplicative factor for 10-minute maximum sustained wind	–	0.88	–	0.871
Multiplicative factor for SI units	0.514	0.514	0.514	–

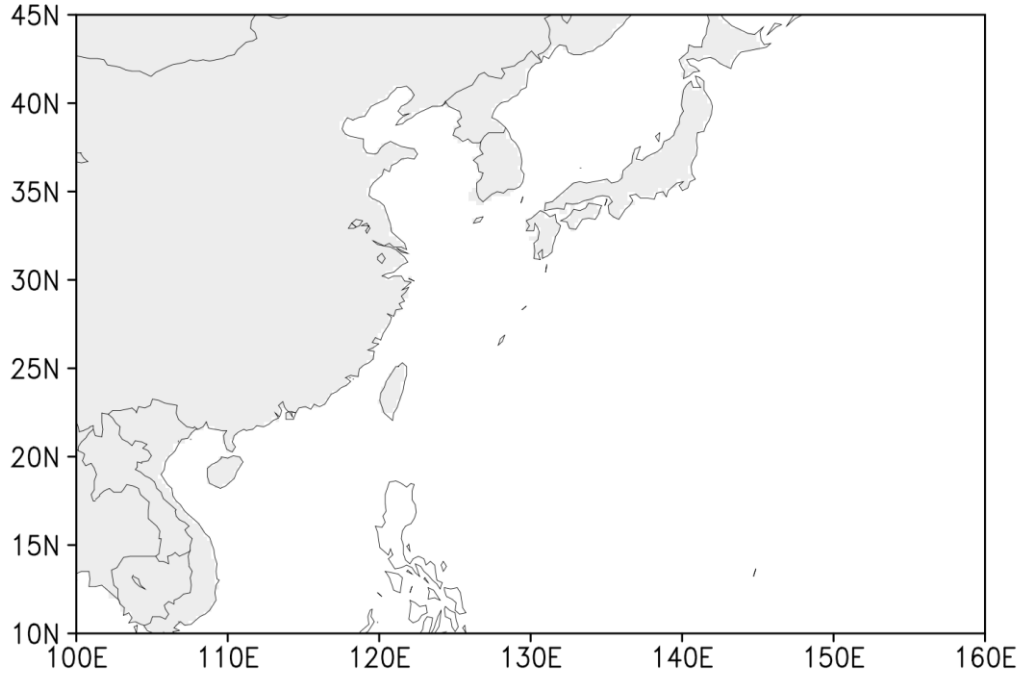

Figure 2. Defined landfall domain (gray shadings).

b. Atmospheric and Oceanic Data

Various datasets were obtained to analyze large-scale environments related to TC intensity. The datasets include atmospheric reanalysis data from the European Centre for Medium-Range Weather Forecasts (ERA-interim) [*Dee et al*., 2011], SST data from the National Oceanic and Atmospheric Administration (NOAA) Optimum Interpolation SST version 2 [*Reynolds et al*., 2002], and oceanic analysis data from the National Centers for Environmental Prediction (NCEP) Global Ocean Data Assimilation System (GODAS) [*Behringer et al*., 1998]. The ERA-interim provides the atmospheric state variables with troposphere, such as temperature, relative vorticity, horizontal/vertical winds, specific/relative humidity, and sea level pressure at a 1.5° horizontal resolution for the period 1979−2010, while the NCEP GODAS provides the ocean sub-surface temperatures at 40 geometric depth levels with a 1/3° horizontal resolution for the period 1980−2010. The NOAA Optimum Interpolation SST covers the shorter period starting from 1982, at a 1° horizontal resolution.

3. Spatial Distribution of Tropical Cyclone Activity over the western North Pacific

3.1 Inhomogeneous Spatial Distribution of Trends in Tropical Cyclone Intensity

There are many TC intensity-related definitions widely used, such as power dissipation index (PDI) [*Emanuel*, 2005], accumulated cyclone energy (ACE) [*Bell et al*., 2000], and number of intense TCs classified by Saffir-Simpson category [*Webster et al*., 2005]. However, these definitions have some limitations. PDI and ACE complexly depend on lifetimes, frequencies, and intensity of TCs [*Emanuel*, 2007]. The categorized frequencies cannot perceive tiny changes in maximum wind speed within each bound of the categories. Thus, in this study, the intensity-related definition used is seasonal average of peak wind speed of each TC. This definition, hereafter just called as TC intensity, is only dependent on maximum wind speed and very sensitive to wind speed change.

Figure 3a and 3b show the spatial patterns of climatology and linear trends in TC intensity during the analysis period (1977−2010), respectively. As seen in Figure 3a, the maximum of climatological TC intensity is located in the northeast of Taiwan. The region is one of main paths for TCs recurving from the eastern tropics to the midlatitudes over the WNP [*Ho et al*., 2004; *Wu et al*., 2005; *Tu et al*., 2009]. Because these types of the recurving TCs generally have enough time to develop over the warm ocean basin, they can become very powerful TCs, thereby accounting for the location of maximum intensity. The contour intervals

are relatively broad around this maximum core region, while narrowing down toward the East Asian continent, the Philippines, and eastern tropics. This implies that TCs may rapidly develop (decay) over the eastern tropics (after landfall). In addition, the coastal regions facing the South China Sea generally suffer less from intense TCs than those bordering the WNP including the Philippines, Taiwan, East China, South Korea, and Japan.

The overview of spatial distribution of the linear trends in TC intensity can be characterized by opposite signs between the south and the north of the WNP (Figure 3b). The sub-regions were properly divided into two regions by considering the signs, significances, and localities: the southern Japan and its southeastern ocean (SJ; 25°−36°N, 130°−148°E) and the tropical Philippine Sea (TP; 10°−18°N, 127°−144°E). In the SJ region, positive signs are predominant, whereas negative signs are prevalent in the TP region. In general, all four TC best-track datasets show consistent signs of trends with the average trend from the mean of the four datasets in the grid points where the trends are discernible. The grid points with three or more datasets showing a statistically significant trend at the 90% confidence level mostly reside in the SJ and TP regions. The grid points in which all datasets show a significant trend are mainly distributed over the southeastern ocean in SJ and the central part of TP. In contrast, the imperceptible trends for all datasets are observed around the region where the climatological maximum of TC intensity appeared (Figure 3a). This result is in line with *Webster*

et al. [2005], who found that there is a negligible change in the time series of the annual maximum TC wind speeds over the WNP.

Figure 4 presents the time series of TC intensity for the individual datasets, averages and their confidence intervals of the four best track data except the UW/NCDC data in the two box regions. The confidence interval ($p < 0.1$) was acquired from bootstrap resampling with 10,000 replicates based on the annually four values of best track data [*Hall*, 1988], assuming that the accuracy of each best track data may be same. To test the significance of trend, both the two-tailed *t*-test and nonparametric Mann-Kendall test were utilized together, because the linear trend is generally subject to some assumptions. The merits of the nonparametric Mann-Kendall test are 1) that it is unnecessary to hypothesize normality and 2) that the test is less sensitive to outliers since it detects the monotonic trend which is not essentially linear (Table 1) [*McLeod et al*. 1990; *Chu et al*. 2012].

In the SJ region, all the time series show gradual increments (Figure 4a). The trends range from +0.64 to +1.54 m s^{-1} $decade^{-1}$, which are all positive, but only the UW/NCDC and JTWC data show statistically significant trends at the 90% confidence level (Table 2). In case defining a smaller box over the southeastern ocean of Japan (viz., 25°−33°N, 140°−144°E), the increasing trends of all time series became steeper and statistically significant at the 90% confidence level except the RSMC data (Table 2). The increasing intensity in the SJ region was also reported in previous studies [e.g., *Chan*, 2008; *Wu and Zhao*, 2012].

In contrast, the time series in the TP region show overall decrements (Figure 4b). The negative trends range from −2.75 to −0.81 m s^{-1} $decade^{-1}$, all of which are statistically significant at the 90% confidence level except the UW/NCDC data (Table 2). The decrements were more evident in the central oceanic area of TP (viz., 11°−17°N, 133°−144°E), in which all datasets presented robust and significant decreasing trends. The trend of the UW/NCDC data was not significant in case applying the Mann-Kendall test. However, the decreasing intensity in the TP region is thought to be as evident as the increasing intensity in the SJ region, because the trend was significant when using the Student's *t*-test and its decreasing rates were generally larger than those in the SJ region.

The time series show large interannual fluctuations of TC intensity (Figure 4). Therefore, calculation of the trend was subject to their start and end years. To examine the sensitivity of the trend to a chosen period, sliding regressions using 20-year moving windows (i.e., 1977–1996, 1978–1997, …, 1991–2010) were calculated for the time series of TC intensity estimated from the average of the four best tracks and the UW/NCDC data in the SJ (Figure 5a) and TP (Figure 5b) regions. For the best track data, the sub-trends for the mean intensity were only displayed because the sub-trends for individual best track datasets show very similar variations with the significant correlation coefficients exceeding 0.75.

In the SJ region, the positive sub-trends were dominant for the average intensity of the four best track data, with only two 20-year windows (1981–2000 and 1990–2009) showing weak negative trends (Figure 5a). The former weak

negative trend during 1981–2000 and two near-zero trends surrounding this period (1980–1999 and 1982–2001) can be attributed to both the positive peak near the start year (1982) and the negative peak near the end year (1999). An analogous explanation holds for the latter one (1990–2009) and two weak positive trends (1989–2008 and 1991–2010). On the other hand, the strongest upward trends were found for the 20-year windows in the early (1977–1996, 1978–1997) and middle periods (1985–2004, 1986–2005), where the start year is near the lowest point and the end year is near the peak point (Figure 4a). The sign of the trend became more sensitive to the start and end years when applying a shorter period. Nevertheless, it is unlikely to be the fallacy that TC intensity in the SJ region has increased since 1977, since the majority of sub-trends (Figure 5a) as well as all the trends for the entire period (Table 2) shows upward tendencies.

On the other hand, the TP region showed conspicuous negative trends in TC intensity for the four best track data for all sub-periods (Figure 5b). The negative trends in this region were more prominent than the positive trends in the SJ region. The negative sub-trends were statistically significant for the windows during the mid-period (1981–2000, 1982–2001, 1983–2002, and 1984–2003), which start near the peak of 1985 and end near the lowest year of 1999. The negative trends were relatively weaker without a statistical significance for the windows in the early (1977–1996, 1978–1997, 1979–1998, and 1980–1999) and the middle to late periods (1985–2004, 1986–2005, 1987–2006, 1988–2007, 1990–2009, and 1991–2010). Several dips around 1980 and the strong peak in 2009 contributed to the

weakening of the negative sub-trends (Figure 4b). The 20-year sliding regressions using the UW/NCDC data also showed consistent signs of the trend with those of the best track data for both the SJ and TP regions (open bars in Figure 5). Though uncertainty due to the data quality remains, these results suggest that the opposing trends found in the SJ and TP regions certainly exist during the analysis period (1977–2010).

In addition to the two main analysis regions, some regions exhibited marginal trends with consistent signs among datasets (i.e., dot points in Figure 3b), though only one or two sets have the statistical significance. For example, the southern coast of China and the Philippines were likely experience weakly decreasing TC intensity, while, in the intermediate region between SJ and TP, both negative and positive signs were observed. In the following sub-section, the changes in these regions will be shortly described after discussing the changes in the main regions.

Table 2. Linear trends in TC intensity (m s^{-1} $decade^{-1}$) in SJ and TP regions for averages of four best track data, UW/NCDC, RSMC, JTWC, HKO, and STI during the period 1977–2010. * and † denote the changes are statistically significant at the 90% confidence level when using the Student *t*-test and the Mann-Kendall test, respectively. The values in the parentheses indicate linear trends of core regions of SJ and TP where the changes are larger.

	Mean	UW/NCDC	RSMC	JTWC	HKO	STI
SJ	+0.97† (+1.69*†)	+1.39*† (+2.16*†)	+0.64 (+1.07)	+1.54*† (+2.39*†)	+1.05† (+1.52*†)	+0.66 (+1.78*†)
TP	–2.35*† (–2.95*†)	–0.81 (–1.13*)	–2.28*† (–2.90*†)	–2.00*† (–2.63*†)	–2.75*† (–3.30*†)	–2.36*† (–2.99*†)

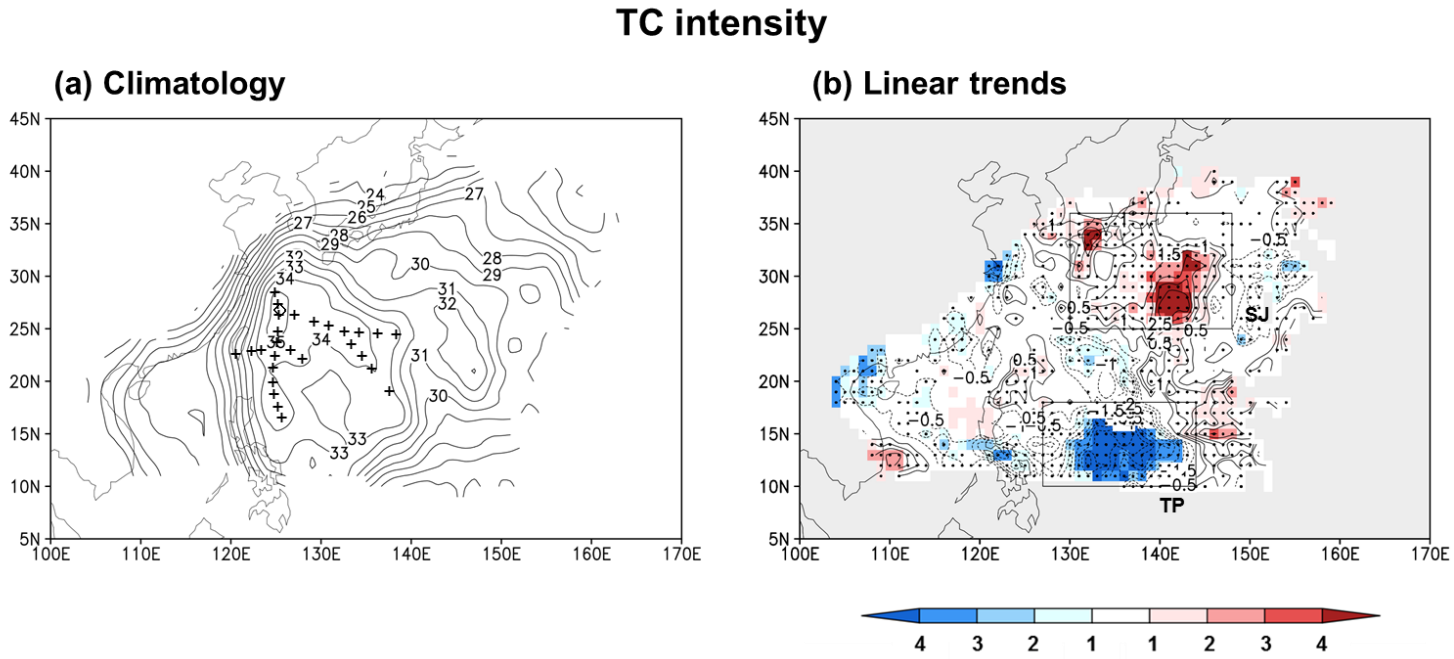

Figure 3. (a) Climatology (m s^{-1}) and (b) linear trends (m s^{-1} $decade^{-1}$) of TC intensity during the period 1977–2010. Contour indicates the average of four best-track datasets, color indicates the number of TC data for which changes are significant at the 90% confidence level, and dot indicates regions where all four TC data show the same sign. Crosses represent ridges of TC intensity.

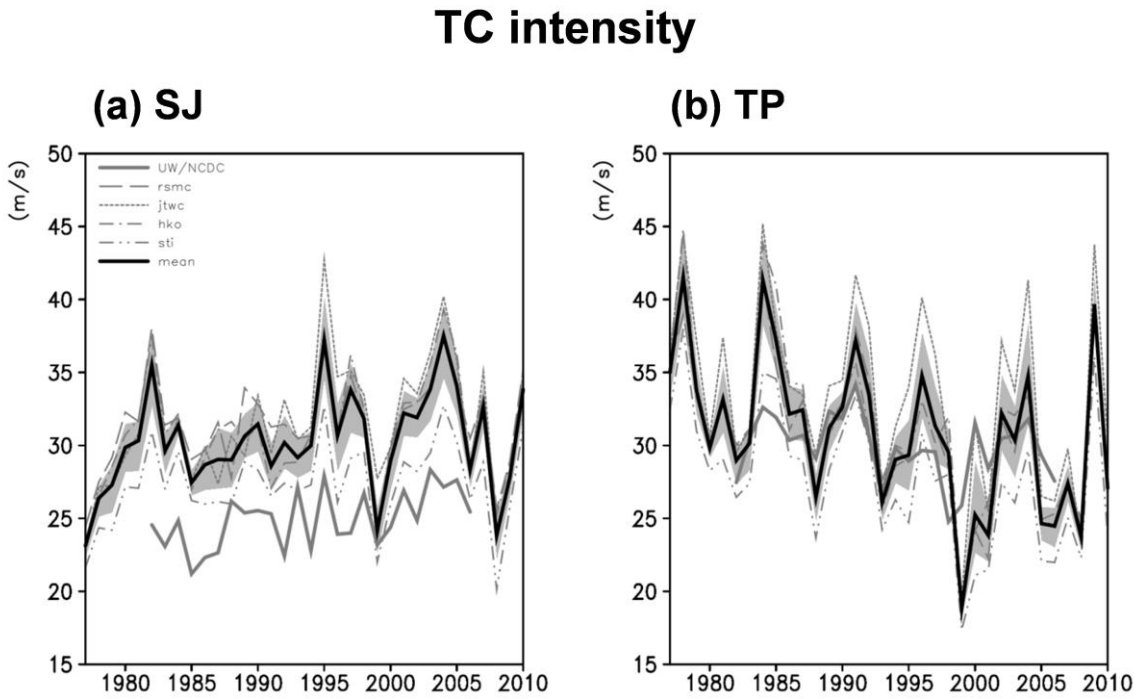

Figure 4. Time series of TC intensity (m s^{-1}) in (a) SJ and (b) TP. Dashed, dotted, dot-dashed, and dot-dot-dashed lines represent annual TC intensity of RSMC, JTWC, HKO, and STI, respectively. Gray and black solid lines indicate the UW/NCDC and the mean of four best track data, respectively. Gray shadings represent the confidence intervals of the mean of best track data.

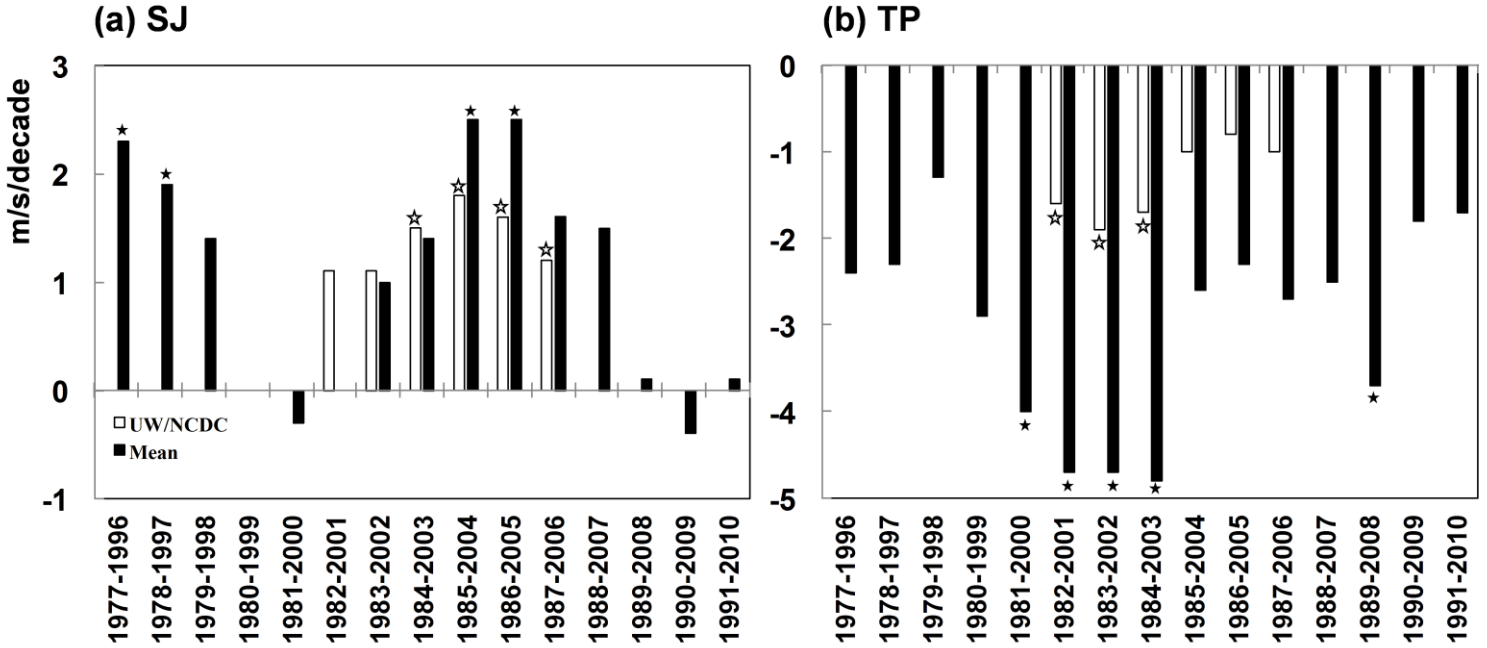

Figure 5. The 20-year sub-trends (m s^{-1} $decade^{-1}$) of TC intensity in (a) SJ and (b) TP during the period 1977–2010. The open and filled boxes indicate UW/NCDC and the mean of four best track data, respectively. Open and filled stars represent that the sub-trends for the UW/NCDC and mean of four best track data are statistically significant at the 90% confidence level, respectively. Small rectangular represents the available period for the UW/NCDCD data.

3.2Associated Other Parameters of Tropical Cyclone Activity

If the intensity trends were computed over the whole life of TCs, the basin-total trends would diverge in various TC best track datasets as shown in preceding studies [*Wu et al*., 2006; *Kamahori et al*., 2006; *Song et al*., 2010; *Ren et al*., 2011], reflecting the effect of reversal trends in the TP and SJ regions. Namely, it is important to interpret the mechanism of the differing trend patterns observed in the two regions. Prior to investigating relevant large-scale environments, the spatial distribution of trends in other TC activity parameters (e.g., TC intensification rate, genesis, track density, and translation speed) that could substantially affect the TC intensity was examined.

a. Intensification Rate

Here, the TC intensification rate, which is defined as an average wind speed change in a unit hour in a grid, was utilized. Figure 6a demonstrates the spatial pattern of climatological TC intensification rate and translational direction for the analysis period (1977−2010). The negative values are distributed over the coastline of the East Asian continents and the north of 25°N, while the positive values are spread over most of entire ocean basin in the tropics. This climatological pattern naturally accounts for the spatial distribution of climatological TC intensity because of the straightforward physical relationship between the TC intensification rate and the TC intensity. Considering the climatological translational direction, it is expected that the zero line of TC intensification rate in the WNP nearly coincides with the ridges of TC intensity

(crosses in Figure 3a). In other words, TCs generally reach their strongest intensity where the TC intensification rate changes its sign from positive to negative. Thus, the spatial distribution of trends in TC intensification rate can account for the spatially inhomogeneous trends in TC intensity with the aid of the climatological translational direction.

Figure 6b displays spatial distribution of linear trends in TC intensification rate. As shown in Figure 6b, the TC intensification rate has been slightly getting slower in the eastern part of TP, while significantly boosted over the vast tropical and subtropical areas. As the TCs in the tropics generally move westward or northwestward according to the climatological translational direction (Figure 6a), this pattern of TC intensification rate can explain that the TCs from the easternmost or eastern outer region of TP experienced the suppression of TC intensification and became weaker over the eastern part of TP. In addition, the increasing intensification rate with climatological west-northwestward TC translation over the center of TP is accountable for the moderate decrease of TC intensity over the eastern offshore of the Philippines (Figures 3b and 6b). Keeping moving on to the west, the reweakened intensification rate just outside of the western boundary of the TP region explains the decreasing intensity trends over the Philippines (Figures. 3b and 6b). The intensification rate shows the largest upward trends over the intermediate region between the TP and SJ regions. In a climatological sense, TCs passing over this region move northward (Figure 6a), so that the more rapid intensification rate there could greatly enhance the TC

intensity to its north (i.e., the SJ region) (Figures. 3b and 6b). This interpretation is reasonable because the trends in TC intensification rate are trivial in the SJ region, which indicates no evidences of further local strengthening of TCs therein. Thus, the spatial distribution of the trend of TC intensification rate is an effective method to interpret the trend of TC intensity.

Figure 7 exhibit correlation coefficients between intensification rate and intensity time series of the SJ and TP regions. The time series of intensity in the SJ are weakly correlated with intensification rate (Figure 7a). This may be because the intensity of TCs in the SJ is affected by broad ocean environments through their lives. Otherwise, due to shorter lives of TCs, spatial patterns of correlation coefficients of intensification rate with intensity in the TP seem to be very similar with reverse pattern of trend in intensification rate (Figure 7b). This suggests that TC intensity in the TP can be considerably affected by changes of intensification rate over the eastern Philippine Sea.

However, the spatial distribution of TC intensification rate is not always a perfect indicator for the TC intensity as displayed in the following regions: 1) The intensification rate has increased over the northern South China Sea, but the TC intensity has slightly weakened along the southern coast of China (Figures. 3b and 6b); 2) The positive trends of TC intensity southeast of Taiwan was not as large as those in the SJ region even though the TCs passing there were also very likely to experience the strong positive trends of TC intensification rate over the western TP region and its north; 3) The declining trends of TC intensification rate are not

large enough to explain the remarkable downturn of TC intensity in the TP region. Accordingly, the interpretation solely by the TC intensification rate with the climatological translation direction is imperfect for those regions. This naturally leads us to investigate other parameters, such as TC genesis frequency, passage frequency, and translation speed.

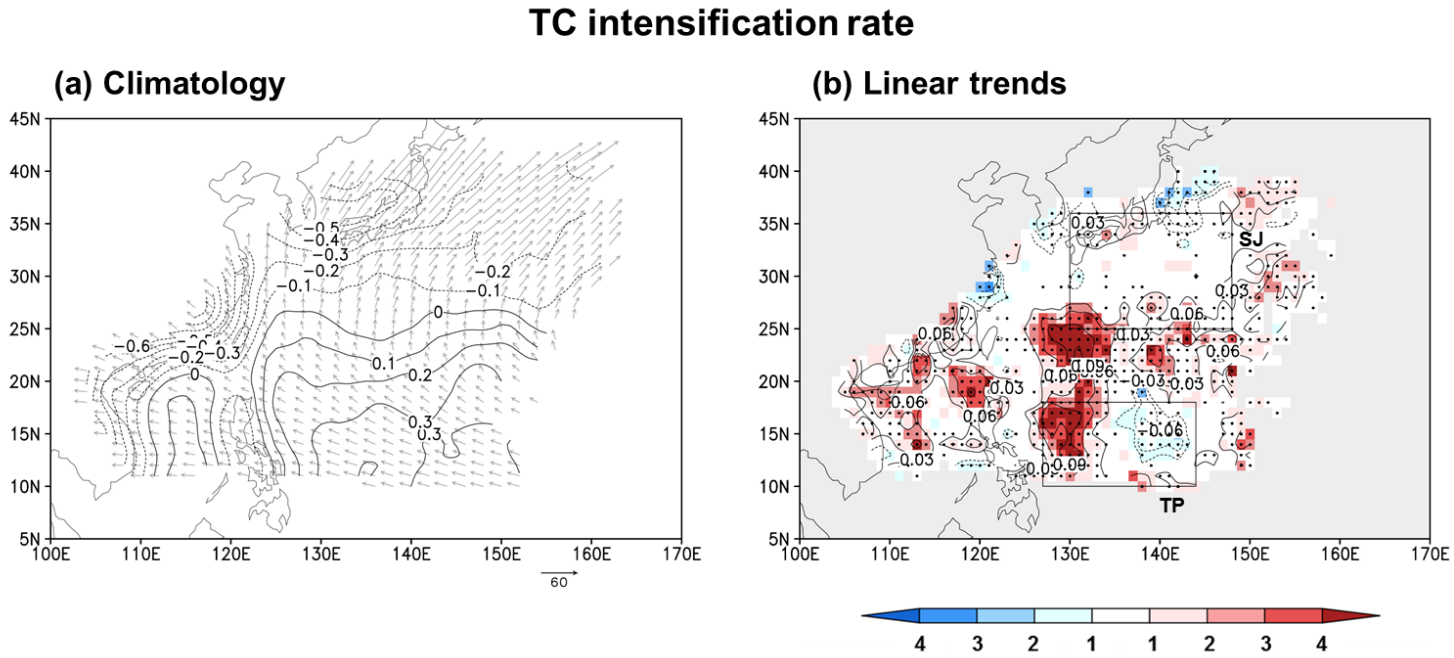

Figure 6. (a) Climatology of TC intensification rate (black contour, m s^{-1} hr^{-1}) and translational direction (gray vector, km hr^{-1}) and (b) linear trends of TC intensification rate (m s^{-1} hr^{-1} $decade^{-1}$) during the period 1977–2010. Contour indicates the average of four best-track datasets, color indicates the number of best-track data for which changes are significant at the 90% confidence level, and dot indicates regions where all four TC data show the same sign.

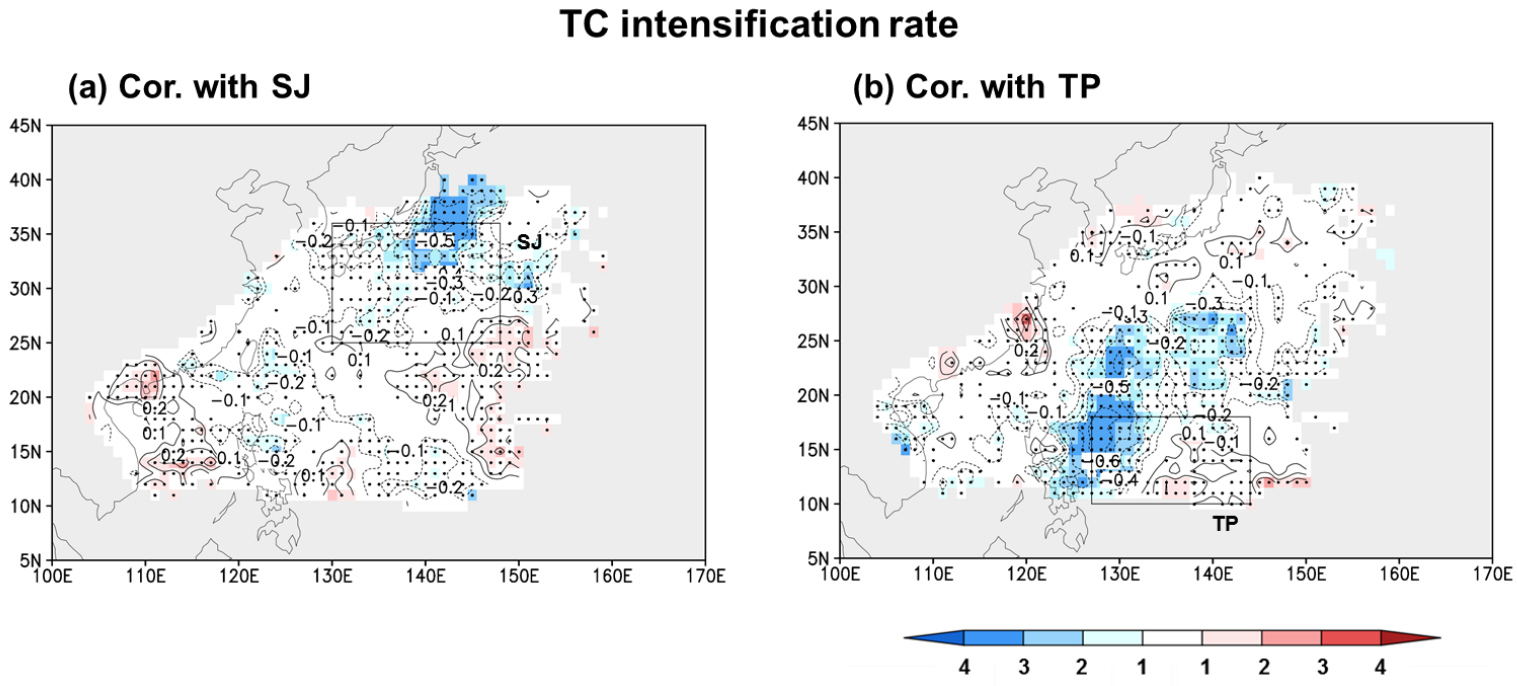

Figure 7. Correlation coefficients between intensification rate and intensity time series of (a) SJ and (b) TP regions.

b. Genesis Frequency

Figure 8a exhibits spatial distribution of climatological genesis frequency, which has three high cores: the South China Sea, the Philippine Sea, and the easternmost Philippine Sea. These cores are positioned over the subtropics that the environmental conditions are favorable for TC development: warm SST above 26.5℃, high humidity, existence of monsoon trough, and weak vertical wind shear [*Gray*, 1968; *Briegel and Frank*, 1997; *Ritchie and Holland*, 1999; *Frank and Ritchie*, 2001]. The location of TC genesis is an influential factor for TC intensity because TCs can have more or less time to develop over a warm ocean basin depending on the genesis location [*Camargo and Sobel*, 2005; *Wu and Wang*, 2008; *Ha et al*., 2012]. Hence, particularly in the low latitudes, the TC intensity could be considerably affected by genesis frequency.

Figure 8b represents spatial distribution of linear trends in genesis frequency. As seen in Figure 8b, the frequency of TC genesis has decreased considerably over the large domain of the tropical eastern WNP basin (i.e., east of the TP region) and the west and east sides of the Philippines. Conversely, it has increased in the south of Hainan Island, northern South China Sea, north of the TP region near 130℃E, and the heart of the TP region.

TCs at their genesis locations must have the intensity slightly above 17 m s^{-1} in the best track data, since it is the minimum threshold of TC intensity in this study. Thus, it is natural to say that the newly generated TCs are weaker than the developed TCs. Considering this point, the average intensity in the grid point

should be reduced if more newly generated TCs are included. Therefore, with the genesis frequency, the insufficient interpretation of the trends in TC intensity can be improved by the TC intensification rate in the three regions, such as the southern coast of China, southeast of Taiwan, and the TP region.

First, more TC genesis in the northern South China Sea and less TC genesis west and east of the Philippines (Figure 8b) may contribute to the slight weakening of landfalling TCs in the southern coast of China (Figure 3b). That is, the trends of TC genesis counteracted the trends of TC intensification rate in the northern South China Sea. As the two responsible factors offset each other, the changes in these regions could not be prominent. Second, the increasing genesis frequency north of the TP region near 130°E may explain the weak increasing trends of TC intensity southeast of Taiwan. Third, the slight increase of new TCs forming in the TP region can have a role in enhancing the weakening trends of TC intensity there. In addition, the great decrease in TC genesis frequency over the large domain of the tropical eastern WNP basin can contribute to the weakening of TC intensity in the TP region together with the suppressed TC intensification rate (Figures 6b and 8b). This is because fewer number of developed TCs reached the eastern TP region. Considering that TCs in the low latitudes, where most of TCs form, will generally intensify and propagate westward, this seems to be a reasonable speculation.

The TC genesis frequency can account for the large parts of decreasing intensity trends over the tropical and subtropical WNP regions, in combination

with the intensification rate. However, the trivial local genesis frequency in the SJ region hardly affected the TC intensity therein since the climatological genesis location lies south of 25°N (figure not shown). Accordingly, it is natural to say that the trends of TC intensity in the SJ region were determined by the intensification rate at the southern entrance region of the domain.

To clarify the relationship between genesis frequency and intensity, their correlation coefficients were calculated (Figure 9). In the SJ, decreasing genesis frequency in recent decade over the easternmost Philippine Sea may be a negative role for intensity because they are positively correlated (Figure 9a). However, the notably increasing intensification rate in the center of the WNP may decide the intensity increase in the SJ (Figure 6b). Meanwhile, in the TP, the correlations in middle and east of the TP are negatively and positively correlated (Figure 9b). This indicates that recent increment and decrement of genesis frequency in the middle and east of the TP are one of the major roles for the intensity in the TP (Figure 8b).

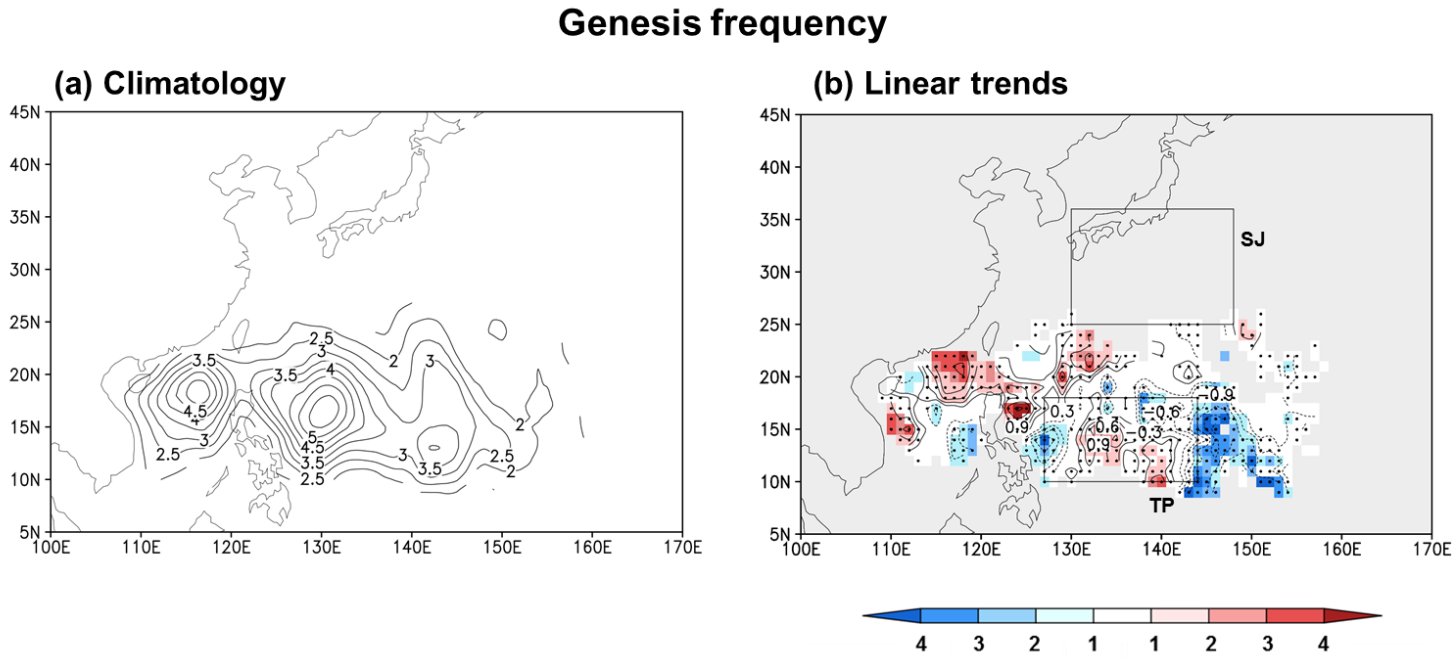

Figure 8. (a) Climatology of TC genesis frequency (black contour, %) and (b) linear trends of TC genesis frequency (% decade^{-1}) during the period 1977–2010. Contour indicates the average of four best-track datasets, color indicates the number of best-track data for which changes are significant at the 90% confidence level, and dot indicates regions where all four TC data show the same sign.

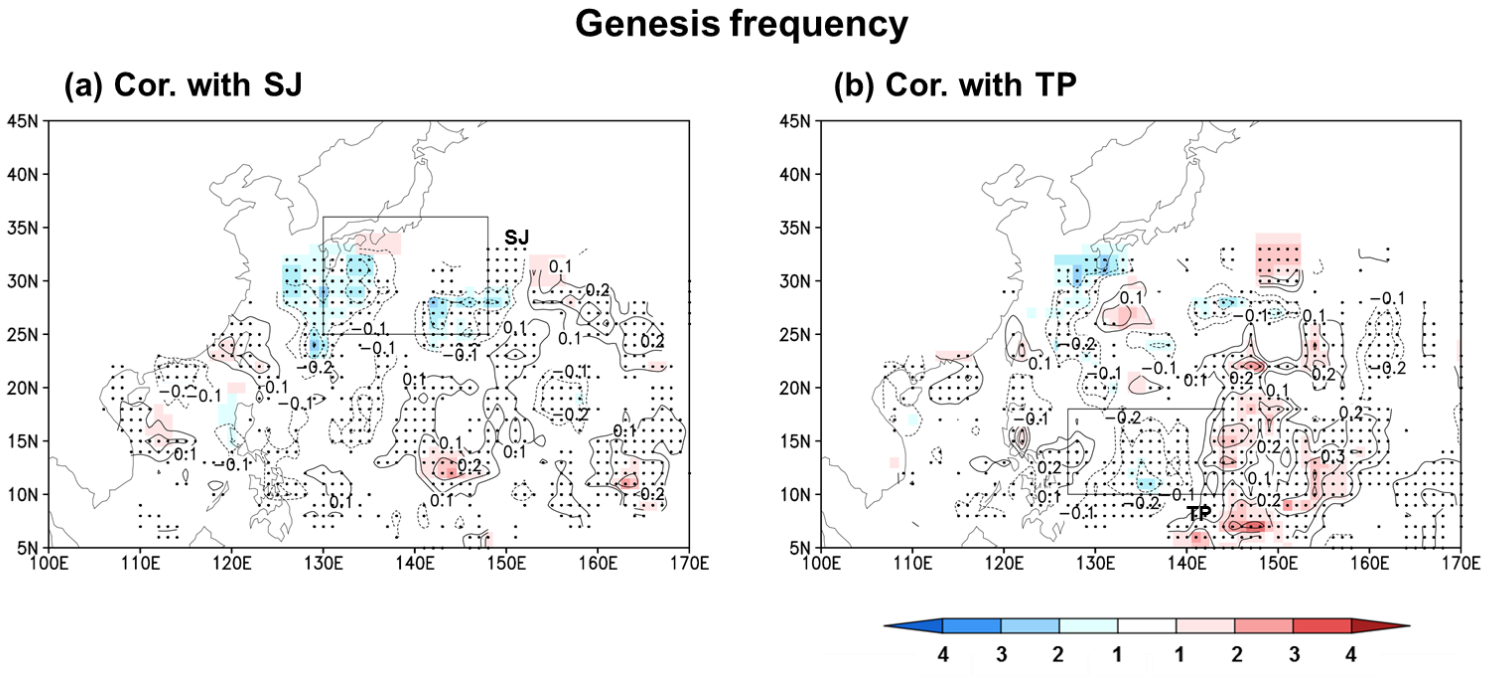

Figure 9. Correlation coefficients between genesis frequency and intensity time series of (a) SJ and (b) TP regions.

c. Track Density

The TC track density was defined as the ratio of seasonal number of TCs passing through each grid box to total number of seasonal TCs. Figure 10a and 10b display climatology and linear trends in track density, respectively. Climatological track density is classified to two branches: westward straight toward the South China Sea and northeastward recurved to Korea and Japan (Figure 10a) [*Ho et al*., 2004; *Wu et al*., 2005; *Tu et al*., 2009; *Kim et al*., 2011]. The peak value of track density is observed in east of Luzon strait (i.e., a narrow sea between Taiwan and Luzon island) that is located on climatological translational way from the highest core of the genesis frequency in the Philippine Sea (Figures 6a, 8a, and 10a). This implies that the TC track density is a function of TC genesis locations and movements [*Ho et al*., 2004]. The TC intensity in a certain grid also depends on the TC passage frequency of intense TCs [*Wu and Wang*, 2008].

Figure 10b presents that the TC track density has decreased significantly over the two large tropical areas, the East China Sea, and eastern subtropical area of the WNP, whereas it has increased significantly around Taiwan and marginally near the east coast of Japan. Considering the distribution of genesis frequency trends (Figure 8a) and climatological translation direction (Figure 6a), it is natural to expect large changes in TC track density to the west and north of the regions where large changes in TC genesis frequency were observed (Figures 8b and 10b). Previous studies already identified this pattern of change [*Wu et al*., 2005; *Tu et*

al., 2009]; More frequent TC movements to Taiwan and Japan were related with the enhanced monsoon trough and the northeastward shift of the WNP subtropical high.

Although both the spatial patterns of trends in TC passage frequency and intensity have similar signs in the tropics and midlatitudes (Figures 3b and 10b), the significant regions are not exactly coincident with each other. For example, the major decreasing region of TC intensity (i.e., the TP region) flanks on the two large regions with declining TC passage frequency. The significant increments of TC intensity appear in the SJ region, in which no considerable changes in TC passage frequency are detected. Taiwan and its vicinity do not show an appreciable intensity change in spite of the significant increase in TC passage frequency.

Especially, the area around Taiwan is interesting to discuss in more detail. As a majority of TCs affecting Taiwan comes from the southeast [*Chu et al*., 2010], it is natural to expect that a robust upward trend in TC track density (Figure 10b), together with the intensification rate (Figure 6b), would lead to an increase in TC intensity. However, the intensity trends are trivial or slightly negative in the vicinity of Taiwan (Figure 3b), which lead us to interpreting that the increasing genesis frequency between 120°–130°E along 20°N (Figure 5a) totally offsets the other two factors. To sum up, the changes in TC passage frequency have less to do with TC intensity, compared with the changes in TC intensification rate and genesis frequency.

Figure 11 shows correlation coefficients between track density and intensity in the SJ and TP. In the SJ, high correlations are spread along the lines where the significant increasing signal in track density appears. This implies that track density can be one of the reasons why intensity in the SJ has increased. However, it is hard to regard track density as a critical factor for intensity because the core of track density is westward shifted from that of intensity in the SJ. On the other hand, the correlation coefficients for the TP suggest that genesis frequency in the east of TP is the focal factor for intensity of the TP region; the highest values locate over the east of TP.

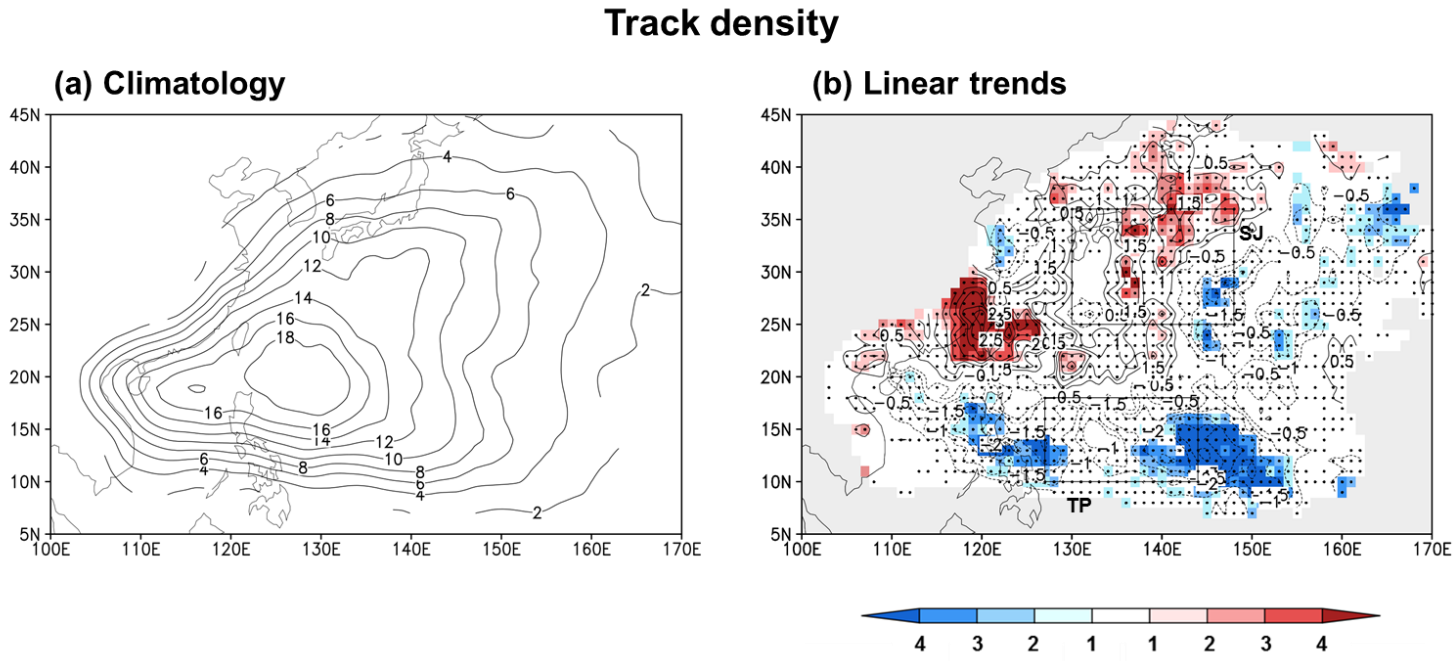

Figure 10. (a) Climatology of TC track density (black contour, %) and (b) linear trends of TC track density (% decade^{-1}) during the period 1977–2010. Contour indicates the average of four best-track datasets, color indicates the number of best-track data for which changes are significant at the 90% confidence level, and dot indicates regions where all four TC data show the same sign.

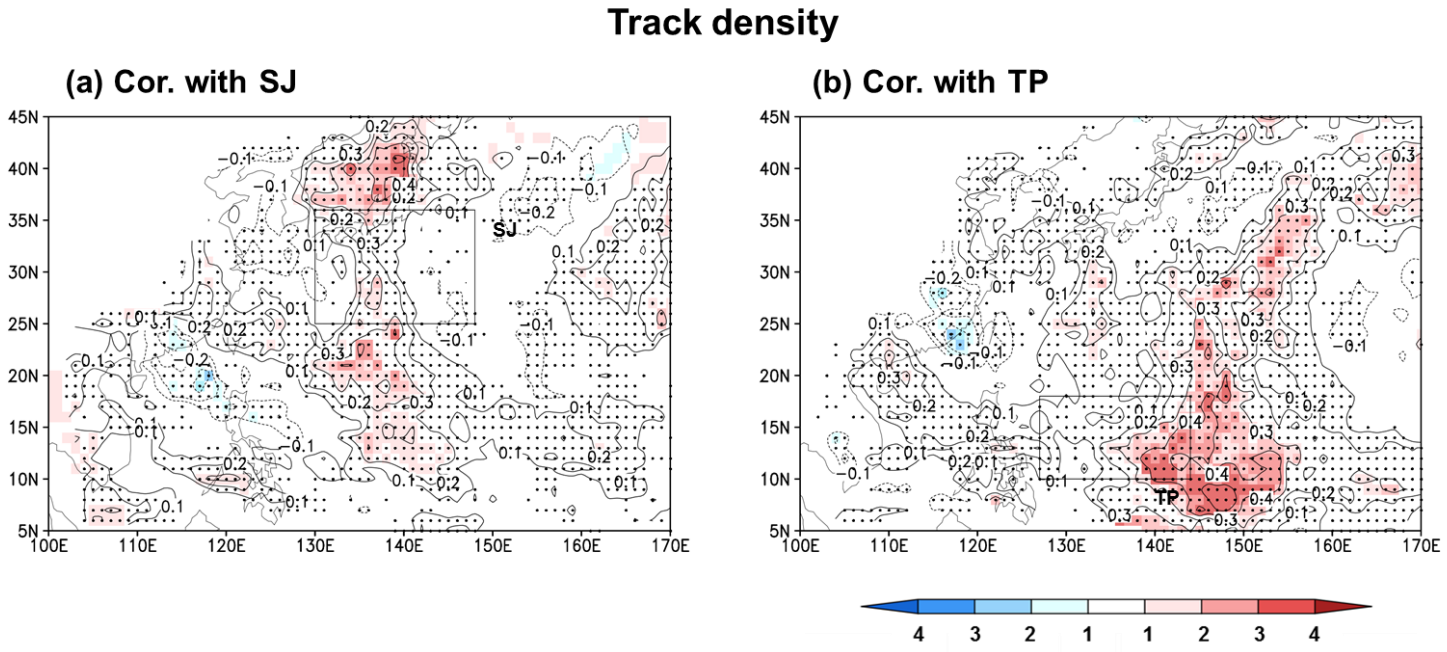

Figure 11. Correlation coefficients between track density and intensity time series of (a) SJ and (b) TP regions.

d. Translation speed

The combination of TC intensification rate and genesis frequency successfully explain the spatial distribution of trends in TC intensity over the WNP. In addition to them, the possible contribution of TC translation speed needs a validation because it has been known to affect TC intensity through modulation of the effect of TC-induced SST cooling on the intensification rate [*Bender and Ginis*, 2000]. Its effect on the intensification rate can vary depending on various factors, such as the residence time, depth of the mixed layer, and TC-induced wind speed [*Wada and Usui*, 2007; *Lin et al*., 2009].

To examine the effect of TC translation speed on the intensification rate, the spatial distribution of climatology and trends in the TC translation speed was examined (Figures 12a and 12b). According to Figure 12a, TCs generally travel at the highest speed over Korea and Japan and at the lowest speed in the Philippine Sea; existence of upper tropospheric jet in the midlatitudes could accelerate TC movements therein while TCs usually move slowly in their early stages in the low latitudes [*Zeng et al*., 2007]. As seen in Figure 12b, in contrast with the aforementioned studies, the translation speed seems not to be an effective factor on the intensification rate in climatological sense since it has not been considerably changed over the regions where the intensification rate has changed significantly during the analysis period. The unchanged translation speed is inconsistent with *Chu et al*. [2012], who found a significant decrease in TC translation speed in the subtropics during the period of 1958-2010, which is

attributed to the shorter analysis period in this study (i.e., 1977–2010) than that of *Chu et al*. [2012]. Thus, not all changes in the intensification rate were influenced by the changes in the translation speed during the analysis period of this study.

To clarify this point, changes in TC intensification with consideration of the residence time of TCs in a grid box (i.e., intensification rate × residence time) were calculated. This modified intensification rate is more physically linked with the translation speed, as the residence time in a grid box itself implies the translation speed. Figure 13 shows the spatial pattern of trends in the modified intensification rate, which is almost similar to that of the original intensification rate. This indicates that the intensification rate is a major factor to explain the spatial distribution of the trends in TC intensity, rather than the translation speed. In the following sub-section, the intensification rate and genesis frequency will be mainly discussed with large-scale tropospheric and oceanic environmental changes.

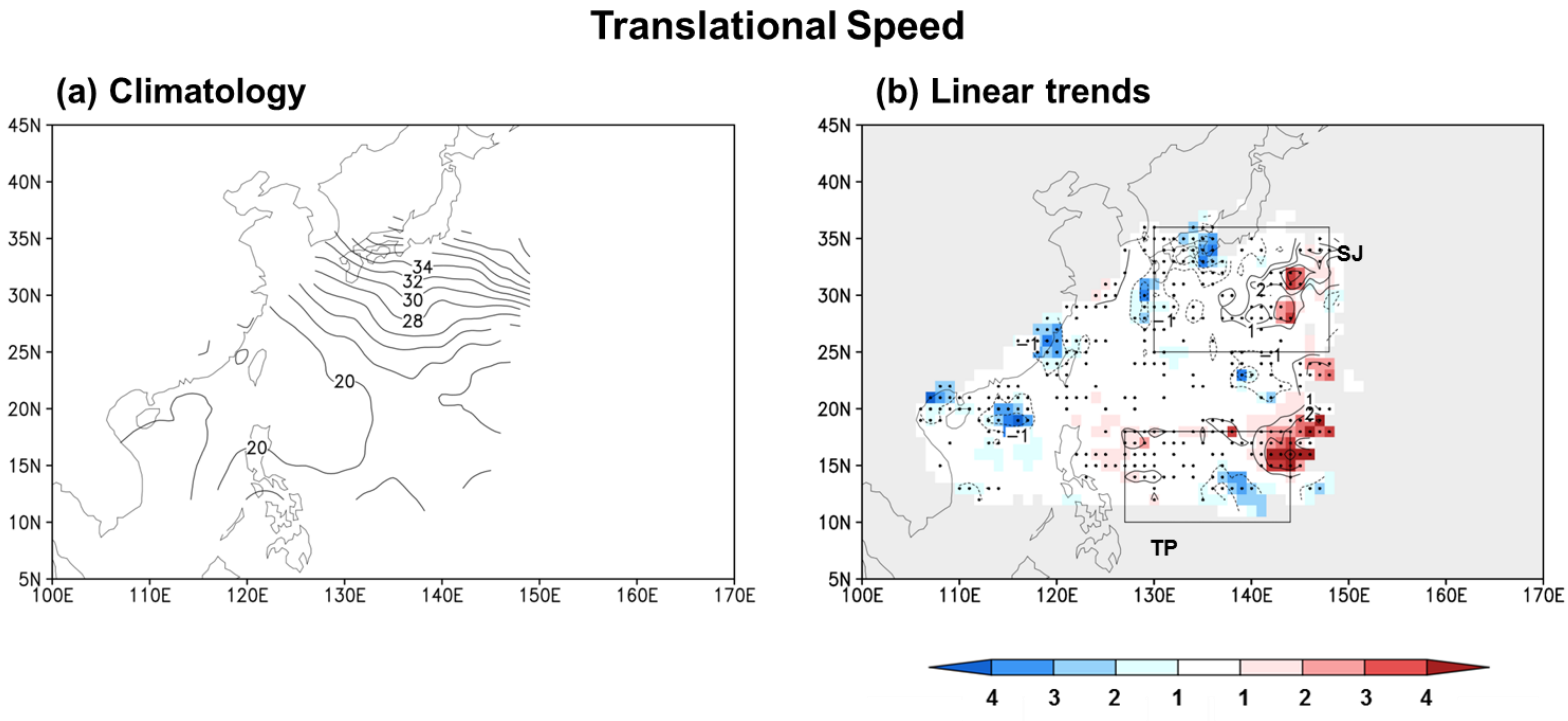

Figure 12. (a) Climatology of TC translational speed (black contour, km hr^{-1}) and (b) linear trends of TC translational speed (km hr^{-1} $decade^{-1}$) during the period 1977–2010. Contour indicates the average of four best-track datasets, color indicates the number of best-track data for which changes are significant at the 90% confidence level, and dot indicates regions where all four TC data show the same sign.

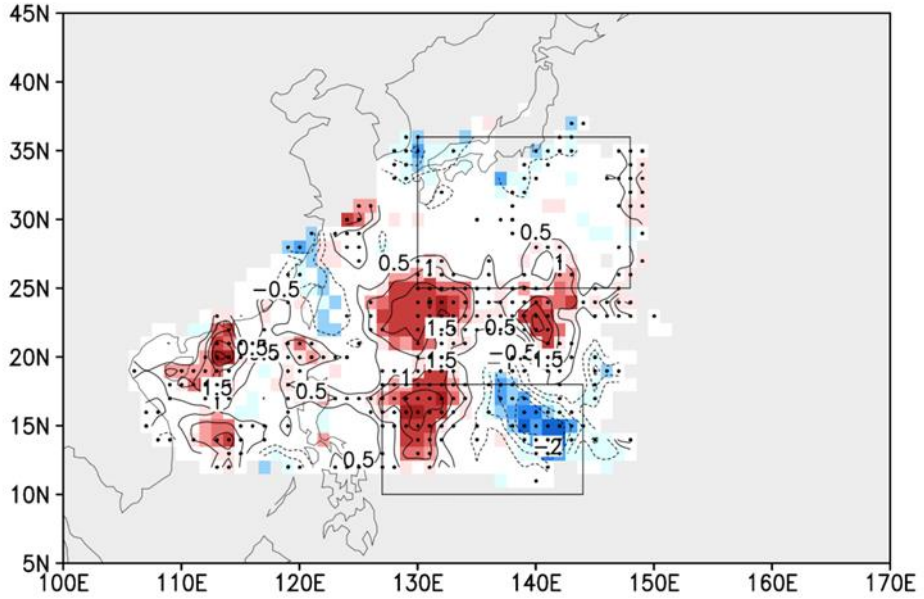

Figure 13. Linear trends of modified intensification rate (m s^{-1} $decade^{-1}$) during the period 1977–2010. Contour indicates the average of five TC datasets, color indicates the number of TC data for which changes are significant at the 90% confidence level, and dot indicates regions where all five TC data show the same sign.

3.3Relevant Thermodynamic and Dynamic Environmental Changes

To reveal possible mechanisms for the regionally varying trends in TC intensity via the combination of the trends in TC intensification rate and genesis frequency, both thermodynamic- and dynamic-related variables for the TC development were examined. The thermodynamic variables were represented by three factors: maximum potential intensity (MPI), SST, and 26℃ isothermal ocean depth [*Gray*, 1968; *Emanuel*, 1987; *Bister and Emanuel*, 1998; *Wada and Usui*, 2007; *Wada and Chan*, 2008]. The MPI is generally referred to as the theoretical maximum intensity of a TC. The basic concept of the MPI came from the Carnot cycle, which was regarded as the energy cycle of a TC. The MPI was computed by

$$MPI = \mu \times \sqrt{\frac{T_s}{T_0} \times CKCD \times (CAPE_s - CAPE)},$$

where μ is the factor to reduce gradient wind to 10-m wind; T_s is the SST; T_0 is the outflow layer temperature; $CKCD$ is the ratio of the exchange coefficient for enthalpy to the drag coefficient; $CAPE_s$ is the saturation convective available potential energy (CAPE) at radius of maximum winds; $CAPE$ is the CAPE at radius of maximum winds. The μ and $CKCD$ was taken by 0.8 and 0.9, respectively. The MPI comprises two independent variables, which are CAPE and thermal efficiency. The CAPE denotes the limit of potential TC energy under the given status of variables in the troposphere and surface, such as moisture, temperature, and pressure. If the troposphere is unstable, high CAPE can be achieved. The thermal efficiency can be thought of as how many rates of

the potential TC energy are released into the troposphere to generate the TC wind. Thus, high MPI can be regarded as a favorable thermodynamic condition for the TC development. Figure 14a and 14b shows climatology and linear trends in the MPI, respectively. As shown in Figure 14a, the highest MPI is observed in the western tropics and the MPI gradually drops as latitude increases. Meanwhile, the MPI has significantly increased over most areas of the WNP since 1977, which means that the thermodynamic condition over the WNP basin has become more favorable for the TC development (Figure 14b).

In addition to the MPI, oceanic conditions such as the depth of the 26℃ isotherm and SST were also investigated. The depth of the 26℃ isotherm can determine how deep the warm mixed-layer of the ocean extends below the ocean surface, which is an essential factor to calculate the ocean thermal energy (i.e., TC heat potential). This parameter provides important oceanic information for the TC intensity and its intensification rate [*Wada and Usui*, 2007] because the warm SST of more than 26.5℃ is a necessary condition for the TC development [*Gray*, 1968]. It is noted that the SST can easily drop below 26.5℃ over those regions where the depth of the thermocline is shallow, since TC-induced strong winds can cause mixing of upper and lower seawater, thereby effectively cooling the oceanic mixed-layer by the upwelling process [e.g., *Lin et al*., 2005; *Lin et al*., 2008; *Wu et al*., 2008]. Figure 15 displays climatology and linear trends in isotherm depth. The climatological 26℃ isotherm is the deepest (i.e., about 120 meters depth) over east part of the Philippine Sea and it continually decrease until zero lines in the

midlatitudes (Figure 15a). As shown in Figure 15b, the 26℃ isotherm has deepened across the WNP basin, though the deepening trend is relatively weaker along the subtropical belt of the Philippine Sea, of which reason is unclear and needs a further investigation. The deepening of 26℃ isothermal depth would provide oceanic conditions favoring the TC development in the WNP.

Figure 16 exhibits climatology and linear trends in SST. The climatology of SST shows very similar pattern with that of MPI (Figure 16a), which means that MPI is highly dependent on SST in the WNP. Moreover, the zero lines of 26℃ isotherm depth nearly correspond with 26℃ lines of SST whereas, interestingly, the cores of isotherm depth and SST are not coincident each other. As shown in Figure 16b, the SST has also increased considerably over the entire WNP as is well known [*Emanuel*, 2005; *Webster et al*., 2005]. Thus, it is represented that the atmospheric and oceanic thermodynamic fields have been more favorable for the TC development over almost the entire WNP, but these results cannot fully explain the spatially inhomogeneous distribution of the TC intensity trends that results from the combined changes in TC intensification rate and genesis frequency. For instance, the TC intensification rate and genesis frequency have decreased around the Philippines and the tropical eastern WNP. This may imply the thermodynamically favorable conditions over these regions have been masked by unfavorable dynamic conditions.

The anomalous SST distribution is informative to understand the large-scale atmospheric circulations. As shown in Figure 16b, the SST trends vary signs from

the west to the east over the tropical Pacific Ocean. This reflects the steeper zonal SST gradient (i.e., La Niña-like SST pattern) [*Trenberth*, 1997], owing to stronger warming in the western Pacific warm pool region. This increasing SST gradient during last three decades can be dynamically linked with the enhancement of the Walker circulation through the Bjerknes feedback in the near-equatorial ocean-atmosphere coupled process [*Sohn and Park*, 2010; *An et al*., 2011]. Figure 17 shows in the cross section of the climatology and trends in the zonal and vertical winds averaged between the latitudes of 5°S−10°N. The climatological pattern clearly presents the Walker circulation; there are upward motions in the warm pool of the western Pacific and downward motions in the cold tongue of the eastern Pacific (Figure 17a). On the other hand, the trend represents an increasing clockwise overturning over the equatorial western-to-central Pacific sector (Figure 17b).

Associated with this enhanced Walker circulation, dynamic environments relevant to the TC activity were also examined, such as the horizontal winds and relative vorticity at 850 hPa, and the magnitude of the vertical wind shear between 200 hPa and 850 hPa (Figures. 18 and 19). Figure 18 shows climatology and linear trends in 850-hPa horizontal winds and relative vorticity. Climatologically, in the low latitudes of the WNP, cyclonic flows are dominantly distributed possibly due to the monsoon trough, otherwise, large anticyclonic circulations locate over the subtropics (Figure 18a). Meanwhile, the recently increasing low-level easterlies near the equator have formed the meridional wind shear, inducing

the low-level flows more anticyclonic along the tropics including the eastern TP region (Figure 18b). Figure 19 displays climatological vertical wind shear and its linear trend. Strong vertical wind shear is observed in the midlatitudes and the easternmost of the Philippine Sea (Figure 19a); in the midlatitudes, upper tropospheric jet strengthens vertical wind shear while the Walker circulation causes high values of the vertical wind shear in the eastern Philippine Sea. Thus, the recently strengthening of the Walker circulation also has increased the magnitude of the vertical wind shear in the tropical North Pacific, with the maximum increments near the dateline (Figure 19b). The eastern part of TP region is also the part of a region of increased vertical wind shear, though it is not significant. In the eastern part of TP area, both the low-level flows and vertical wind shear have been more unfavorable, so that it would be reasonable to regard them as main reasons for the decrease in TC intensification rate and genesis frequency, thereby reducing TC intensity in the TP region. The similar interpretation can be made to explain the decreasing TC intensity around the Philippines (i.e., the western TP region). The anomalous anticyclonic flow over the Philippines may be a factor to suppress TC intensification rate and genesis frequency therein, resulting in the weaker TCs in the Philippines and the southern coast of China.

In contrast, there are an anomalous large-scale cyclonic flow and weak vertical wind shear in the western part of TP and almost parts of the subtropics including the northern part of the South China Sea, the south of Taiwan and Japan

(Figures 18b and 19b). The anomalous cyclonic flow is thought to be the result of anomalous anticyclonic flows in the tropics, and the weak vertical wind shear is closely related to the recently weakened- and northward-shifted jet stream [e.g., *Kwon et al*., 2007; *Archer and Caldeira*, 2008]. Both of these changes could increase TC intensification rate and genesis frequency with the thermodynamic conditions over the same regions, thereby accounting for the significantly stronger TCs in the SJ region and also weaker TCs in the southern coast of China related with increasing TC genesis frequency over the northern South China Sea.

To clarify this interpretation, correlation coefficients of SST, 850-hPa vorticity and wind, and vertical wind shear with intensity time series in SJ and TP were investigated, respectively (Figures 20, 21, and 22). Figures 20a and 20b indicate that spatial patterns of correlations for SJ and TP are consistently El Niño-like SST warming patterns. In case of TP, the spatial distribution of correlations of SST is very similar with that of linear trend of SST; they are negatively coincident. This means that recent La Niña-like SST warming pattern probably reduces the intensity of TCs in the TP region. Correlation coefficients of vertical wind shear for SJ and TP also display similar spatial patterns of their linear trends (Figure 21). It is noted that positive correlations appear in the SJ and TP regions, respectively. This implies that vertical wind shear may not influence TC intensity, directly. In addition, correlations of 850-hPa vorticity and wind also exhibit similar shapes of their linear trends (Figure 22).

Consequently, it is essential to consider both thermodynamic and dynamic conditions when investigating spatial distribution of linear trends in TC intensity through the intensification rate and genesis frequency. In addition, in the TP regions, dynamic variables seem to act as a more decisive role for TC intensification rate and genesis frequency than thermodynamic variables.

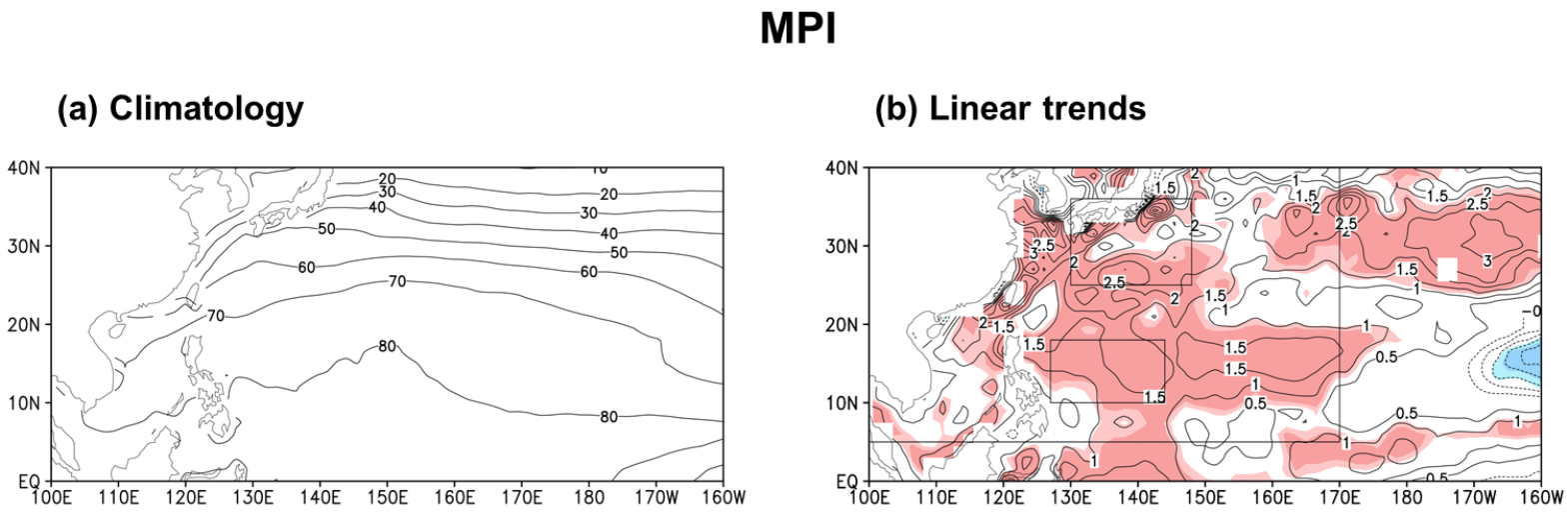

Figure 14. (a) Climatology of maximum potential intensity (m s^{-1}) and (b) linear trends of maximum potential intensity (m s^{-1} $decade^{-1}$), during the period 1979–2010. Light and dark shaded red and blue indicate that the changes are significant at the 90% and 95% confidence levels, respectively. The largest rectangle (5°−45°N, 100°−170°E) indicates the WNP basin.

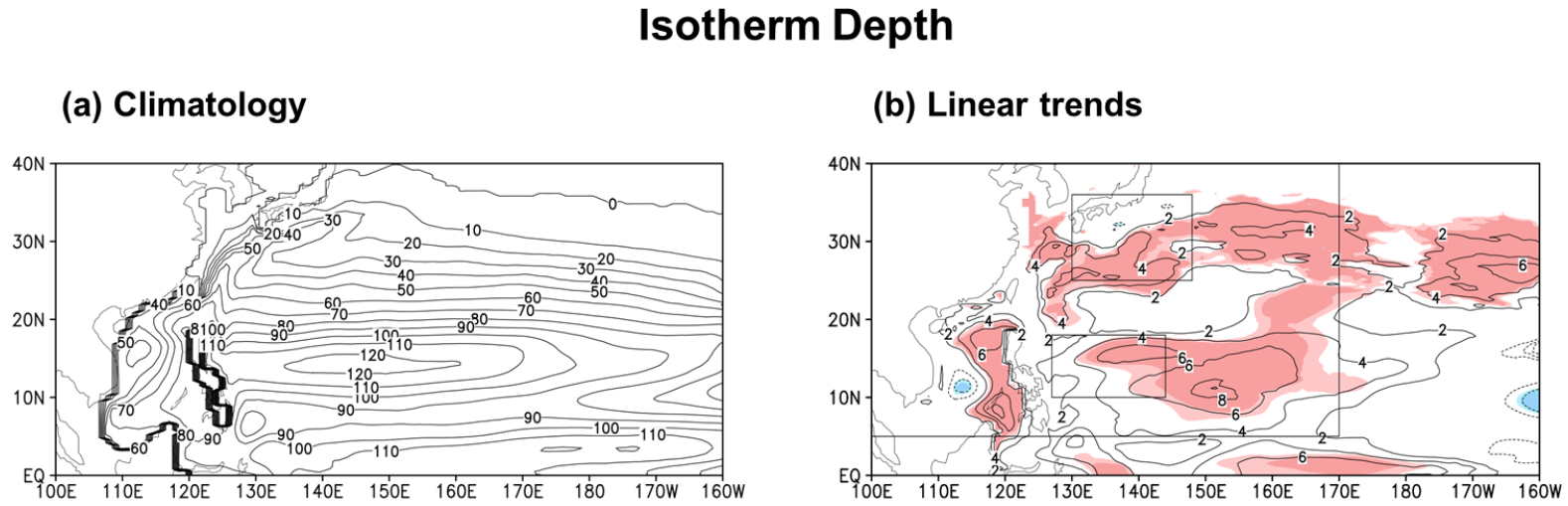

Figure 15. (a) Climatology of 26℃ isotherm geometric depth below sea surface (m) and (b) linear trends of 26℃ isotherm geometric depth below sea surface (m decade^{-1}), during the period 1979–2010. Light and dark shaded red and blue indicate that the changes are significant at the 90% and 95% confidence levels, respectively. The largest rectangle (5°−45°N, 100°−170°E) indicates the WNP basin.

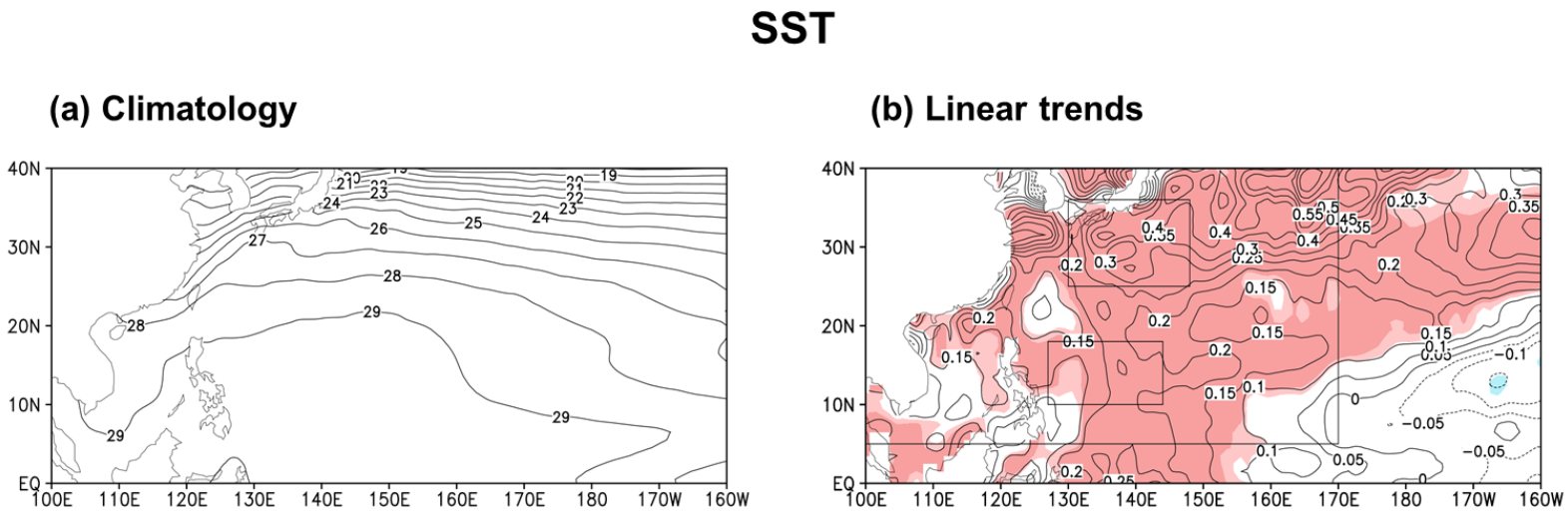

Figure 16. (a) Climatology of SST (℃) and (b) linear trends of SST (℃ decade^{-1}), during the period 1979–2010. Light and dark shaded red and blue indicate that the changes are significant at the 90% and 95% confidence levels, respectively. The largest rectangle (5°−45°N, 100°−170°E) indicates the WNP basin.

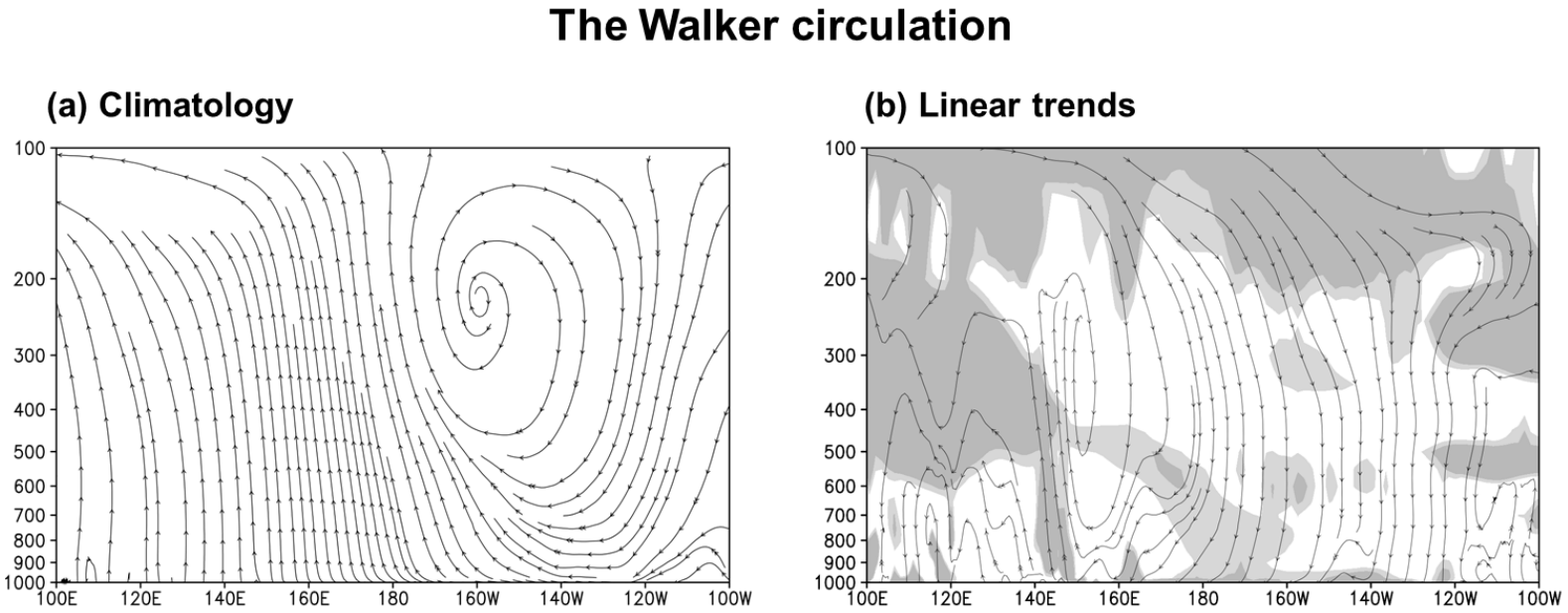

Figure 17. (a) Climatology of meridional-mean circulation along the region 5°S−10°N and (b) linear trends of meridional-mean circulation along the region 5°S−10°N, during the period 1979–2010. Light and dark shaded gray indicate that the changes are significant at the 90% and 95% confidence levels, respectively.

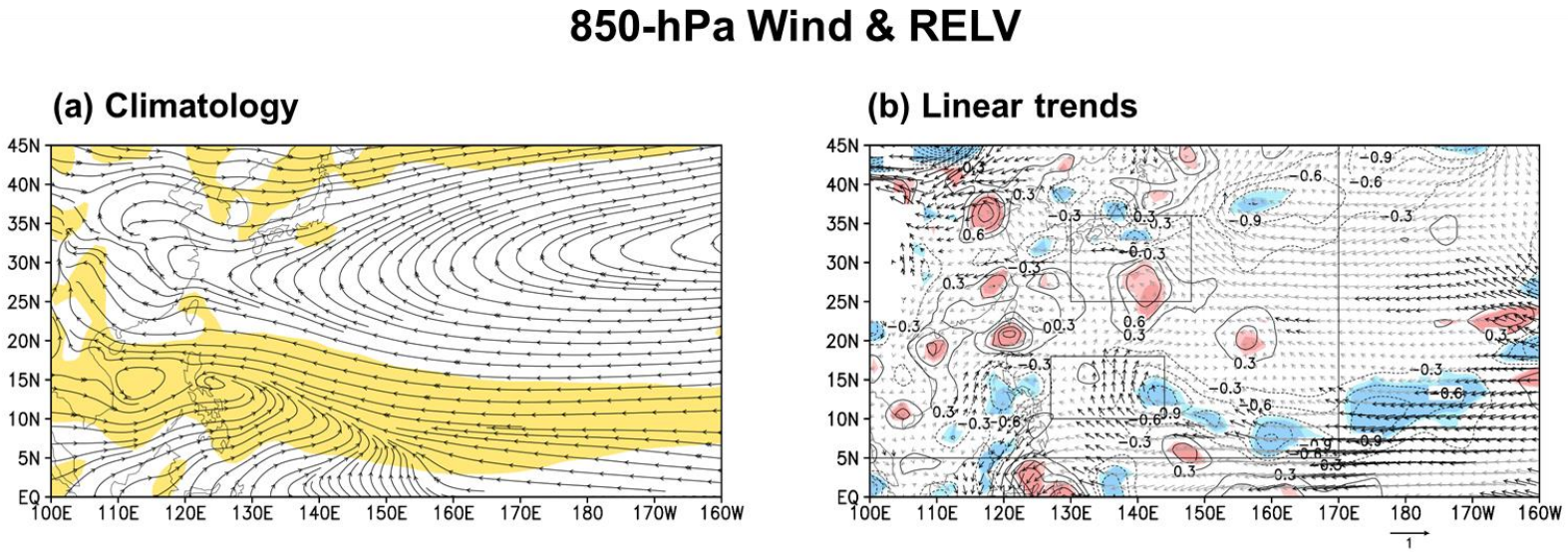

Figure 18. (a) Climatology of 850-hPa wind and relative vorticity; yellow shades indicate that there is positive vorticity, and (b) linear trends of 850-hPa wind (m s^{-1} $decade^{-1}$) and relative vorticity (10^{-6} s^{-1} $decade^{-1}$) during the period 1979–2010. Light and dark shaded red and blue indicate that the changes are significant at the 90% and 95% confidence levels, respectively. The largest rectangle (5°−45°N, 100°−170°E) indicates the WNP basin.

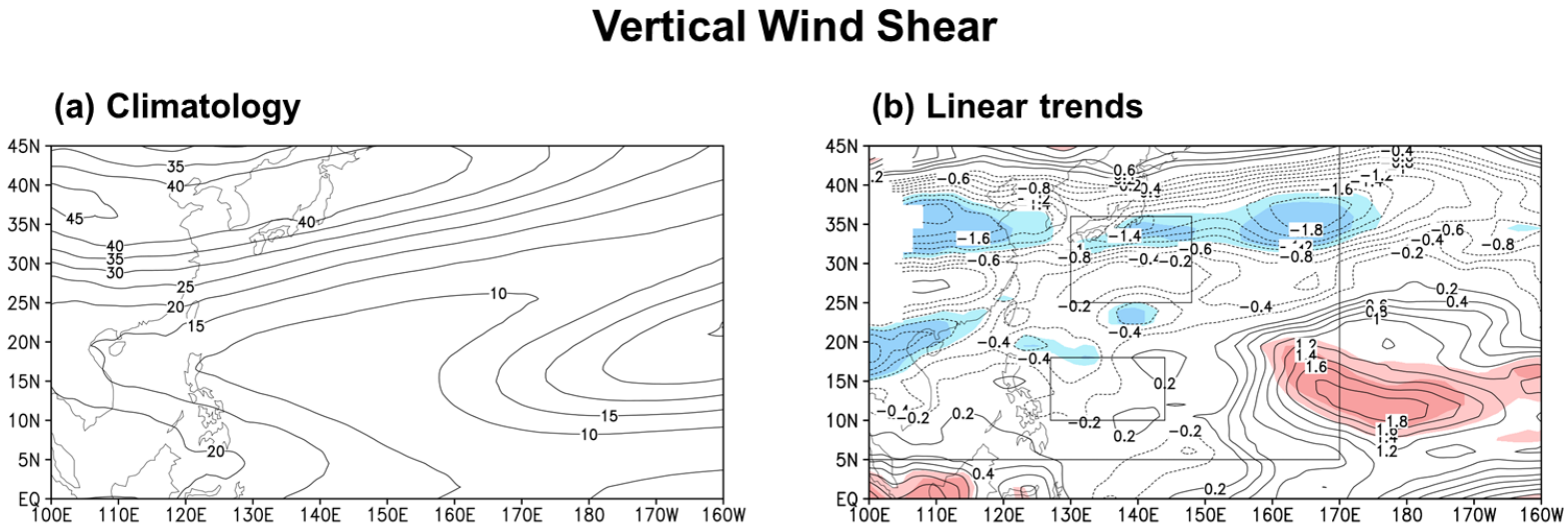

Figure 19. (a) Climatology of vertical wind shear (m s^{-1}) and (b) linear trends of vertical wind shear (m s^{-1} $decade^{-1}$), during the period 1979–2010. Light and dark shaded red and blue indicate that the changes are significant at the 90% and 95% confidence levels, respectively. The largest rectangle (5°−45°N, 100°−170°E) indicates the WNP basin.

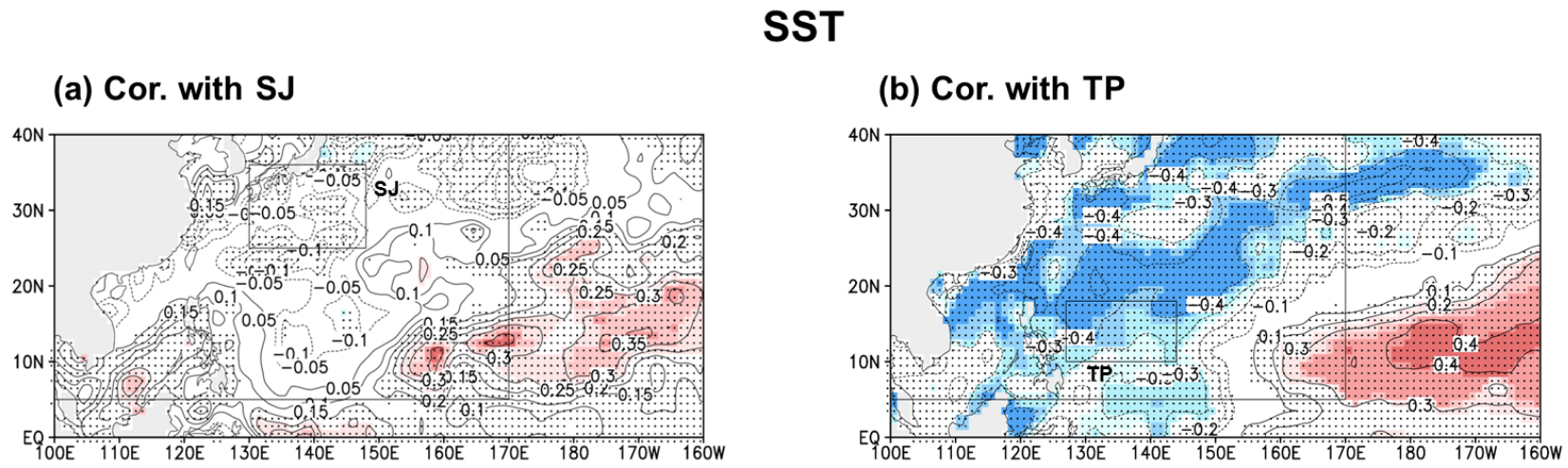

Figure 20. Correlation coefficients between SST and intensity time series of (a) SJ and (b) TP regions.

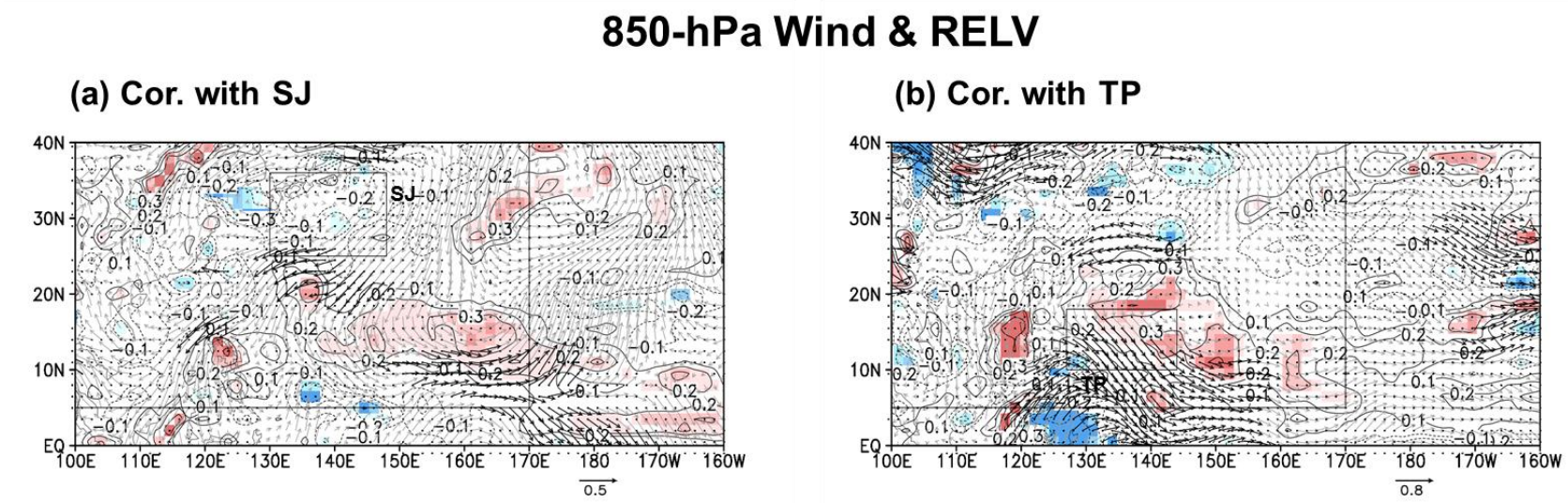

Figure 21. Correlation coefficients of 850-hPa wind and relative vorticity with intensity time series of (a) SJ and (b) TP regions.

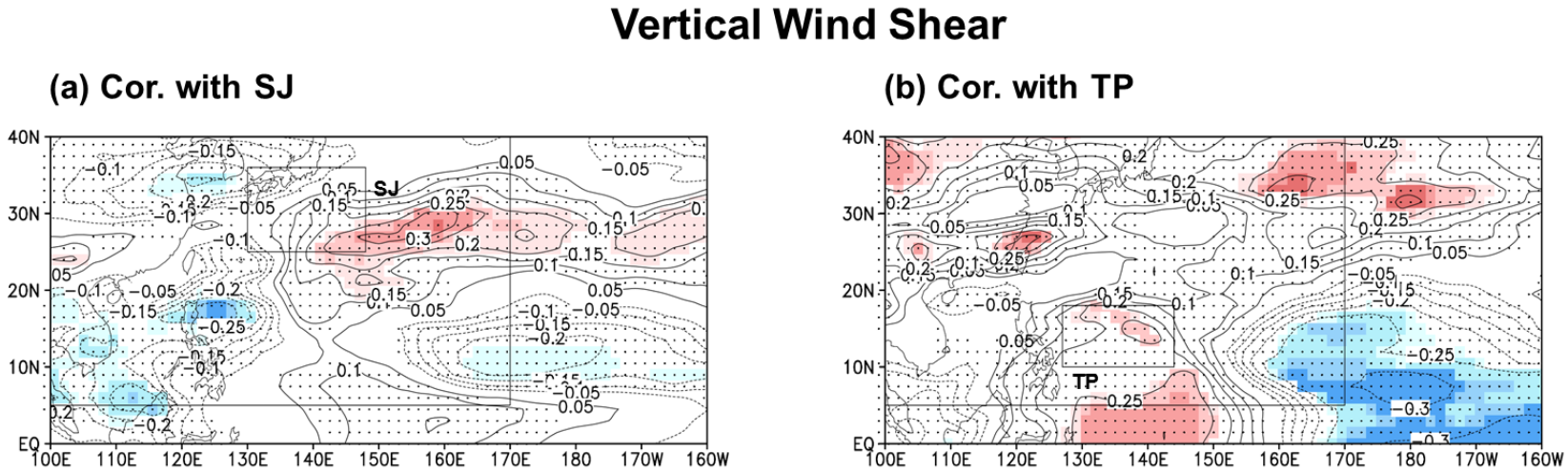

Figure 22. Correlation coefficients between vertical wind shear and intensity time series of (a) SJ and (b) TP regions.

4. Tropical Cyclone Intensity at Landfall on East Asia

4.1 Shifts in Spatial Position of Maximum Intensity of Tropical Cyclones

Recent changes in oceanic and atmospheric environments over the western North Pacific (WNP) seem to imperil coastal countries in East Asia with TCs, as shown in the previous section. The section 3 demonstrated that spatially distinct changes in dynamic environments have affected the corresponding pattern of changes in TC intensity in recent decades. As shown in Figure 23, the notable warming in sea surface temperature (SST) in the western Pacific accompanied by cooling in the tropical central and eastern Pacific, referred to as a La-Niña-like warming pattern [*An et al*., 2011; *Zhang et al*., 2011], has driven a strengthening of the Pacific Walker circulation. This enhanced circulation subsequently resulted in an anticyclonic anomaly and strengthened vertical wind shear over the eastern Philippine Sea. These anomalous fields have suppressed TC development, despite the general SST warming. Along the coastal sea of East Asia, however, anomalous cyclones and weakened vertical wind shear, in combination with the warmer SST have encouraged TCs to increase in strength. In other words, TCs may reach their maximum state more frequently closer to the East Asian continent; TCs could intensify or sustain their strength up to the brink of landfall. Accordingly, a trend of increasing intensity of landfalling TCs would be expected along the East Asian coastlines.

As mentioned above, it is expected that the principal region in which many TCs attain peak intensity during their lifetime would be translocated. Figure 24a illustrates the climatology of the location of maximum intensity (contour) and its linear trend (shading), averaged for all best-track data, during the analysis period. Here, the location of maximum intensity represents the ratio of the number of TCs showing lifetime maximum intensity at a grid point to the total genesis count. According to the climatology, the majority of TCs reached their strongest state within their lifetime at the western boundary of the Philippine Sea and the southern shore of China. The linear trend shows a notable increase in the location of maximum intensity in a belt along the continental shoreline south of 30°N, while the corresponding decrement is predominant to the south and southeast of this increasing belt. These features demonstrate that the expected changes based on the large-scale environmental changes (Figure 23) have indeed been occurring over the WNP basin.

The TC intensification rate and track density are helpful in interpreting the recent change in the location of maximum intensity. Figure 24b shows the climatology of the TC intensification rate (contour) and its linear trend (shading), averaged for all best-track data. Climatology of the intensification rate is negative along the coastal seas of East Asia and over the Philippines (contour), meaning that TCs begin to decay after entering these regions. Thus, it is natural that the climatological ridges showing the location of maximum intensity (asterisks in Figure 24a) almost correspond to the zero lines of the intensification rate (Figure

24b). The linear trend in the location of maximum intensity is also explained by the linear trend in the intensification rate. Except for in East Asia, a negative trend in the intensification rate is seen over the limited area of the southeastern Philippine Sea (around 140°E and 15°N), whereas a positive trend is broadly distributed south of 30°N (shading). In the midlatitudes, no apparent trend of the intensification rate is detected, despite the increase in SST and the weakening of vertical wind shear (shading). This may be due to a weak anomalous anticyclonic flow that counteracts the positive effects of the SST and vertical wind shear on the intensification rate over Korea and Japan (Figure 23). However, confirmation of this is beyond the scope of this study.

Figure 24c represents the climatology (contour) and linear trend (shading) for averages of the TC track density from all the best-track data. Climatology of the track density can explain two high cores in climatology of the location of maximum intensity near the Hainan Island and Taiwan (contour of Figures 24a vs. 24c); this could be supported by the fact that most TCs pass by these two high cores. It can be easily supposed that TCs have more chance to attain their maximum intensity in a grid if a greater number of TCs pass through that grid. The two cores also lie on two main passing routes of the TCs, which are characterized by westward straight and northward curvy tracks from the eastern tropics of the WNP (black arrows in Figure 24c) [*Ho et al*., 2004; *Wu et al*., 2005; *Tu et al*., 2009; *Kim et al*., 2011]. Similar to this relationship, the linear trend in the track density could also account for the shifting of the location of maximum

intensity toward the East Asian continent (shading). Comparable spatial patterns are observed between the track density and the location of maximum intensity; there are positive signs along the East Asian coasts and negative signs in the tropical WNP. However, the track density cannot fully explain the location of maximum intensity, since the changes are not exactly coincident with each other (shading of Figures 24a vs. 24c). For instance: (1) the largest increment in the track density is located over Taiwan, while the location of maximum intensity has noticeably increased over the east and southwest sides of Taiwan; and (2) there is the minor trend in the track density along the eastern shoreline of Vietnam, but a significant positive sign in the location of maximum intensity exists there. Thus, climatology and the linear trend in the location of maximum intensity can be successfully understood when both the intensification rate and the track density are considered.

Given that TC intensity is highly affected by genesis frequency in the main genesis region, spatial changes in the main genesis locations should be examined. Figure 24d depicts climatology (contour) and linear trend (shading) in the genesis frequency for the averages of all best-track datasets. Usually newly generated TCs have the weakest intensity, 17 m s^{-1}, and increasing genesis frequency in a certain region can reduce the average TC intensity over the local and surrounding regions. Notice that most TCs form over the South China Sea and the Philippine Sea (contour), which are located near the southern coast of East Asia. Furthermore, as shown by the shadings in Figure 24d, there is a notable increase in TC genesis

over the northern South China Sea. This may decrease landfall intensity over the southern part of East Asia, including Vietnam, south China, and Taiwan. To verify this genesis effect on landfall intensity, the East Asian coastlines were divided into two subareas, Northeast and Southeast Asia, to the north and south of 25°N, respectively (thick black line in Figure 24d). Hereafter, landfall TCs over Northeast and Southeast Asia will be analyzed in addition to the entire East Asia.

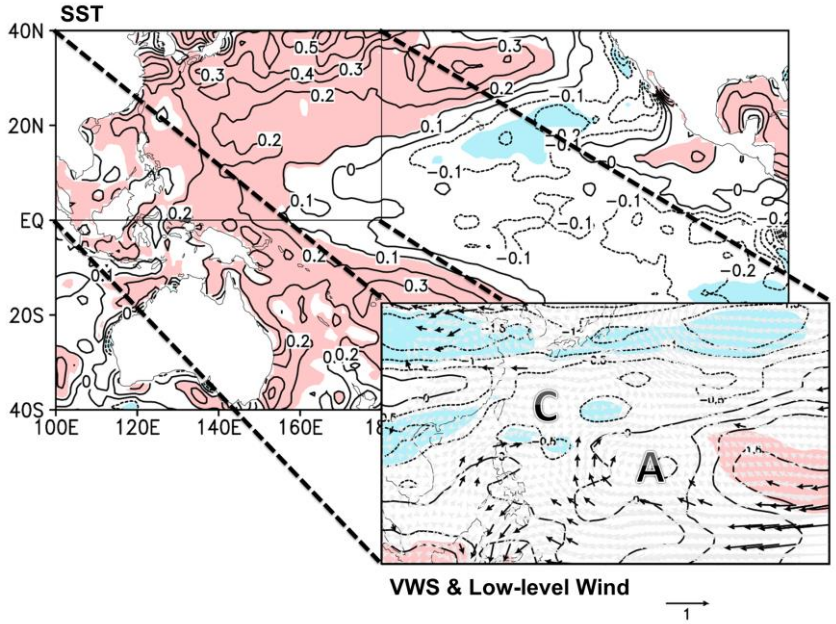

Figure 23. Linear trends in the SST (℃ decade^{-1}) over the Pacific, the 850-hPa horizontal winds (vectors, m s^{-1} decade^{-1}), and the vertical wind shear between 850 and 200 hPa (contours, m s^{-1} decade^{-1}) over the WNP during the period 1979–2010. Gray shading indicates that the trend is statistically significant at the 90% confidence levels there. Gray and black vectors denote statistically insignificant and significant trends in horizontal winds at the 90% confidence levels, respectively.

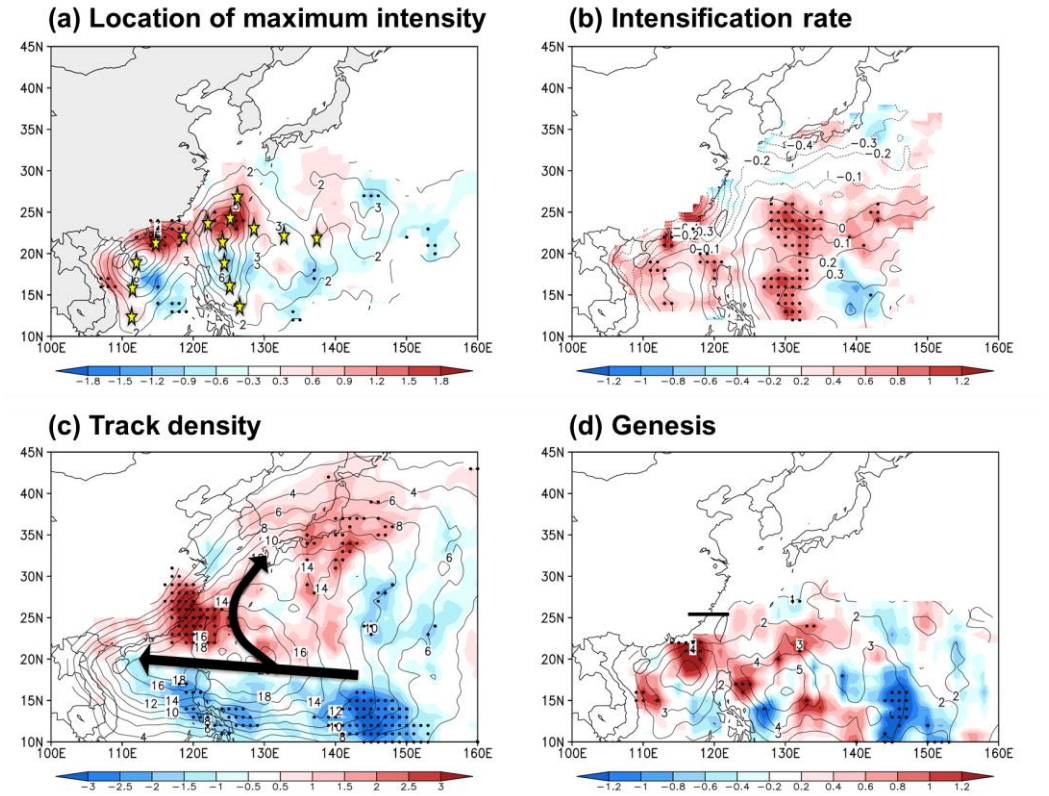

Figure 24. Climatology (contours) and linear trends (red and blue shading) in (a) the location of maximum intensity (% decade^{-1}), (b) intensification rate (m s^{-1} hr^{-1} decade^{-1}), (c) track density (% decade^{-1}), and (d) genesis locations (% decade^{-1}) during the period 1977–2010. All values are averaged for the four best-track data. Dots are marked for grid points where the linear trends are statistically significant at the 90% confidence level for three or more best-track data. Yellow asterisks denote the ridges of the location of maximum intensity. Black arrows represent the main tracks of TCs.

4.2 Growing Threat of Intense Tropical Cyclones to East Asia

Figure 25 displays the time series of maximum intensity, landfall intensity, and landfall frequency for the analysis domains: East, Northeast, and Southeast Asia. Notice that only landfall TCs are considered when calculating the maximum intensity, which gives the peak intensity prior to landfall. Accordingly, landfall TCs may become stronger even if the maximum intensity does not change during the analysis period, because the maximum states of TCs more frequently occur nearer to East Asia (Figure 24a). Figure 25a describes the case where the entire East Asia region is defined as a landfall domain. There are neither clear upward nor downward tendencies in the maximum intensity (blue lines), and there is a negligible trend (+0.01 m s^{-1} $decade^{-1}$) for the UW/NCDC dataset as well. As expected, however, the time series of landfall intensity show clear increasing trends (red lines). All of the best-track datasets display positive trends with magnitudes from 0.58 to 1.81 m s^{-1} $decade^{-1}$, although the positive trend (+0.56 m s^{-1} $decade^{-1}$) for UW/NCDC is not statistically significant at the 90% confidence level (Table 3). The insignificance of this trend seems to be attributed to the genesis effects that may reduce landfall intensity in Southeast Asia.

Since the number of landfall TCs may affect the landfall intensity, the landfall frequency is also examined in Figure 25a. There is little connection between frequency and intensity of landfall TCs. The landfall frequency has hardly increased, in contrast to the rising landfall intensity (black lines), and correlation coefficients between the frequency and the intensity are negligible for

all datasets. Here, the weak tendencies in the landfall frequency over East Asia may be considered somewhat abnormal, because it has been shown that significantly more TCs have headed toward Taiwan and Japan [*Wu et al*., 2005; *Tu et al*., 2009]. The cause of this weak trend in landfall frequency may be that the total TC genesis frequency has significantly decreased since the 1990s [*Matsuura et al*., 2003; *Fengjin and Ziniu*, 2010; *Liu and Chan*, 2012].

Figure 25b illustrates the time series for the case of TCs striking Northeast Asia. Mixed tendencies in the maximum intensity are still seen among the best-track datasets (blue lines); yet the trend for UW/NCDC is not meaningful (+0.52 m s^{-1} $decade^{-1}$). In contrast, the landfall intensity has notably increased for all best-track datasets (red lines); all of their linear trends including UW/NCDC dataset are statistically significant at the 90% confidence level, ranging from 1.01 to 2.35 m s^{-1} $decade^{-1}$ (Table 3). This is because the landfall intensity would be scarcely affected by the genesis effect over Northeast Asia, as it is separated from the main TC genesis regions (i.e., the South China Sea and the Philippine Sea). The landfall frequency still shows weak relationship with the landfall intensity; the trends are insubstantial (black lines) and the correlation coefficients between them are not significant.

The time series for TCs landfalling on Southeast Asia are illustrated in Figure 25c, which shows that the maximum intensity has consistently decreased for all of the best-track datasets (blue lines); a slight negative trend (–0.99 m s^{-1} $decade^{-1}$) is also observed for the UW/NCDC, although it is not statistically significant at the

90% confidence level. This can be due to the genesis effect; a greater number of TCs have formed near the south coast of China since 1977, but fewer over the southern part of the South China Sea (Figure 24d). Hence, the shortened lifetimes of TCs over the ocean may have reduced the maximum intensity. TCs could sustain their peak intensity nearer to land in the recent few decades (Figure 24a), while the landfall strength of TCs was not decreasing but instead remained unchanged (red lines); thus their tendencies among the best-track datasets are mixed (Table 3). For UW/NCDC datasets, the trend (–0.40 m s^{-1} $decade^{-1}$) is also very weak and insignificant (Table 3). The landfall frequency also shows little tendency (black lines), and is not a factor that influences the landfall intensity, showing no notable correlation coefficients between them for all datasets.

Interestingly, the landfall intensity does not exceed but just approaches the maximum intensity during the analysis period, in both Northeast and Southeast Asia. Most of the linear trends of the differences: the maximum intensity minus the landfall intensity, show substantial negative values over Northeast (–1.6 to –0.9 m s^{-1} $decade^{-1}$) and Southeast (–1.7 to –0.5 m s^{-1} $decade^{-1}$) Asia although two specific cases (i.e., over East and Northeast Asia for JTWC dataset) show a weak positive trend. Correlation coefficients between maximum and landfall intensity are high and significant (correlation coefficient, r = 0.39–0.72) for all best-track datasets. Those for UW/NCDC are notable over Southeast Asia (r = 0.36) but not over Northeast Asia (r = 0.22). Thus, these results suggest that the landfall

intensity over East Asia may strongly depend on the maximum intensity and its location, although there are a few exceptions.

Table 3. Linear trends in landfall intensity (m s^{-1} $decade^{-1}$) for RSMC, JTWC, HKO, STI, and UW/NCDC, respectively. * denotes that the trend is statistically significant at the 90% confidence levels for the two-tailed student *t*-test.

	RSMC	JTWC	HKO	STI	UW/NCDC
East Asia	+0.58	+1.81*	+0.92	+0.79*	+0.56
Northeast Asia	+1.29*	+2.35*	+2.04*	+1.01*	+1.43*
Southeast Asia	−0.43	+0.63	−0.45	+0.08	−0.40

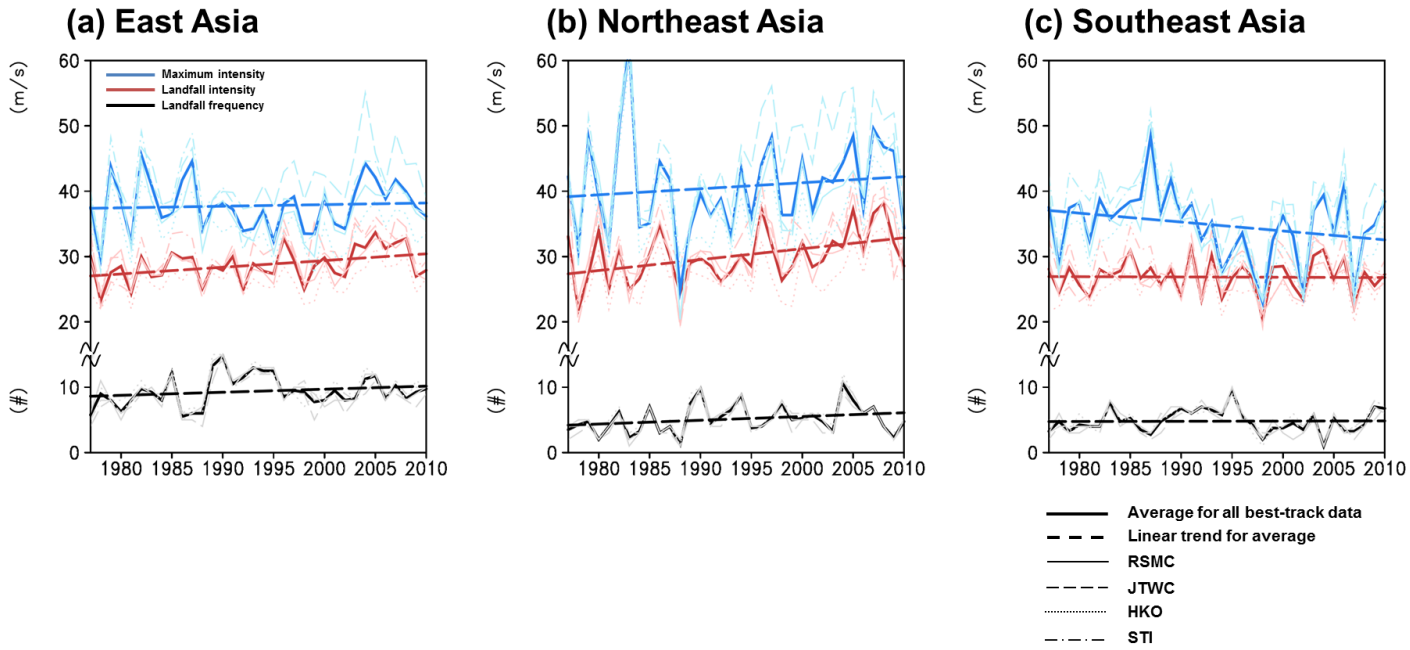

Figure 25. Time series of seasonal averages of maximum (blue lines) and landfall (red lines) intensity, and seasonal accumulation of landfall frequency (black lines) over (a) East Asia, (b) Northeast Asia, and (c) Southeast Asia. Faint-colored solid, dashed, dotted, and dot-dashed lines denote the RSMC, JTWC, HKO, and STI data, respectively. Thick solid and thick dashed lines denote the average of the four best-track data and the trend of the average, respectively.

4.3 Increasing Potential Impacts by Tropical Cyclones on Korea and Japan

Here, four parameters are used to characterize the TC impacts on Korea and Japan: PDI, TC-induced rainfall, number of landfall TCs, and TC duration. These parameters represent the TC potential impact for each year, and they have been used in many studies in the past [*Emanuel*, 2005; *Kamahori et al.*, 2006; *Kim et al.*, 2006; *Emanuel*, 2007; *Englehart et al.*, 2008; *Lee et al.*, 2010]. A TC directly affects Korea and Japan when its center is at a distance of 1° from the coastal lines of these two countries (Figure 26). Hereafter, this kind of TC is called as "an influential TC". Moreover, only the TC activity during the season (June–October), when 90% of TCs approach Korea and Japan [*Kim et al.*, 2005], was determined in these analyses. The "accumulated" and "mean" values of the parameters were separately determined. The "accumulated" value is defined as the sum of each parameter for all influential TCs during a TC season and the "mean" is the ratio of the accumulated value to the total number of influential TCs. Therefore, the "mean" value is the averaged potential impact of one TC.

The accumulated TC duration is the duration for which the influential TC remains in the target region. The accumulated PDI is defined as

$$Accumulated\ PDI = \sum_{n=1}^{N}\sum_{t=1}^{T} v_{\max}^{3}\ , \qquad (1)$$

where N is the total number of influential TCs every year, and T is the duration for which each TC remains in the target region. This definition of the accumulated PDI is obtained from *Emanuel* [2005]. The accumulated TC-induced rainfall is

calculated by the summation of the amounts of rainfall caused by influential TCs. the 0.5° × 0.5° grid gauge pixel data pertaining to daily precipitation for the period 1979–2010, obtained from the Climate Prediction Center, the National Oceanic and Atmospheric Administration (NOAA), was used [*Xie et al.*, 2007]. Since this dataset is only based on the rain-gauge data recorded at the weather stations in the target region, which includes a sufficient number of stations, the dataset is more homogeneous in time than satellite-based rainfall datasets. TC-induced rainfall is defined as the rainfall occurring when the center of a TC is within 5° of the grid points in Korea and Japan [e.g., *Kim et al.*, 2006; *Lee et al.*, 2010].

Figure 27 shows the time series of the number of influential TCs in Korea and Japan, the total number of TC genesis events in the WNP, and the ratio of the number of influential TCs in Korea and Japan to the total number of TC genesis events in the WNP. While the interannual variations are large, the number of influential TCs has increased since the early 1977 (Figure 27a); however, the trends are not statistically significant. On the other hand, the total number of TC genesis events in the WNP increased gradually until the mid-1990s but decreased rapidly afterwards and stabilized at a number same as that in the 1970s (Figure 27b). Consequently, the ratio of the total number of influential TCs (Figure 27a) to the total number of WNP TCs (Figure 27b) (i.e., a/b × 100%) shows a steeper increasing trend even though the trend is still not significant (Figure 27c). While about 17% of the WNP TCs influence the target region in the earlier decade, about

25% of the WNP TCs influence the target region in the later decade. This increased influential frequency has been reported in previous studies [*Choi and Kim*, 2007; *Liu and Chan*, 2008; *Tu et al.*, 2009].

Figure 28 represents the time series of the accumulated TC duration, PDI, and TC-induced rainfall within Korea and Japan as seen in Figure 26. These TC-related parameters are considered the potential impacts of influential TCs over the region. A considerable increase in all the parameters is observed; the increments for duration and TC-induced rainfall are not statistically significant at the 90% confidence levels. Nevertheless, the mean amplitudes of the TC duration nearly doubled in the later decade in each TC dataset. An increase in the accumulated TC-induced rainfall was observed as well; this is in good agreement with the rain-gauge observation in Korea (see Figure 2 in *Kim et al.*, 2006). Otherwise, the PDI represents notable increase with significance at the 90% confidence levels, only except for the STI dataset. The impact of the influential TCs is well correlated with the number of TCs shown in Figure 27a; the correlation coefficients of the three parameters are significant at 99% and are higher than 0.8. It is very likely that the increased total impacts of the influential TCs are highly related with the increase in the influential frequency.

The mean or normalized values (obtained by dividing the accumulated values by the number of influential TCs) used to investigate the impacts of each TC are shown in Figure 29. Unlike the number of influential TCs (Figure 27a), the mean TC duration within Korea and Japan shows a gradual increase (Figure 29a). The

mean TC durations have significantly increased for all datasets. Averaged lifetime of TCs over Korea and Japan has been rising about 2 hours every decade. This indicates that, in recent decades, TCs could damage more and more on these two countries as sustaining their intensity strong enough.

As in the case of the mean TC duration, a significant increase is observed in the mean PDI at the 95% confidence level for all datasets (Figure 29b). According to *Emanuel* [2007], the accumulated PDI shows the cumulative impact of the number of TCs, TC duration, and maximum wind speed. Here, the mean PDI is strongly correlated with the mean TC duration (correlation coefficient r = 0.75). The potential destructive power of a TC increases because of the long duration of the TC over the countries. The mean TC-induced rainfall showed a substantial increase in the late 1990s, followed by a decrease in the late 2000s (Figure 29c). Further, there was a large amount of TC-induced rainfall in the late 1970s. The increased TC durations partially affect the temporal variability of the TC-induced rainfall over the region (r = 0.43, significant at the 95% confidence level). The time series of the mean TC-induced rainfall showed a decadal variability, unlike the TC duration or PDI. This discrepancy does not imply that uncertainty exists in the rainfall dataset because the rainfall data over land area would definitely be accurate. This discrepancy is due to the strong influence of various factors, such as synoptic structure, topography, and moisture distribution, on the TC-induced rainfall [e.g., *Kim et al.*, 2006; *Park and Lee*, 2007].

The increased number and duration of influential TCs are key indicators of

the enhanced TC impact over Korea and Japan. Why did TCs live longer over the land in a later decade? Several factors, such as intensity, weakening rate, track, and translation speed of the TC, can be responsible. All possible factors are investigated whether they are major or minor roles related with the increased TC duration. The TC translation speed decreases slightly in the 2000s. The TC tracks tend to follow the Japanese islands more in the later decade (figure not shown). Partially related with the change in the TC tracks, the mean drift length of TCs over Korea and Japan has also increased since the late 1980s (not shown). However, these changes in the TC translation speed and TC tracks are not significant, indicating that they may be minor factors for the increased TC duration in the domain.

Intensity is identified as the main factor that induces the increase in the TC duration. Table 4 presents the linear trends in landfall strength of TCs. All of TC datasets, includes UW/NCDC, display statistically significant increasing trends ranging from 1.32 to 2.02 m s^{-1} $decade^{-1}$. These results are consistent with those of Section 4.2 and those reported by *Choi and Kim* [2007] and *Chan* [2008]. *Choi and Kim* [2007] reported an increase in the intensity of landfall TCs over the Korean peninsula. *Chan* [2008] showed that the number of intense TCs heading for the mid-latitude region has increased. Consequently, the more intense TCs could be a major factor to cause a longer TC duration over Korea and Japan because the other factors, such as weakening rate, tracks, translational speed, were not notably changed during the analysis period.

Table 4. Linear trends in landfall intensity (m s^{-1} $decade^{-1}$) for RSMC, JTWC, HKO, STI, and UW/NCDC, respectively. * denotes that the trend is statistically significant at the 90% confidence levels for the two-tailed student *t*-test.

RSMC	JTWC	HKO	STI	UW/NCDC
+1.58*	+2.02*	+1.73*	+1.32*	+1.79*

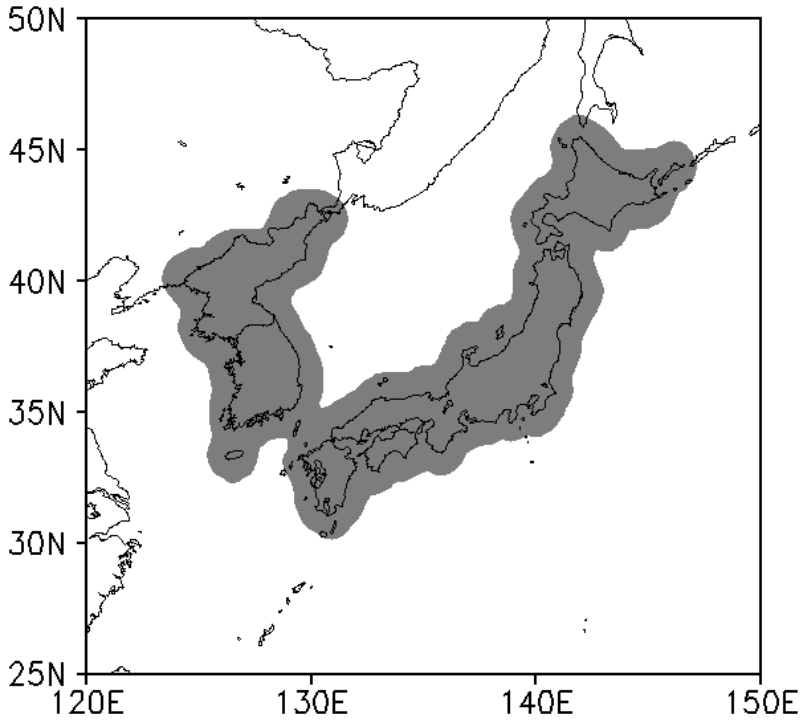

Figure 26. Analysis domain indicated by the shaded area.

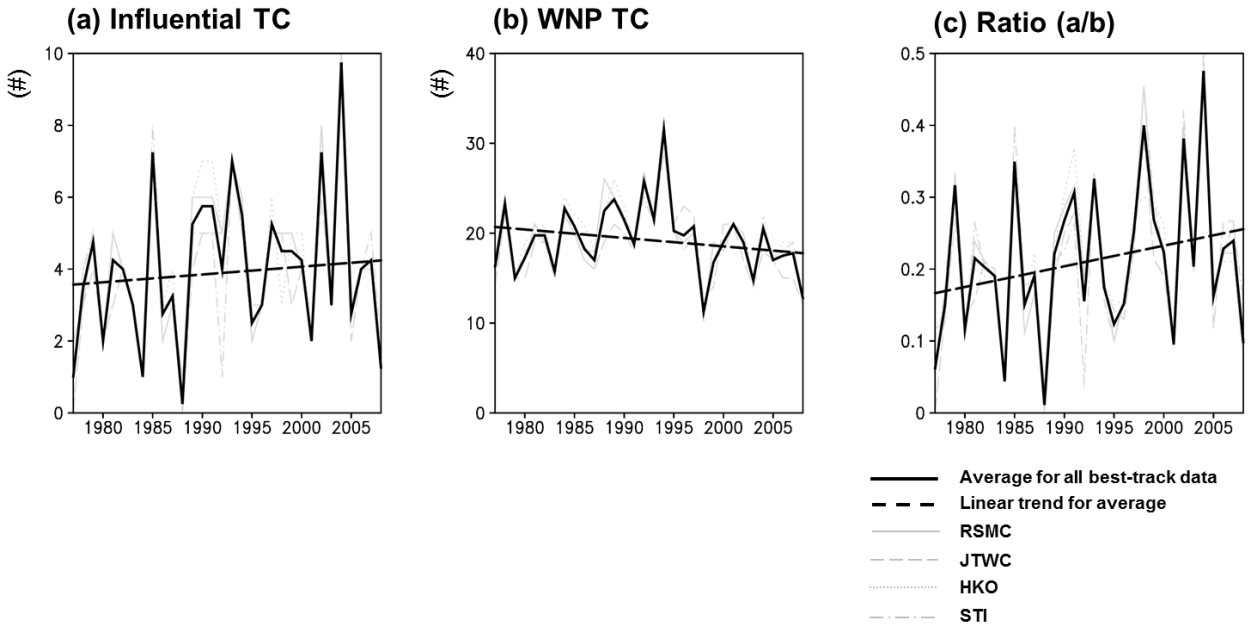

Figure 27. Time series of (a) the number of influential TCs over Korea and Japan, (b) the number of TC genesis events over the WNP, and (c) the ratio of number of influential TCs over Korea and Japan to the number of TC genesis events over the WNP. Gray solid, dashed, dotted, and dot-dashed lines denote the RSMC, JTWC, HKO, and STI data, respectively. Thick solid and thick dashed lines denote the average of the four best-track data and the trend of the average, respectively.

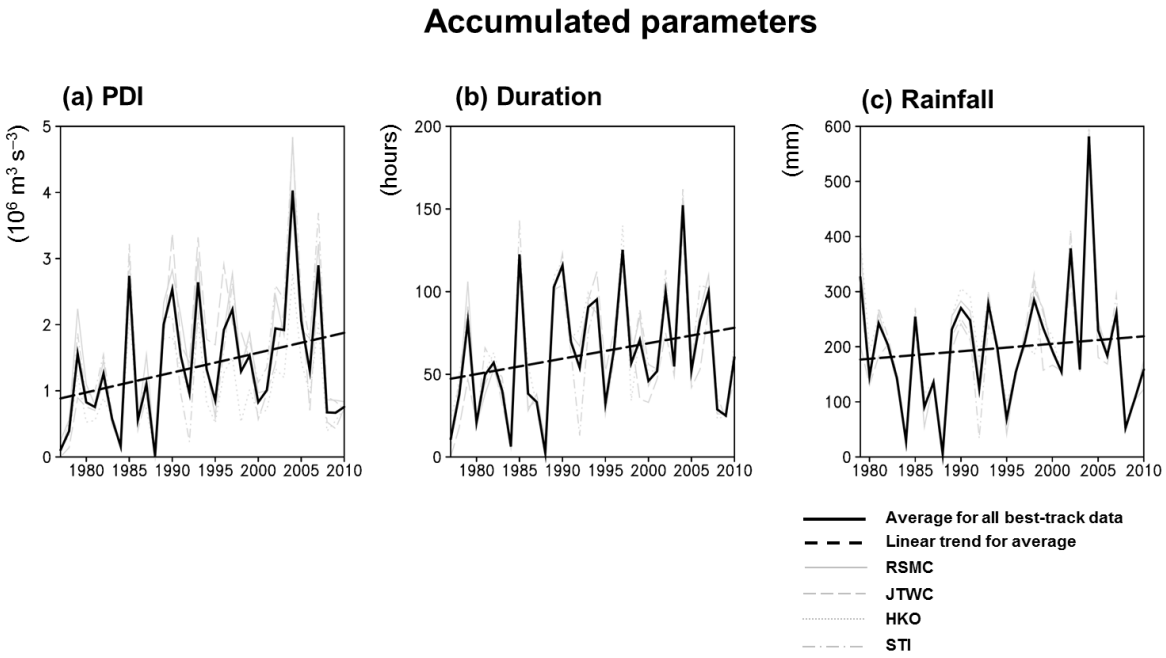

Figure 28. Time series of (a) the accumulated TC duration (hours), (b) the accumulated PDI (10^6 m^3 s^{-3}), and (c) the accumulated TC-induced rainfall (mm) for the influential TCs. Gray solid, dashed, dotted, and dot-dashed lines denote the RSMC, JTWC, HKO, and STI data, respectively. Thick solid and thick dashed lines denote the average of the four best-track data and the trend of the average, respectively.

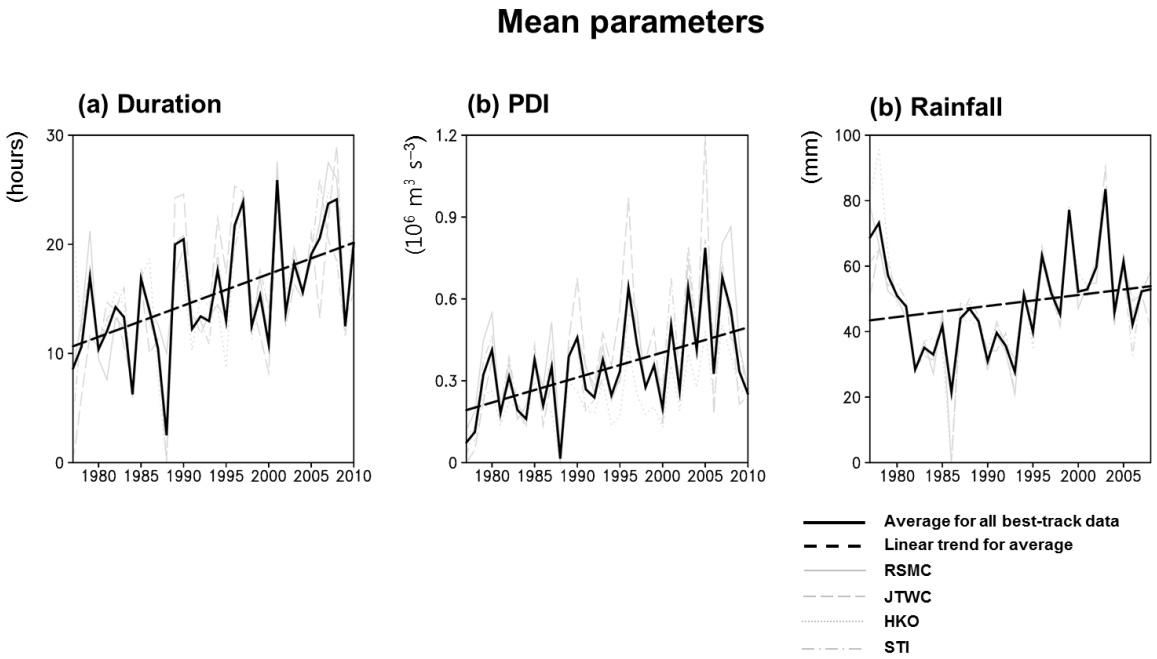

Figure 29. Time series of the mean values of (a) the TC duration (hours), (b) the PDI (10^6 m^3 s^{-3}), and (c) the TC-induced rainfall (mm) for the influential TCs.

5. Socioeconomic Damages by Tropical Cyclones on South Korea

5.1 Changes in Socioeconomic Damages

Here, the long-term trends in TC potential damage parameters and its real damages were examined as 51 TCs that striking South Korea were focused. The data for casualties and property losses by TCs were obtained from National Disaster Information Center. The economic losses are classified into five fields: agriculture, vessels, public facilities, buildings, and the rest. The data cover the period 1979–2010. Some landfall TCs were missing or excluded because their damages overlapped with those by summer monsoon, referred as Chang-Ma. Consequently, only 51 TCs were selected as the analysis objects even though more number of TCs affected Korea for the last three decades.

The TC intensity-related parameters were calculated by using station-based observations, include maximum wind speed and precipitation, on 56 weather stations. Because best-track datasets only provide maximum intensity of a TC, it is hard to know how wide area of South Korea is seriously affected by the TC. Some agencies recently issue radius of maximum wind, but the record length is too short to perform climatological analysis. Thus, from station-based data, TC potential damage parameters were acquired. Figure 30 exhibits locations of used weather stations, which are spread almost uniformly across the country. The stations were regarded as under influence of TCs if their daily amount of rainfall

is larger than 80 mm or daily maximum wind speed exceeds 14 m s^{-1} during the TC impact period; the thresholds of 14 m s^{-1} and 80 mm are the standards of weather advisory of Korea Meteorological Administration (KMA). TC-induced rainfall and wind are defined as summations of daily rainfall and maximum wind each station under influence. By these methods, the defined potential damage parameters can involve both of the intensity and the influence range of TCs. To check whether this method works well, tracks of TCs stroke South Korea were classified into four clusters by fuzzy cluster analysis during the period 1951–2010 (Figure 31) [*Kim et al*., 2011], and then the spatial distribution of potential damages were examined for each cluster (Figure 32). Four clusters are characterized by east-passing, south-landing, southwest-decaying, and west-landing cases (Figure 31). The east passing cases mostly affect the eastern coasts of South Korea (Figures 32a and 32b). The south-landing and south-west decaying cases influence entire domain of South Korea, particularly southern coasts focused (Figures 32c, 32d, 32e, and 32f). The west-landing case also seems to cause nation-wide damages (Figures 32g and 32h).

Because societal growth is one of the most important factors for the recent increasing TC damages [*Pielke et al.*, 2003; *Pielke et al*., 2008; *Fengjin and Ziniu*, 2010], casualties and property losses were normalized by using the following equations, which were suggested by *Pielke et al*. [2008].

$$L_{2005} = L_y \times I_y \times DRW_y$$

$$C_{2005} = C_y \times P_y$$

The equations above indicate normalization of each year's TC damage to 2005's. L_{2005} is the normalized economic loss, and C_{2005} is the normalized casualties. L_y and C_y are the values of each year's reported damages. I_y, DRW_y, and P_y are the ratio of inflation, domestic real wealth and population each year based on 2005.

Figure 33 shows annual averages of original and normalized casualties and property losses. While original casualties have decreased, property losses have abruptly increased (Figures 33a and 33b). The decreasing trends in casualties were also reported in other nations [*Fengjin and Ziniu*, 2010]. This is maybe in virtue of the improvements of various fields, such as medical skill, early-warning system, weather forecast and so on. On the other hand, the strong upward tendency is mainly due to the record breaking damages of 2002 and 2003 in which two extreme TCs stoke the country. For instance, in 2002, typhoon Rusa brought about torrential downpour (870.5 mm/day) in Gangneung, the highest rainfall records in Korea. In 2003, typhoon Maemi took the top of the strongest wind records of Korea, 60 m s^{-1} in Gosan. Thus, it can be said that the notable increasing trend would be led by only these two TCs. This thought is consistent with some previous studies [*Crompton et al*., 2011; *Emanuel*, 2011], who argued that only a few intense TCs can lead the trends of economic damages.

Figures 33c and 33d represent the time series of normalized casualties and property losses. As shown in Figures 33c, the casualties have remarkably dropped for the analysis period. The normalized losses also display very weak rising trend

since the damages in the early period are raised after the normalization. Furthermore, after excluding two extreme TCs, Rusa and Maemi, the trend becomes negative. Noticeable uplift of economic losses appears in 1987 due to typhoon Thelma, which also caused the highest number of casualties during the analysis period. The large amount of socioeconomic damages by Thelma is not only due to its destructiveness but also because KMA failed to forecast its track; most of the losses came from sinking of ships unprepared for Thelma.

Figure 34 exhibits time series of annual averages of TC-induced rainfall and wind. TC-induced rainfall has slightly increased whereas TC-induced wind has no specific trend (Figure 34a). The increased TC-induced rainfall is consistent with the result of Section 4.3 (Figure 29c). However, the timid trend in TC-induced wind is different from the result of Section 4.3 (Figure 29b). This is because TC-induced wind only considers the influential range of TCs but not PDI.

The results generally indicate that TC-caused property losses show weak tendency after adopting normalization method, so that recent increasing tendency is mostly attributable to economic growth of the country. Otherwise, the number of casualties has notably decreased even though TC-induced rainfall and wind have slightly increased. In case of property losses, if typhoons Rusa and Maemi are excluded, the evident downward tendency can be observed. These hint that TCs may have caused less and less socioeconomic damages at same intensity.

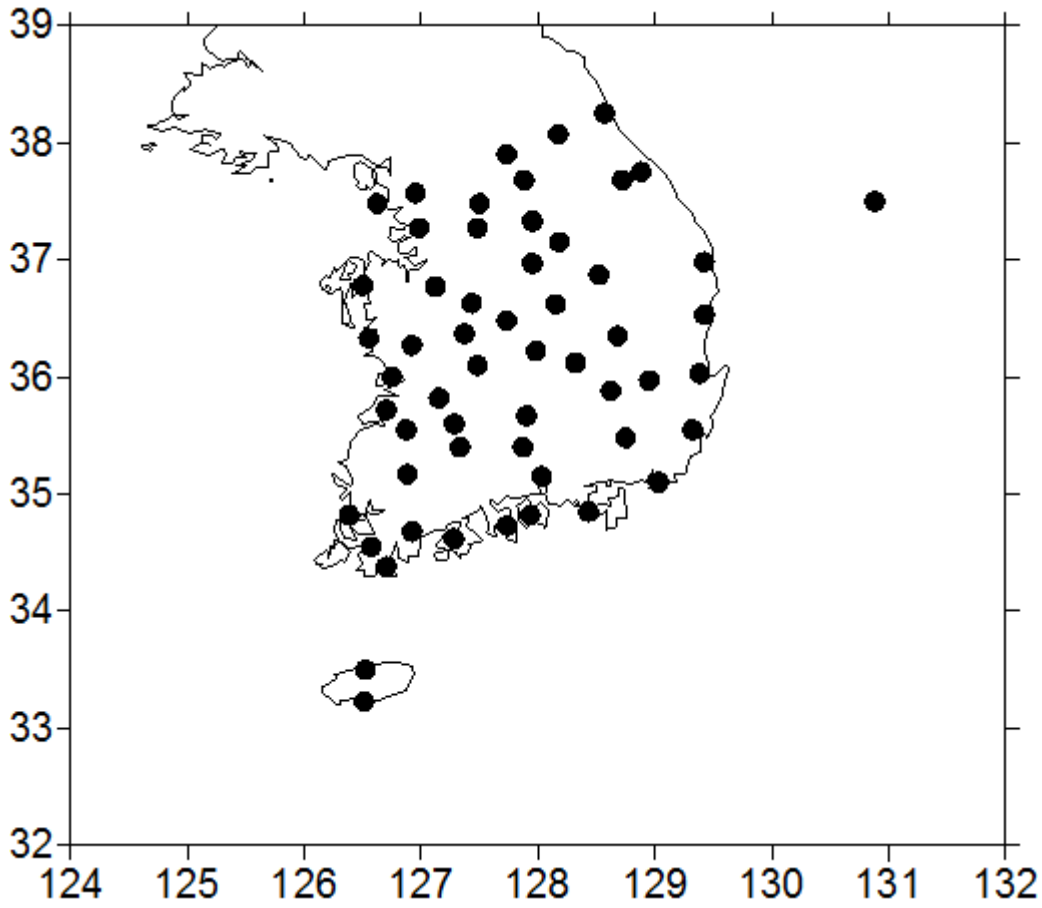

Figure 30. Locations of 56 weather stations used.

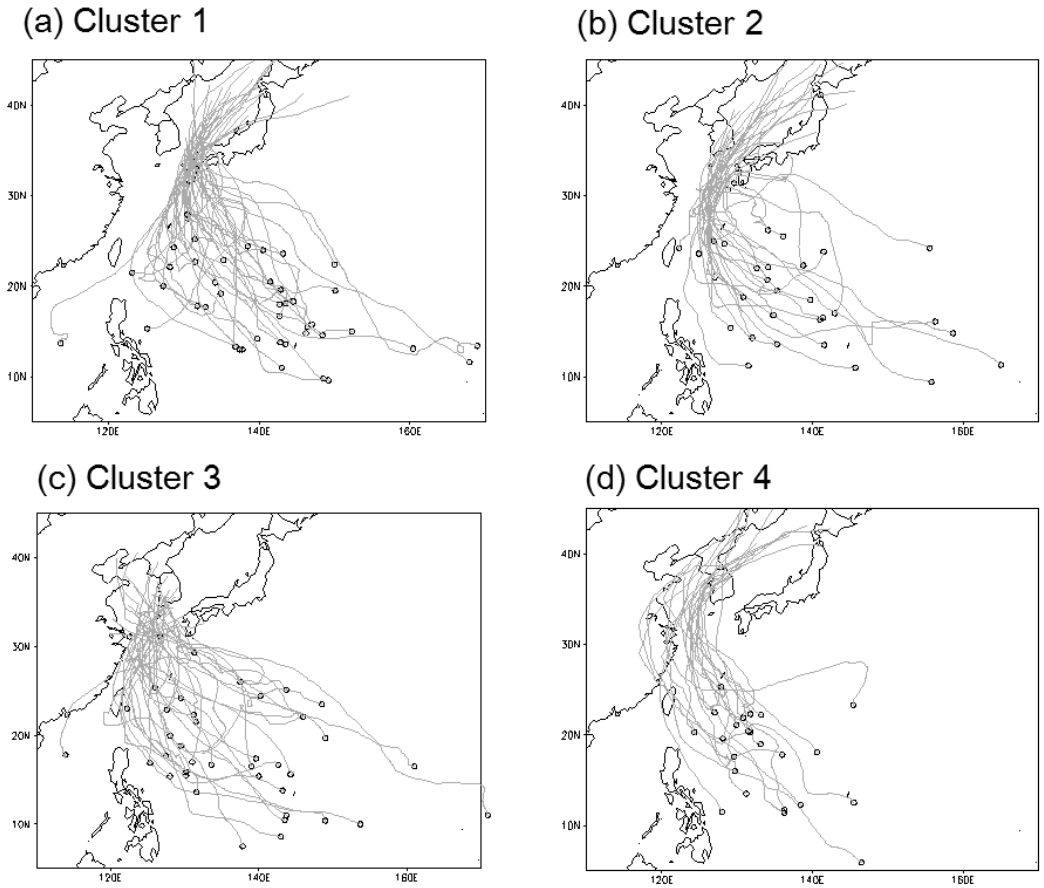

Figure 31. Clusters of tracks of TCs stroke South Korea during 1951–2010.

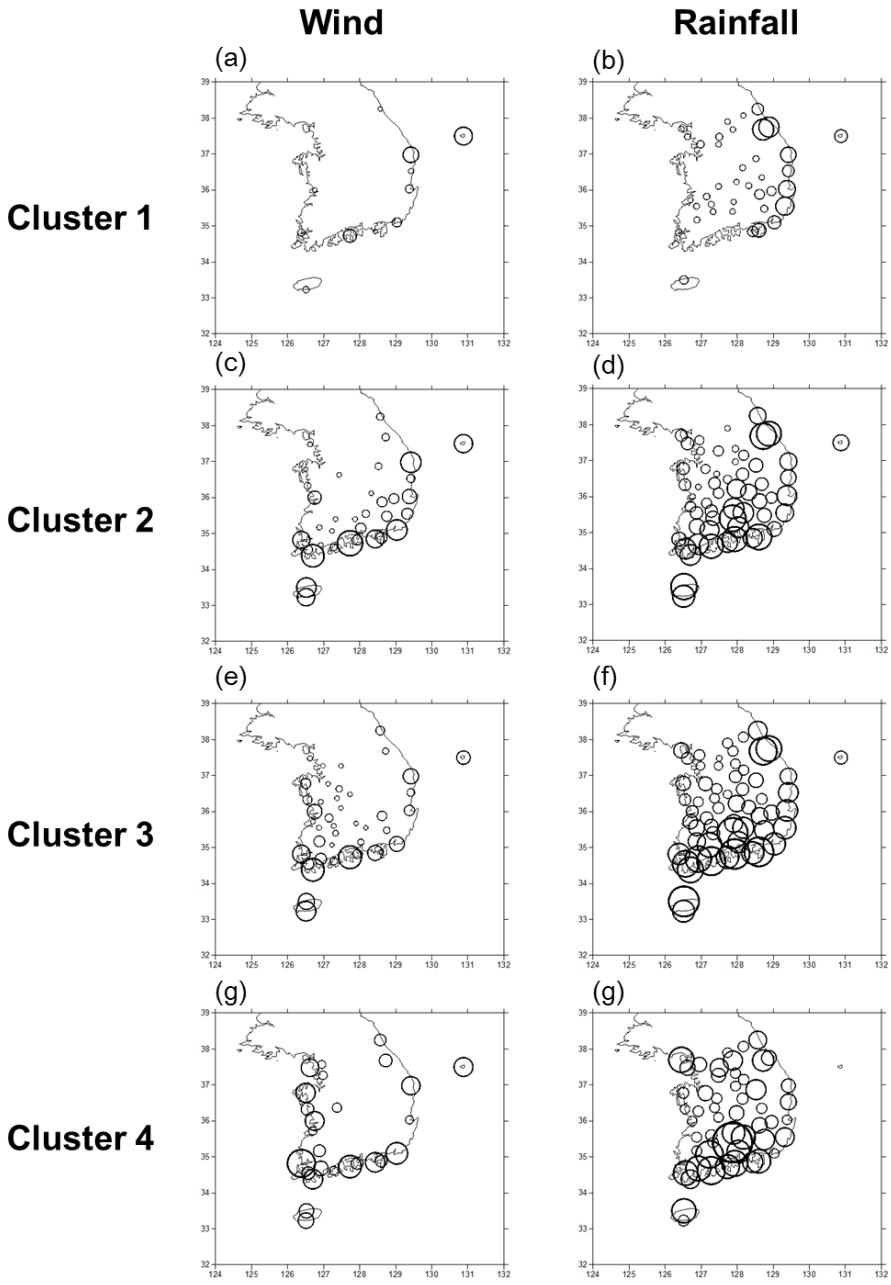

Figure 32. Accumulated wind and rainfall for each cluster of TC track over South Korea during 1973–2010.

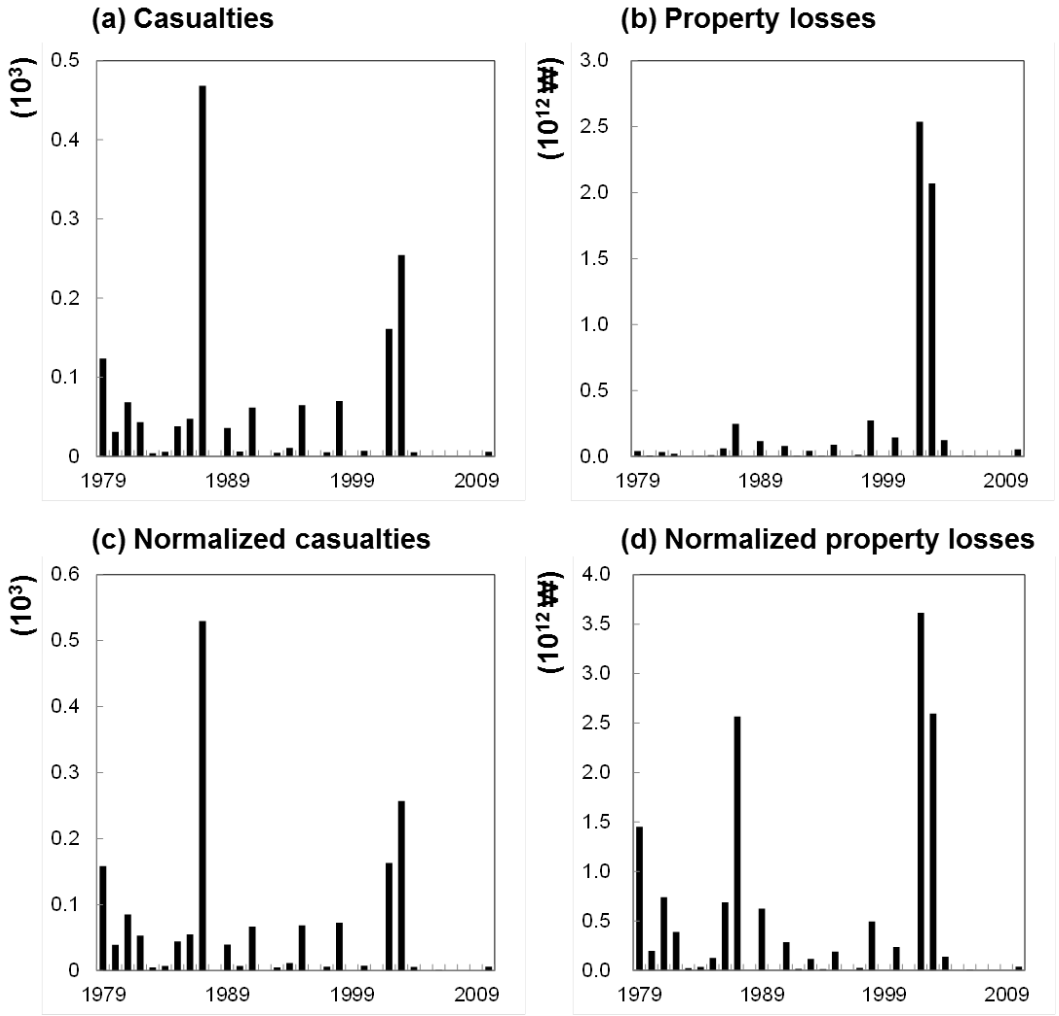

Figure 33. Time series of annual averages of (a) casualties, (b) property losses, (c) normalized casualties, and (d) normalized property losses in South Korea. The basis year for normalization is 2005.

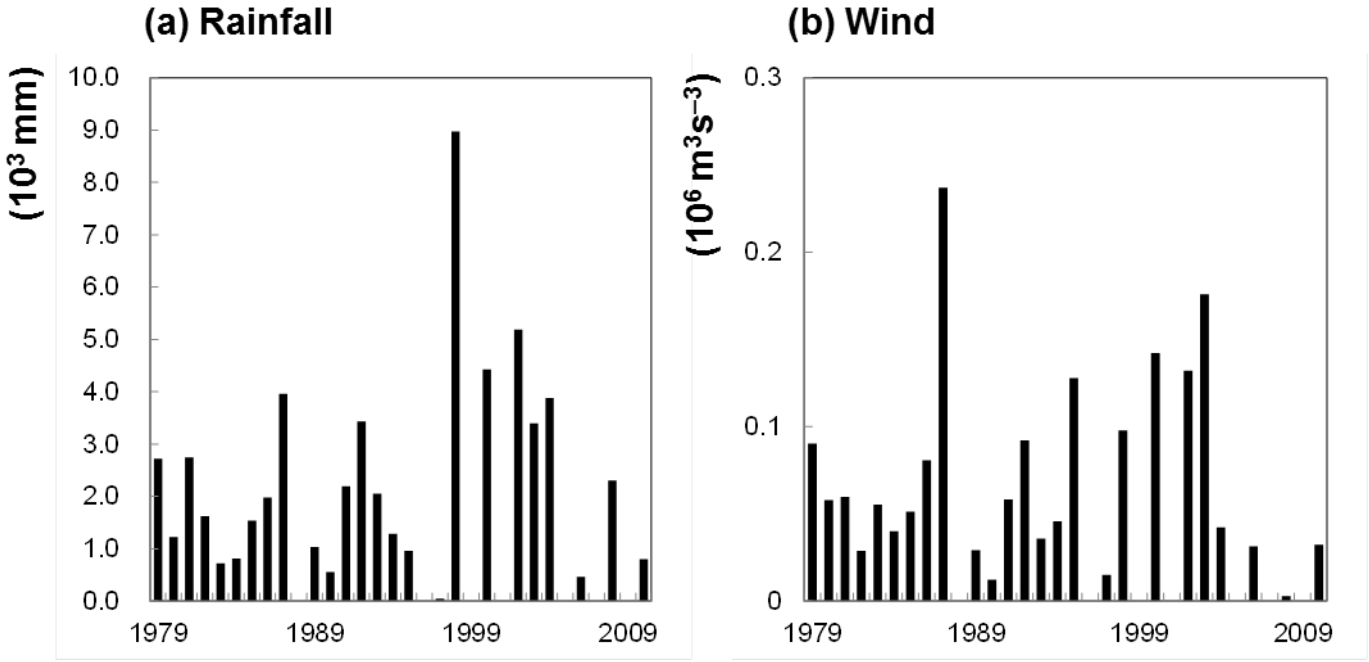

Figure 34. Time series of annual averages of (a) TC-induced rainfall and (b) TC-induced wind over South Korea.

5.2Reduced Vulnerability of Tropical Cyclones

The statistical relationships between TC intensity and damages were investigated. In this study, in order to test changes in sensitivity between TC intensity and damages, the entire periods were divided into two periods (1979–1990 and 1991–2010); the early and later periods include 24 and 27 TCs, respectively. Figure 35 reveals how TC intensity affects damages. Based on basic statistic assumption of homoscedasticity, casualties and economic losses had their best fitting of regression of rainfall and wind in linear straight line (Figure 35). The gradient regression lines of rainfall with casualties and property losses for the former period (1979–1990) are much steeper than those for the latter period (1991–2010) (Figures 35a and 35b). This means the ratio of normalized casualties and property losses to intensity decreased over time. The regression lines of wind with casualties also show same result, which indicate TC-caused casualties reduce to same intensity in the recent periods (Figures 35c and 35d).

Despite of some exceptions, these results consistently suggest that the vulnerability of TCs in South Korea has reduced for one cause or another. The societal development is thought to be the major cause of the reduced vulnerability. Figure 36 represents time series of economic losses by five different fields: agriculture, vessels, public facilities, buildings, and the rest. The clear decreasing tendency is particularly found in two areas, agriculture and vessels, which can be declined by to the improved technologies, such as weather forecasting and disaster prevention. Moreover, TC-caused flooding area has considerably diminished for

the analysis period possibly due to the advanced disaster reduction technologies (Figure 37).

Actually, this supposition makes sense because notable investments for natural disaster preventions were conducted in South Korea during the analysis period (1979–2010). Figure 38 presents the improved technologies and infrastructures to restrain TC-caused damages. KMA has applied 12-hr and 24-hr forecast to TC track since 1984. Nowadays, 72-hr forecast to track and 48-hr forecast to intensity are performed. Moreover, numerical weather prediction has been utilized since 1991 and supercomputer has been operated since 1999 only for weather forecasting. In 2008, KMA established National Typhoon Center that is an organization exclusively for typhoon forecast. On the other hand, Korea also found National Institution of Disaster Prevention in 1997 and National Emergency Management Agency in 2004, which are composed by experts of technologies and policies for disaster reduction.

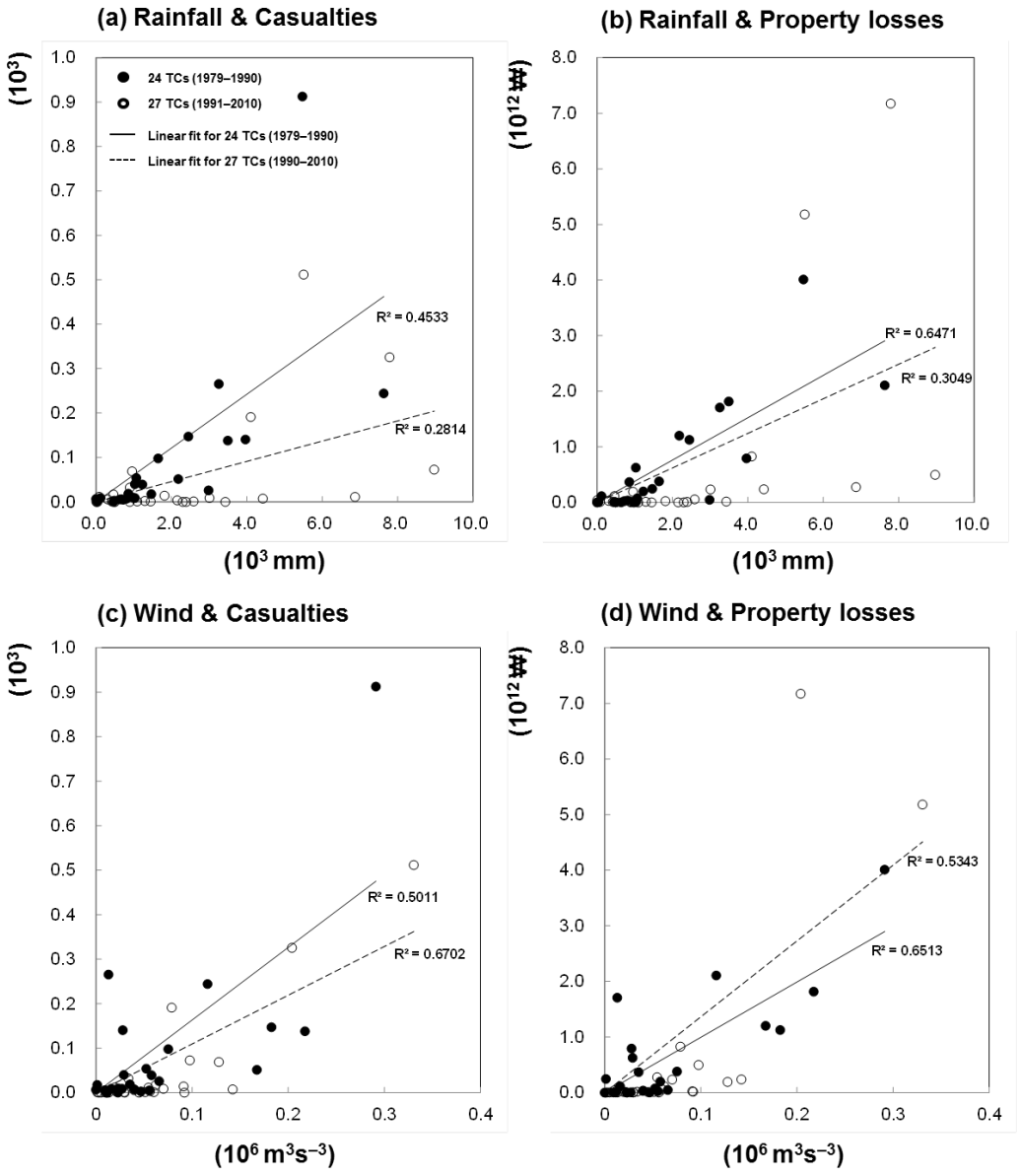

Figure 35. Statistical relationships of TC-induced rainfall with (a) normalized casualties and (b) normalized property losses, and those of TC-induced wind with (c) normalized casualties and (d) normalized property losses between the early (1979–1990) and later periods (1991–2010).

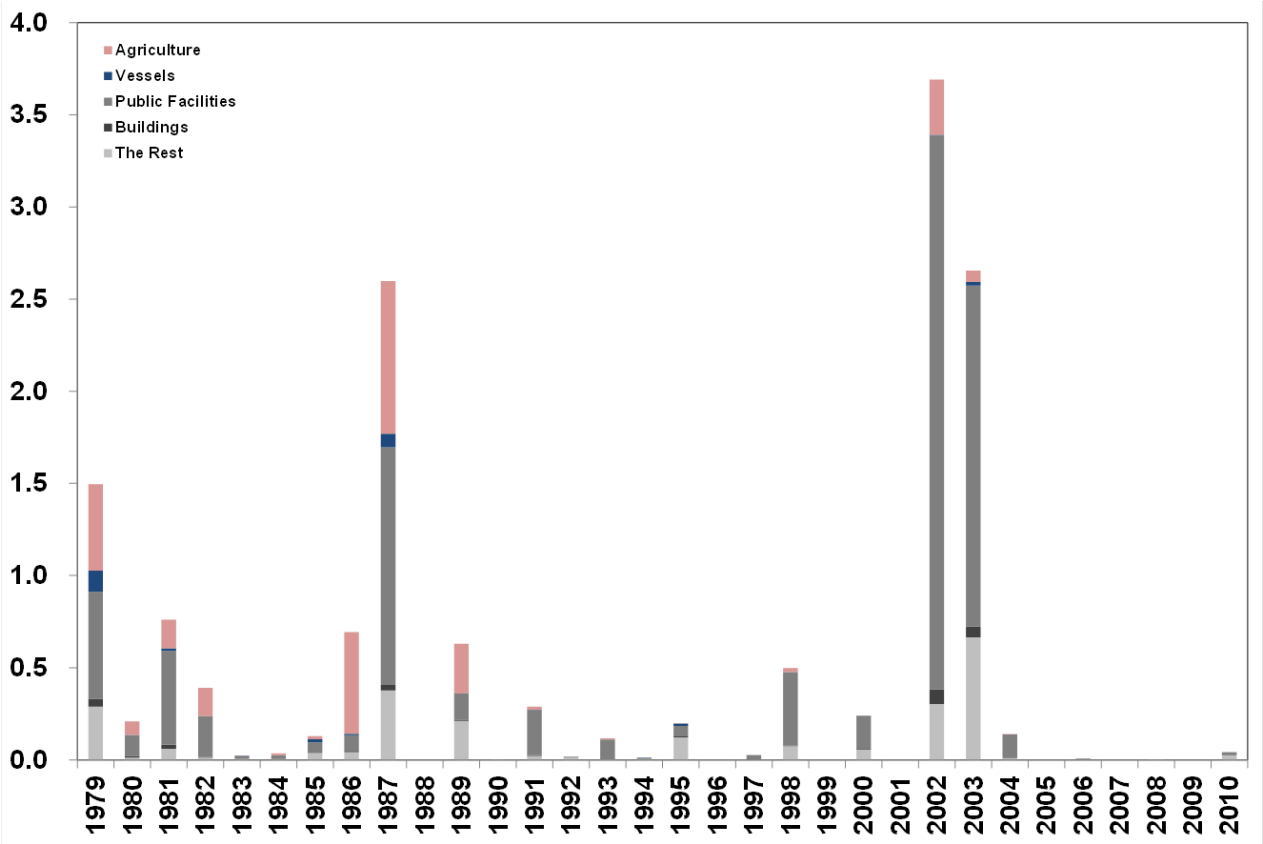

Figure 36. Time series of normalized property losses in each field: agriculture, vessels, public facilities, buildings, and the rest in South Korea.

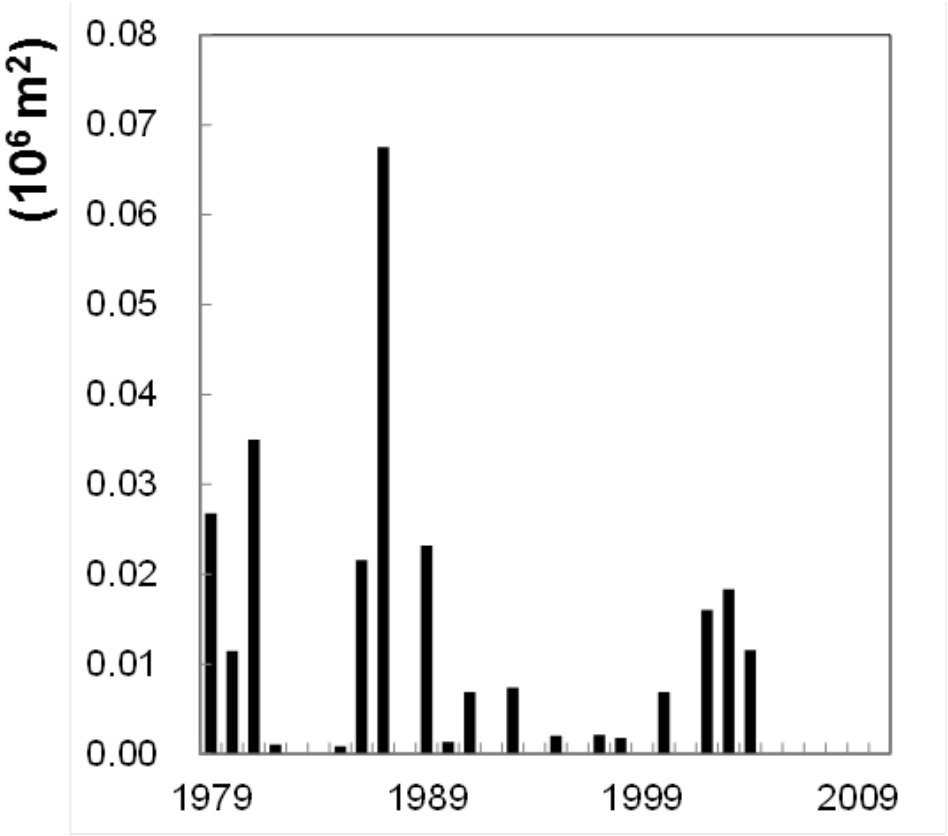

Figure 37. Time series of flooding area by TCs over South Korea.

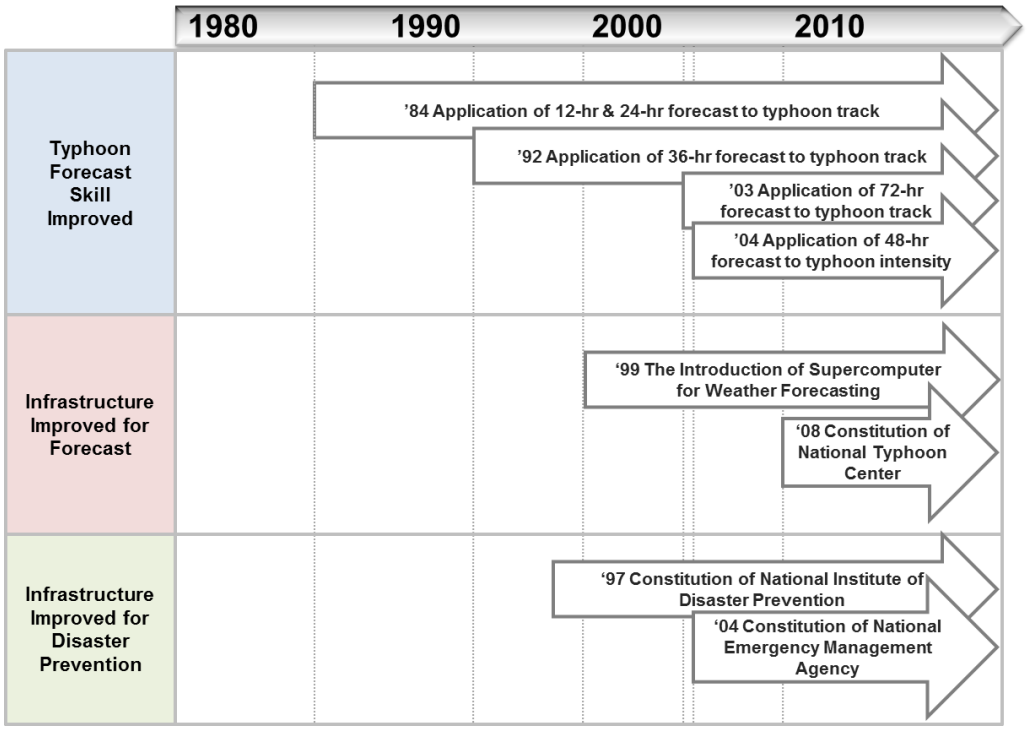

Figure 38. Timeline of the improvement of typhoon forecast and disaster prevention infrastructures in South Korea.

6. Concluding Remarks

This study examined spatial distribution of long-term changes in TC intensity over the WNP and its impacts on coastal countries of East Asia, especially South Korea focused. To find spatial distribution of trends in TC intensity, five TC datasets were used for the period 1977−2010. While unclear and inconsistent long-term changes in TC intensity were observed with regard to the whole life of TCs in the WNP [*Wu et al*., 2006; *Kossin et al*., 2007], consistent trends for all TC datasets were newly identified in the TP and SJ regions. For all TC datasets, the TC intensity consistently strengthened in the SJ region, whereas it weakened in the TP region. These opposing trends in TC intensity were mainly affected by TC intensification rate and genesis frequency. In particular, the changes in TC intensification rate could mostly support spatial distribution of linear trends in TC intensity. The suppressed (increased) TC intensification rate in the eastern part of TP (the subtropics and the western part of TP) weakened (strengthened) TCs in the TP (SJ) region. However, in the tropics, the TC intensification rate could not sufficiently account for the spatial change in TC intensity, but rather the TC genesis frequency could explain it: decrease (increase) in the eastern part of TP and the Philippines (the center of TP and northern part of the South China Sea). Thus, it is suggested that both TC

intensification rate and genesis frequency have been the decisive factors for regionally inhomogeneous intensity trends.

The increased TC intensification rate and genesis frequency in the subtropics and the western part of TP were driven by both thermodynamic and dynamic climate variables: the high MPI, deeper 26℃ isotherm, warm SST, weak vertical wind shear, and anomalous cyclonic large-scale flow in the same region. However, the reduced TC intensification rate and genesis frequency around the east of TP were attributable to unfavorable dynamic variables: the low-level anomalous anticyclonic flows and strong vertical wind shear therein, which canceled out and overcame effect of the favorable thermodynamic conditions. These changes in dynamic variables were closely linked with the recently enhanced Walker circulation over the Pacific. Thus, it is suggested that the dynamic variables (e.g., relative vorticity and vertical wind shear) could have more conclusive roles for the changes in TC intensity in the eastern part of TP. This conclusion supports those of *Chan* [2009], who suggested that dynamic fields might be more dominant factors than thermodynamic fields in determining TC intensity over the WNP, as thermodynamic environments could not fully explain the variation in TC intensity.

This significant increase of SST over the western Pacific, known as the La-Niña-like SST pattern, could move the location of maximum intensity of TCs

closer to the East Asian coastline over the analysis period. Note that this horizontal distribution of SST over the Pacific can intensify the Walker circulation, thereby causing anticyclonic anomalies and strong vertical wind shear over the tropical eastern Philippine Sea, and vice versa along the East Asian continent. These counter changes in large-scale environment may directly result in the shifts in the location of maximum intensity. A larger fraction of TCs heading for Taiwan and Japan is another possible reason for the shift of the location of maximum intensity towards East Asia. Consequently, the location of maximum intensity of TCs approaching East Asia can extensively strengthen the landfall intensity in Northeast Asia, even when the maximum intensity itself is unchanged. In contrast, the landfall intensity in Southeast Asia has scarcely changed due to a substantial decrease in maximum intensity. This decrease in the maximum intensity is attributable to the enormous influence of the significant increase in newly generated weak TCs over the northern part of the South China Sea near Southeast Asia. Overall, the growing threat of intense TCs characterizes the recent change in the intensity of landfalling TCs over East Asia.

Due to these stronger landfall TCs, the average impact of one TC per a year also show significant increase over Korea and Japan. Linear increases are observed in the mean TC duration and mean PDI, implying that they are well correlated with each other. In contrast, the TC-induced rainfall shows a dramatic

increase in the late 1990s. Since rainfall can be affected by various factors apart from the TC intensity [e.g., *Kim et al.*, 2006; *Park and Lee*, 2007], the increase in the rainfall does not necessarily depend on the increase in the TC duration. Thus, in addition to the increased landfall frequency, the increased mean TC duration is another important factor responsible for the recent enhancement in the TC activity over Korea and Japan. It can be said that the high-intensity TCs sustained their intensity for a longer duration after landfall because the dissipation time required for these intense TCs to weaken is expected to be longer than that required for moderate TCs. This is the case because more number of typhoons and intensive typhoons made landfall in the region in a later decade. The other factors (i.e., tracks, translation speeds, mean drift lengths, and weakening rates of TCs) could be also important for TC duration. The TC translation speeds have been slightly slower since the 2000s. The TC tracks have been shifted towards Japan. The mean drift lengths of TCs over the landfall domain have also increased since the late 1980s. The weakening rates of TCs have been a little bit faster in the later decade. However, these changes in four factors are not significant, indicating that they might have a minor role in the increased TC duration in the domain.

Finally, changes in statistical sensitivity between TC potential damage parameters and socioeconomic damages were investigated as 51 TCs that stroke

South Korea were focused during the period 1979–2010. The intensity-related parameters were made with station-based wind speed and precipitation. The results showed that typhoon-induced gale and downpour have slightly increased, whereas normalized casualties and property losses have decreased and increased, respectively. The rising property losses were mainly due to two extreme events; Rusa (2002) and Maemi (2003). After these events excluded, the losses also tended to decrease. Thus, TCs seem to have caused less and less socioeconomic damages at same intensity. This reduced TC vulnerability could be explained by the improved prevention against TCs in South Korea.

References

An, S.-I., J.-W. Kim, S.-H. Im, B.-M. Kim, and J.-H. Park, 2011: Recent and future sea surface temperature trends in tropical pacific warm pool and cold tongue regions. *Clim Dyn*, **39**, 1373–1383, doi:10.1007/s00382-011-1129-7.

Archer, C. L., and K. Caldeira, 2008: Historical trends in the jet streams. *Geophys. Res. Lett*, **35**, L08803, doi:10.1029/2008GL033614.

Behringer, D. W., M. Ji, and A. Leetmaa, 1998: An improved coupled model for ENSO prediction and implications for ocean initialization. Part I: The ocean data assimilation system. *Mon. Wea. Rev*, **126**, 1013–1021.

Bell, G. D. M. S. Halpert, R. C. Schnell, R. W. Higgins, J. Lawrimore, V. E. Kousky, R. Tinker, W. Thiaw, M. Chelliah, and A. Artusa, 2000: Climate assessment for 1999. *Bull. Amer. Meteor. Soc*, **81**, s1–s50.

Bender, M. A., and I. Ginis, 2000: Real-case simulations of hurricane-ocean interaction using a high-resolution coupled model: Effects on hurricane intensity. *Mon. Wea. Rev*, **128**, 917–946.

Bister, M., and K. A. Emanuel, 1998: Dissipative heating and hurricane intensity. *Meteorol Atmos Phys*, **65**, 233–240.

Briegel, L. M., and W. M. Frank, 1997: Large-scale influences on tropical cyclogenesis in the western North Pacific. *Mon. Wea. Rev*, **125**, 1397–

1413.

Camargo, S. J., and A. H. Sobel, 2005: Western North Pacific tropical cyclone intensity and ENSO. *J. Climate*, **18**, 2996–3006.

Cane, M. A., A. C. Clement, A. Kaplan, Y. Kushnir, D. Pozdnyakov, R. Seager, S. E. Zebiak, and R. Murtugudde, 1997: Twentieth-Century Sea Surface Temperature Trends. *Science*, **275**, 957–960.

Chan, J. C. L., 2005: Interannual and interdecadal variations of tropical cyclone activity over the western North Pacific. *Meteorol Atmos Phys*, **89**, 143–152.

Chan, J. C. L., 2006: Comment on "Changes in Tropical Cyclone Number, Duration, and Intensity in a Warming Environment." *Science*, **311**, 1713b–1713b, doi:10.1126/science.1121522.

Chan, J. C. L., 2008: Decadal variations of intense typhoon occurrence in the western North Pacific. *Proceedings of the Royal Society A: Mathematical, Physical and Engineering Science*, **464**, 249–272, doi:10.1098/rspa.2007.0183.

Chan, J. C. L., and J.-E. Shi, 1996: Long-term trends and interannual variability in tropical cyclone activity over the western North Pacific. *Geophys. Res. Lett*, **23**, 2765–2767, doi:10.1029/96GL02637.

Chan, J. C. L., and K. S. Liu, 2004: Global warming and western North Pacific

typhoon activity from an observational perspective. *J. Climate*, **17**, 4590–4602.

Choi, K.-S. and B.-J. Kim, 2007: Climatological characteristics of tropical cyclones making landfall over the Korean peninsula, *J. Korean Meteorol. Soc.*, **434**, 97–109.

Chu, P.-S., J.-H. Kim, and Y. R. Chen, 2012: Have steering flows in the western North Pacific and the South China Sea changed over the last 50 years? *Geophys. Res. Lett*, **39**, L10704.

Chu, P.-S., X. Zhao, C.-H. Ho, H. S. Kim, and M. M. Lu, 2010: Bayesian forecasting of seasonal typhoon activity: A track-pattern-oriented categorization approach. *J. Climate*, **23**, 6654–6668.

Crompton, R. P., R. A. Pielke Jr, and K. J. McAneney, 2011: Emergence timescales for detection of anthropogenic climate change in US tropical cyclone loss data. *Environ. Res. Lett*, **6**, 014003, doi:10.1088/1748-9326/6/1/014003.

Dee, D. P., S. M. Uppala, A. J. Simmons, P. Berrisford, P. Poli, S. Kobayashi, U. Andrae, M. A. Balmaseda, G. Balsamo, P. Bauer, P. Bechtold, A. C. M. Beljaars, L. van de Berg, J. Bidlot, N. Bormann, C. Delsol, R. Dragani, M. Fuentes, A. J. Geer, L. Haimberger, S. B. Healy, H. Hersbach, E. V. Hólm, L. Isaksen, P. Kållberg, M. Köhler, M. Matricardi, A. P. McNally, B. M.

Monge-Sanz, J.-J. Morcrette, B.-K. Park, C. Peubey, P. de Rosnay, C. Tavolato, J.-N. Thépaut, and F. Vitart, 2011: The ERA-Interim reanalysis: Configuration and performance of the data assimilation system. *Q.J.R. Meteorol. Soc*, **137**, 553–597.

Dvorak, V. F., 1975: Tropical cyclone intensity analysis and forecasting from satellite imagery, Mon. Wea. Rev., **103**, 420–430.

Emanuel, K. A., 1986: An air-sea interaction theory for tropical cyclones. Part I: Steady-state maintenance. *J. Atmos. Sci*, **43**, 585–605.

Emanuel, K. A., 1987: The dependence of hurricane intensity on climate. *Nature*, **326**, 483–485.

Emanuel, K. A., 2005: Increasing destructiveness of tropical cyclones over the past 30 years. *Nature*, **436**, 686–688, doi:10.1038/nature03906.

Emanuel, K. A., 2007: Environmental factors affecting tropical cyclone power dissipation, *J. Climate*, **20**, 5497–5509.

Emanuel, K. A., 2011: Global warming effects on US hurricane damage. *Weather, Climate, and Society*, **3**, 261–268, doi:10.1175/WCAS-D-11-00007.1.

Englehart, P. J., M. D. Lewis, and A. V. Douglas, 2008: Defining the frequency of near-shore tropical cyclone activity in the eastern North Pacific from historical surface observations (1921–2005), *Geophys. Res. Lett.*, **35**, L03706, doi:10.1029/2007GL032546.

Fengjin, X., and X. Ziniu, 2010: Characteristics of tropical cyclones in China and their impacts analysis. *Nat Hazards*, **54**, 827–837, doi:10.1007/s11069-010-9508-7.

Frank, W. M., and E. A. Ritchie, 2001: Effects of vertical wind shear on the intensity and structure of numerically simulated hurricanes. *Mon. Wea. Rev*, **129**, 2249–2269.

Gray, W. M., 1968: Global view of the origin of tropical disturbances and storms. *Mon. Wea. Rev*, **96**, 669–700.

Grossmann, I., and M. G. Morgan, 2011: Tropical cyclones, climate change, and scientific uncertainty: what do we know, what does it mean, and what should be done? *Climatic Change*, **108**, 543–579, doi:10.1007/s10584-011-0020-1.

Ha, K.-J., S.-J. Yoon, K.-S. Yun, J.-S. Kug, Y.-S. Jang, and J. C. L. Chan, 2012: Dependency of typhoon intensity and genesis locations on El Niño phase and SST shift over the western North Pacific. *Theor. Appl. Climatol*, **109**, 383–395, doi:10.1007/s00704-012-0588-z.

Hall, P., 1988: Theoretical comparison of bootstrap confidence intervals. *The Annals of Statistics*, 927–953.

Ho, C.-H., J.-J. Baik, J.-H. Kim, D.-Y. Gong, and C.-H. Sui, 2004: Interdecadal changes in summertime typhoon tracks. *J. Climate*, **17**, 1767–1776.

Holland, G. J., 1997: The maximum potential intensity of tropical cyclones. *J. Atmos. Sci*, **54**, 2519–2541.

Kamahori, H., N. Yamazaki, N. Mannoji, and K. Takahashi, 2006: Variability in Intense Tropical Cyclone Days in the Western North Pacific. *SOLA*, **2**, 104–107, doi:10.2151/sola.2006-027.

Kim, H.-S., J.-H. Kim, C.-H. Ho, and P.-S. Chu, 2011: Pattern Classification of Typhoon Tracks Using the Fuzzy c-Means Clustering Method. *J. Climate*, **24**, 488–508, doi:10.1175/2010JCLI3751.1.

Kim, J.-H., C.-H. Ho, C.-H. Sui, and S. K. Park, 2005: Dipole structure of interannual variations in summertime tropical cyclone activity over east Asia, *J. Clim.*, **181**, 5344–5356.

Kim, J.-H., C.-H. Ho, M.-H. Lee, J.-H. Jeong, and D. Chen, 2006: Large increase in heavy rainfall associated with tropical cyclone landfalls in Korea after the late 1970s, *Geophys. Res. Lett.*, **33**, L18706, doi:10.1029/2006GL027430.

Kim, J.-H., C.-H. Ho, and P.-S. Chu, 2010: Dipolar redistribution of summertime tropical cyclone genesis between the Philippine Sea and the northern South China Sea and its possible mechanisms. *J. Geophys. Res*, **115**, D06104, doi:10.1029/2009JD012196.

Knutson, T. R., J. L. McBride, J. Chan, K. Emanuel, G. Holland, C. Landsea, I.

Held, J. P. Kossin, A. K. Srivastava, and M. Sugi, 2010: Tropical cyclones and climate change. *Nature Geoscience*, **3**, 157–163, doi:10.1038/ngeo779.

Knapp, K. R., and J. P. Kossin, 2007: New global tropical cyclone data set from ISCCP B1 geostationary satellite observations. *J. Appl. Remote Sens*, **1**, 013505, doi:10.1117/1.2712816.

Knapp, K. R., and M. C. Kruk, 2010: Quantifying interagency differences in tropical cyclone best-track wind speed estimates, *Mon. Wea. Rev.*, **138**, 1459–1473.

Kossin, J. P., K. R. Knapp, D. J. Vimont, R. J. Murnane, and B. A. Harper, 2007: A globally consistent reanalysis of hurricane variability and trends. *Geophys. Res. Lett*, **34**, L04815, doi:10.1029/2006GL028836.

Kwon, M., J.-G. Jhun, and K.-J. Ha, 2007: Decadal change in east Asian summer monsoon circulation in the mid-1990s. *Geophys. Res. Lett*, **34**, L21706, doi:10.1029/2007GL031977.

Landsea, C. W., B. A. Harper, K. Hoarau, and J. A. Knaff, 2006: CLIMATE CHANGE: Can We Detect Trends in Extreme Tropical Cyclones? *Science*, **313**, 452–454, doi:10.1126/science.1128448.

Landsea, C. W., G. A. Vecchi, L. Bengtsson, and T. R. Knutson, 2010: Impact of Duration Thresholds on Atlantic Tropical Cyclone Counts*. *J. Climate*,

23, 2508–2519.

Lee, M.-H., C.-H. Ho, and J.-H. Kim, 2010: Influence of tropical cyclone landfalls on spatiotemporal variations in typhoon season rainfall over South China, *Adv. Atmos. Sci.*, **27**, 443–454.

Lin, I. I., C.-C. Wu, I.-F. Pun, and D.-S. Ko, 2008: Upper-Ocean Thermal Structure and the Western North Pacific Category 5 Typhoons. Part I: Ocean Features and the Category 5 Typhoons' Intensification. *Mon. Wea. Rev*, **136**, 3288–3306, doi:10.1175/2008MWR2277.1.

Lin, I. I., C.-C. Wu, K. A. Emanuel, I.-H. Lee, C.-R. Wu, and I.-F. Pun, 2005: The interaction of Supertyphoon Maemi (2003) with a warm ocean eddy. *Mon. Wea. Rev*, **133**, 2635–2649.

Lin, I. I., I.-F. Pun, and C.-C. Wu, 2009: Upper-ocean thermal structure and the western North Pacific category 5 typhoons. Part II: Dependence on translation speed. *Mon. Wea. Rev*, **137**, 3744–3757.

Liu, K. S., and J. C. L. Chan, 2012: Inactive period of Western North Pacific Tropical Cyclone Activity in 1998-2011. *J. Climate*, doi:10.1175/JCLI-D-12-00053.1.

Matsuura, T., M. Yumoto, and S. Iizuka, 2003: A mechanism of interdecadal variability of tropical cyclone activity over the western North Pacific. *Clim Dyn*, **21**, 105–117, doi:10.1007/s00382-003-0327-3.

McLeod, A. I., K. W. Hipel, and B. A. Bodo, 1991: Trend analysis methodology for water quality time series. *Environmetrics*, **2**, 169–200.

Mendelsohn, R., K. A. Emanuel, S. Chonabayashi, and L. Bakkensen, 2012: The impact of climate change on global tropical cyclone damage. *Nature Climate Change*, **2**, 205–209, doi:10.1038/nclimate1357.

Merrill, R. T., 1988: Environmental influences on hurricane intensification. *J. Atmos. Sci*, **45**, 1678–1687.

Park, S. K. and E. Lee, 2007: Synoptic features of orographically enhanced heavy rainfall on the east coast of Korea associated with Typhoon Rusa (2002), *Geophys. Res. Lett.*, **343**, L02803, doi:10.1029/2006GL028592.

Pielke, R. A., Jr, and C. W. Landsea, 1998: Normalized hurricane damages in the United States: 1925-95. *Wea. Forecasting*, **13**, 621–631.

Pielke, R. A., Jr, J. Gratz, C. W. Landsea, D. Collins, M. A. Saunders, and R. Musulin, 2008: Normalized hurricane damage in the United States: 1900–2005. *Natural Hazards Review*, **9**, 29–42.

Pielke, R. A., Jr, J. Rubiera, C. Landsea, M. L. Fernández, and R. Klein, 2003: Hurricane vulnerability in Latin America and the Caribbean: Normalized damage and loss potentials. *Natural Hazards Review*, **4**, 101–114.

Rayner, N. A., D. E. Parker, E. B. Horton, C. K. Folland, L. V. Alexander, D. P. Rowell, E. C. Kent, and A. Kaplan, 2003: Global analyses of sea surface

temperature, sea ice, and night marine air temperature since the late nineteenth century. *J. Geophys. Res.*, **108**, D14, 4407, doi:10.1029/2002JD002670.

Ren, F., J. Liang, G. Wu, W. Dong, and X. Yang, 2011: Reliability Analysis of Climate Change of Tropical Cyclone Activity over the Western North Pacific. *J. Climate*, **24**, 5887–5898, doi:10.1175/2011JCLI3996.1.

Reynolds, R. W., N. A. Rayner, T. M. Smith, D. C. Stokes, and W. Wang, 2002: An improved in situ and satellite SST analysis for climate. *J. Climate*, **15**, 1609–1625.

Ritchie, E. A., and G. J. Holland, 1999: Large-scale patterns associated with tropical cyclogenesis in the western Pacific. *Mon. Wea. Rev*, **127**, 2027–2043.

Sohn, B. J., and S.-C. Park, 2010: Strengthened tropical circulations in past three decades inferred from water vapor transport. *J. Geophys. Res*, **115**, D15112, doi:10.1029/2009JD013713.

Song, J.-J., Y. Wang, and L. Wu, 2010: Trend discrepancies among three best track data sets of western North Pacific tropical cyclones. *J. Geophys. Res*, **115**, D12128, doi:10.1029/2009JD013058.

Trenberth, K. E., 1997: The definition of El Niño, 1997, *Bull. Amer. Meteor. Soc.*, **78**, 2771–2777.

Tu, J.-Y., C. Chou, and P.-S. Chu, 2009: The abrupt shift of typhoon activity in the vicinity of Taiwan and its association with western North Pacific-East Asian climate change. *J. Climate*, **22**, 3617–3628.

Tu, J.-Y., C. Chou, P. Huang, and R. Huang, 2011: An abrupt increase of intense typhoons over the western North Pacific in early summer. *Environ. Res. Lett*, **6**, 034013, doi:10.1088/1748-9326/6/3/034013.

Velden, C. S., T. L. Olander, and R. M. Zehr, 1998: Development of an Objective Scheme to Estimate Tropical Cyclone Intensity from Digital Geostationary Satellite Infrared Imagery. *Wea. Forecasting*, **13**, 172–186.

Wada, A., and J. C. L. Chan, 2008: Relationship between typhoon activity and upper ocean heat content. *Geophys. Res. Lett*, **35**, L17603, doi:10.1029/2008GL035129.

Wada, A., and N. Usui, 2007: Importance of tropical cyclone heat potential for tropical cyclone intensity and intensification in the Western North Pacific. *Journal of oceanography*, **63**, 427–447.

Webster, P. J., G. J. Holland, J. A. Curry, and H. R. Chang, 2005: Changes in tropical cyclone number, duration, and intensity in a warming environment. *Science*, **309**, 1844–1846, doi:10.1126/science.1116448.

Weinkle, J., R. Maue, and R. A. Pielke Jr, 2012: Historical Global Tropical Cyclone Landfalls*. *J. Climate,* **25**, 4729–4735, doi:10.1175/JCLI-D-11-

00719.1.

Wu, C.-R., Y.-L. Chang, L.-Y. Oey, C.-W. J. Chang, and Y.-C. Hsin, 2008: Air-sea interaction between tropical cyclone Nari and Kuroshio. *Geophys. Res. Lett*, **35**, L12605, doi:10.1029/2008GL033942

Wu, L., and B. Wang, 2008: What Has Changed the Proportion of Intense Hurricanes in the Last 30 Years? *J. Climate*, **21**, 1432–1439.

Wu, L., and H. Zhao, 2012: Dynamically Derived Tropical Cyclone Intensity Changes over the Western North Pacific. *J. Climate*, **25**, 89–98, doi:10.1175/2011JCLI4139.1.

Wu, L., B. Wang, and S. Geng, 2005: Growing typhoon influence on east Asia. *Geophys. Res. Lett*, **32**, L18703, doi:10.1029/2005GL022937.

Wu, M.-C., K.-H. Yeung, and W.-L. Chang, 2006: Trends in western North Pacific tropical cyclone intensity. *Eos Trans. AGU*, **87**, 537, doi:10.1029/2006EO480001.

Xie, P., A. Yatagai, M. Chen, T. Hayasaka, Y. Fukushima, C. Liu, and S. Yang, 2007: A gauge-based analysis of daily precipitation over East Asia, *J. Hydrometeorol.*, **88**, 607–626.

Yumoto, M., and T. matsuura, 2001: Interdecadal Variability of Tropical Cyclone Activity in the Western North Pacific. *J. Meteor. Soc. Japan*, **79**, 23–35, doi:10.2151/jmsj.79.23.

Yumoto, M., T. Matsuura, and S. Iizuka, 2003: Interdecadal variability of tropical cyclone frequency over the western North Pacific in a high-resolution atmosphere-ocean coupled GCM. *J. Meteor. Soc. Japan*, **81**, 1069–1086.

Zeng, Z., Y. Wang, and C.-C. Wu, 2007: Environmental Dynamical Control of Tropical Cyclone Intensity—An Observational Study. *Mon. Wea. Rev*, **135**, 38–59, doi:10.1175/MWR3278.1.

Zhang, L., L. Wu, and L. Yu, 2011: Oceanic origin of a recent La Niña-like trend in the tropical Pacific. *Adv. Atmos. Sci*, **28**, 1109–1117, doi:10.1007/s00376-010-0129-6.

Zhang, Q., Q. Liu, and L. Wu, 2009: Tropical Cyclone Damages in China 1983–2006. *Bull. Amer. Meteor. Soc*, **90**, 489–495, doi:10.1175/2008BAMS2631.1.

Zhu, Y., H. Wang, W. Zhou, and J. Ma, 2011: Recent changes in the summer precipitation pattern in East China and the background circulation. *Clim Dyn*, **36**, 1463–1473.

국문초록

강풍과 호우를 동반하는 열대저기압은 대표적인 위험기상으로서 해안국가에 상륙하면 일반적으로 수많은 인명피해와 천문학적 재산피해를 발생시킨다. 이러한 열대저기압의 위험성에도 불구하고 북서태평양에서 태풍의 강도가 최근 이 지역의 뚜렷한 해수면온도 상승과 관련하여 어떻게 변화하였는지에 대해서는 아직까지 명확히 밝혀진 바가 없었다. 그래서 본 연구에서는 지난 1977년에서 2010년 사이에 북서태평양에서 태풍의 강도의 장기경향성을 조사하였다. 이와 함께 동아시아에 상륙 시 태풍강도의 장기변화와 이에 따른 잠재피해가능성과 실제피해에 대해서도 한국을 중심으로 분석하였다.

연구결과, 분석기간 동안 태풍강도는 필리핀해 부근에서는 감소하였으며, 일본 남부해역 부근에서는 증가하는 경향성을 보였다. 이런 지역적으로 상반된 태풍강도 변화의 경향성은 지역별 태풍발달속도와 태풍발생의 변화 차이로 설명할 수 있었다. 일본 남부해역에서 강화된 태풍강도는 북서태평양 중앙부에서 더 빨라진 태풍발달속도로 설명가능하며, 필리핀해 부근의 약화된 태풍강도는 필리핀해 내에서의 태풍발생 증가 및 이 지역 동쪽 부근에서 느려진 태풍발달속도와 감소된 태풍발생으로 설명이 가능하였다.

이처럼 지역적으로 태풍발달속도와 태풍발생이 서로 다르게 변화를 설명하기 위해서는 태풍에 영향을 주는 열역학적 요인과 역학적 요인을 모두 고려해야만 했다. 그 이유는 열역학적 요인 (해수면온도, 잠재최대풍속 등)의 경우, 북서태평양 전역에 걸쳐 태풍이 발달하기에 유리한 조건이어서 필리핀해에서의 태풍강도 약화를 설명할 수 없었기 때문이다. 역학적 요인 (연직시어 및 하층와도)은 필리핀해 부근에서 태풍발달에 최근 더 불리하게 작용하고 있었으며, 나머지 지역에서는 더 유리하였다. 즉, 필리핀해 부근에서 역학적 요인이 열역학적 요인보다 더 결정적인 역할을 하면서 지역적으로 서로 다른 태풍발달 정도를

보인 것으로 분석된다.

최근의 이런 열역학적 및 역학적 대기해양장의 변화는 또한 태풍의 최대강도가 나타나는 위치를 동아시아 쪽으로 근접시키는 역할을 하였다. 이로 인해 동북아시아 (중국동부, 한국, 일본)에서는 태풍의 상륙강도가 더 강해졌다. 하지만 동남아시아 (중국남부, 베트남)에서는 상륙강도의 뚜렷한 증가를 발견할 수 없었는데 이는 남중국해안에서 태풍발생이 증가하면서 태풍의 전체 강도를 약화시키는 역할을 하였기 때문이었다. 중위도에서의 태풍상륙강도의 증가는 결과적으로 중위도에 위치한 한국과 일본에서 태풍이 더 오랫동안 유지될 수 있게 함으로써 잠재적 피해가능성을 증가시켰다.

마지막으로 실제 한국에서 태풍에 의한 인명 및 재산피해를 분석하기 위해 지난 1979년에서 2010년 동안 한반도에 상륙했던 51개 태풍을 분석하였다. 그 결과, 최근 태풍에 의한 인명 및 재산피해 모두 동일한 강도 대비 큰 폭으로 감소된 것을 확인할 수 있었다. 이는 1990년대를 전후하여 급격히 발달한 방재 관련 기술 및 인프라 (수치모델, 슈퍼컴퓨터 도입, 방재시설 확대 등) 덕분으로 보인다.

주요어: 열대저기압, 태풍, 기후변화, 기후변동, 피해영향평가

학　번: 2009-30862